NTNU – Trondheim
Norwegian University of
Science and Technology

Multi-span Suspension Bridge with Floating Towers

Ørjan Brunstad

Civil and Environmental Engineering
Submission date: June 2013
Supervisor: Ole Andre Øiseth, KT

Norwegian University of Science and Technology
Department of Structural Engineering

Department of Structural Engineering
Faculty of Engineering Science and Technology
NTNU- Norwegian University of Science and Technology

ACCESSIBILITY

MASTER THESIS 2013

SUBJECT AREA:	DATE:	NO. OF PAGES:
Bridge Dynamics	10.06.2013	127

TITLE:

Multi-span suspension bridge with floating towers

Flerspenns hengebru med flytende tårn

BY:

Ørjan Brunstad

SUMMARY:
The Norwegian Public Roads Administration (NPRA) is currently conducting a feasible study of crossing 8 fjords on the west coast of Norway. The most challenging crossing is the 3700 *m* wide Sognefjord. Three main concepts are under development, and one of the concepts of this crossing is a three span suspension bridge on floating towers. The floating foundation suggested is a multi-column pontoon with mooring lines to seabed. The object of this thesis was to study this bridge concept with respect to static deflection and dynamic properties. A preliminary bridge design based on the Hardanger Bridge design and a preliminary design of the pontoons was conducted. The hydrodynamic effects, e.g. added mass and added non-linear damping, were calculated according to potential theory and Morison equation assuming a vertical circular cylinder. The bridge and pontoons were modeled in the finite element program Abaqus/CAE. The static mean wind analysis and static traffic analysis gave reasonable results, but the tolerability of deflections z_{max} = 8.8 *m* for static mean wind and y_{max} =9.8 *m* for traffic load can be disputed. From real and complex eigen-value analysis natural frequencies, mode shapes and damping ratios were conducted. The ten first eigen modes had considerable motion in the pontoons with natural period between 138 *s* and 20 *s*. The first stiffening girder modes in vertical, horizontal and torsional direction have natural periods were 16.5 *s*, 15.1 *s* and 2.6 *s*. The effect of adding hydrodynamic damping resulted in increased damping ratio of 6 % for modes with lateral and longitudinal motion in the pontoons, 2.5 % increased damping ratio for modes with vertical motion in the pontoons and 1 % increased damping ratio for modes with longitudinal rotation in the pontoons. The validity and accuracy of these increased damping ratios is disputable. Simple time-domain response simulations gave considerably larger damping ratio using the logarithmic decrements of the oscillations. Three of the four simulations gave maximum damping forces according to implemented non-linear damping behavior when assuming reasonable maximum velocities.

RESPONSIBLE TEACHER: Ole Andre Øiseth

SUPERVISOR(S) Ole Andre Øiseth (NTNU) and Bjørn Ivar Isaksen (Statens Vegvesen)

CARRIED OUT AT: Department of Structural Engineering

Institutt for konstruksjonsteknikk
FAKULTET FOR INGENIØRVITENSKAP OG TEKNOLOGI
NTNU –Norges teknisk naturvitenskapelige universitet

MASTEROPPGAVE 2013

for

Ørjan Brunstad

Flerspenns hengebru med flytende tårn

Multi–span suspension bridge with floating towers

I forbindelse med prosjektet ferjefri E39 har det blitt langstert et konsept for kryssing av Sognefjorden som består av en hengebru med tre spenn og to flytende tårn. De flytende tårnene settes på pongtonger som forankres til sjøbunnen ved hjelp av forankringsliner.

Denne oppgaven dreier seg om dynamisk analyse av et slikt konsept.

Oppgaven bør inneholde følgende temaer.

- Overslagsberegninger for å finne dimensjonene til pongtonger, tårn, brobjelke og kabler
- Etablering av en modell i programmet Abaqus der de hydrodynamiske effektene modelleres ved hjelp av fjærer, dempere og punktmasser.
- Analyse av statiske utbøyinger, egenfrekvenser og svingeformer.
- Kartlegging av den hydrodynamiske dempingens innflytelse på den totale dempingen av konstruksjonen

Det legges vekt på at studenten må gjøre fornuftige forenklinger for å komme i mål med oppgaven.

Besvarelsen organiseres i henhold til gjeldende retningslinjer.

Veileder(e): Ole Andre Øiseth

Besvarelsen skal leveres til Institutt for konstruksjonsteknikk innen 10. juni 2013

NTNU, 14. januar, 2013

Ole Andre Øiseth
faglærer

Preface

This thesis constitutes the result of the final semester of the master degree's program at Norwegian University of Science and Technology (NTNU), Trondheim, Norway. The thesis has been carried out at the Faculty of Engineering Science and Technology, Department of Structural Engineering under supervision by Associate Professor Ole Andre Øiseth. The thesis is written in cooperation with the Norwegian Public Roads Administration under supervision by Bjørn Ivar Isaksen.

I wish to thank my supervisors for relevant and helpful information when problems have occurred.

Trondheim, June, 2013

Ørjan Brunstad

Abstract

The Norwegian Public Roads Administration (NPRA) is currently conducting a feasible study of crossing 8 fjords on the west coast of Norway. The most challenging crossing is the 3700 *m* wide Sognefjord. Three main concepts are under development, and one of the concepts of this crossing is a three span suspension bridge on floating towers. The floating foundation suggested is a multi-column pontoon with mooring lines to seabed.

The object of this thesis was to study this bridge concept with respect to static deflection and dynamic properties. A preliminary bridge design based on the Hardanger Bridge design and a preliminary design of the pontoons was conducted. The hydrodynamic effects, e.g. added mass and added non-linear damping, were calculated according to potential theory and Morison equation assuming a vertical circular cylinder.

The bridge and pontoons were modeled in the finite element program Abaqus/CAE. The static mean wind analysis and static traffic analysis gave reasonable results, but the tolerability of deflections z_{max} = 8.8 *m* for static mean wind and y_{max} =9.8 *m* for traffic load can be disputed.

From real and complex eigen-value analysis natural frequencies, mode shapes and damping ratios were conducted. The ten first eigen modes had considerable motion in the pontoons with natural period between 138 *s* and 20 *s*. The first stiffening girder modes in vertical, horizontal and torsional direction have natural periods were 16.5 *s*, 15.1 *s* and 2.6 *s*. The effect of adding hydrodynamic damping resulted in increased damping ratio of 6 % for modes with lateral and longitudinal motion in the pontoons, 2.5 % increased damping ratio for modes with vertical motion in the pontoons and 1 % increased damping ratio for modes with longitudinal rotation in the pontoons. The validity and accuracy of these increased damping ratios is disputable. Simple time-domain response simulations gave considerably larger damping ratio using the logarithmic decrements of the oscillations. Three of the four simulations gave maximum damping forces according to implemented non-linear damping behavior when assuming reasonable maximum velocities.

Sammendrag

Vegvesenet arbeider for øyeblikket med et mulighetsstudie hvor det ses på 8 fjordkryssinger på vest landet. Den mest utfordrende krysningen er Sognefjorden med en bredde på 3700 *m*. En av konseptene som er under utvikling er en trespenns hengebru med flytende tårn. Det er foreslått pongtonger som flytende fundamenter bestående av flere sylindere og forankringsliner til sjøbunnen.

Hensikten med denne oppgaven er å studere et slikt konsept med hensyn på statisk nedbøyning og dynamiske egenskaper. Det er blitt gjennomført en brodimensjonering basert på Hardangerbrua og dimensjonering av pongtongene. De hydrodynamiske effektene, som vil si ekstra masse og ekstra ikke-lineær demping, ble beregnet etter potensialteorien og Morisons ligning for en vertikal sirkulær sylinder.

Det ble etablert en elementmetodemodell i Abaqus/CAE. De statiske analysene av gjennomsnittsvindhastighet laster og trafikk laster er antatt å være rimelige, men om utbøyning 8.8 *m* for vind last og nedbøyning 9.8 *m* er akseptabelt kan diskuteres.

Fra de reelle og imaginære egenverdianalysene er egenfrekvenser, svingeformer og dempningstall tatt ut. De de første svingeformene har betydelig bevegelse in pongtongene og egenperiodene til disse svingeformene er mellom 138 *s* og 20 *s*. For svingeformene til brobjelke kan horisontal-, vertikal-, torsjonsformene er den første tilhørende egenperioden 16.5 *s*, 15.1 *s* og 2.6 *s*. Den hydrodynamiske dempningen resulterte i en økning på 6 % for dempningstallene til svingeformene som har betydelig bevegelse i pongtongenes laterale og langsgående retning. Det observeres en økning på 2.5 % til svingeformene som har pongtongbevegelse in vertikal retning og 1 % økning til svingeformene hvor pongtongene roterer om langsgående akse. Gyldigheten og nøyaktigheten til disse økningene kan diskuteres. De enkle tidsserieanalysene gir betydelig høyere dempningstall, når dempningstallene er funnet fra logaritmisk dekrement for svingningene. Tre av de fire tidsserieanalysene gir maksimal dempningskraft som samsvarer med de implementerte ikke-lineære egenskapene når fornuftige makshastigheter er antatt.

Table of Contents

List of Figures

List of Tables

1 Introduction

The Ministry of Transport and Communication have commissioned the Norwegian Public Road Administration (NPRA) to conduct a feasibile study of eliminating all ferries at E39 along the west coast of Norway. There are 7 fjord crossings at E39 between Stavanger and Trondheim, and the crossing of the Sognefjord is considered the most challenging because of its overall vast depth up to 1300 *m* and width 3700 *m*.

The Sognefjord crossing is therefore chosen as a pilot project for development of technology and concepts for extreme bridges, where the idea is if this fjord can be crossed all the other fjord can be crossed too. The objective of the pilot project is to determine, at a conceptual level, whether it will be technically possible to build a fixed link across the Sognefjord between Lavik and Oppedal. Three main concepts are under development, and one of these concepts is a side anchored multi span suspension bridge on floating support. By having a three span suspension bridge the span length reduces from *3700 m* to 1234 *m*. The end pylons can be placed onshore while the two mid pylons must be supported by floating structures. It is suggested pontoons moored to seabed at depth 1250 *m*.

The purpose of this thesis is to investigate this three span suspension bridge with floating towers. The first step is conducting a preliminary design. When carrying out a preliminary design it is natural to look how similar projects have been designed. The Hardanger Bridge is single span suspension bridge currently under construction by NPRA. The bridge is crossing the Hardanger fjord in Hordaland and will have the world's 10^{th} longest span and longest bridge span in Norway with span length of 1310 *m*. Due to moderate traffic the bridge is design for two notional lanes and one pedestrian crossing. This result in a width of only 18.3*m* and making the Hardanger Bridge unique regarding span-to-width ratio compared to international suspension bridges. There are many parallels between the three span bridge concept and the Hardanger Bridge. Firstly, the same traffic volume and traffic load can be assumed the same as for the Hardanger Bridge. Secondly, the wind situation and wind load are in the same range in Sogn and Hardanger. Most importantly the span length proposed to the three span suspension bridge in Sogn is less than 5% shorter compared to the Hardanger Bridge span. Therefore the preliminary design of the three span bridge concept presented in this thesis will be based on the Hardanger Bridge Design given by NPRA [1].

The three span bridge concept will need a floating support system, able of supporting the two mid pylons. Several concepts are possible, but for this thesis floating multi-column pontoons will presented. The floating multi-column pontoons are inspired by the concept of a spar platform. The multi-column pontoon is favorable compared to single column pontoon due to resistance and flooding in case of ship collision. A preliminary design of the pontoons will be carried out considering dead load on the bridge and static wind load on the bridge. The pontoon design method consists of applying hydrostatics principles and methods initially introduced by naval architects to achieve the necessary hydrostatic behavior.

Multi-span suspension bridges on floating support have only been studied once before [2]. As for normal suspension bridges it is typically the dynamic responses and aerodynamic stability which is decisive in bridge design due to the highly flexible suspension bridge structure and the low frequency fluctuating wind.

Therefore, this thesis will also try to characterize some of the dynamic properties of the bridge. The most comprehensive method to achieve this is creating a numerical model using the *Finite Element Method*. The Finite Element model will be created in *Abaqus/CAE*. It is vital to describe the structural properties precisely such that the model behaves correctly. Hence a fair amount of time will be spent creating this model. The modeling of the bridge and pontoon is done in chapter 4.

The hydrodynamic behavior of the floating foundation is of particular interest since these contributions are fairly new to bridge designers. These hydrodynamic effects have been studied by marine engineers and offshore engineers for decades. From hydromechanics and offshore engineering relevant theory can be obtained to describe the hydrodynamic effects. This theory and relevant method is described in chapter 2, while the hydrodynamic properties are added to the FE-model in chapter 4.

The finite element model will be used to run analysis of the static mean wind load and static traffic load. Eigen–value analysis will be used to investigate the natural frequencies, mode shapes and effective damping ratios. It is of interest to see how the dynamic properties of the bridge change due to the floating support and therefore analysis both including and excluding these the floating support system will be carried out. The effect of the hydrodynamic damping is of particular interest and complex frequency of models including and excluding hydrodynamic damping will be compared. Simple time-history response simulations will be carried out to see the effect of the hydrodynamic damping forces.

2 Hydrostatics and Hydrodynamics

For the purpose of preliminary design of the floating support system theory, principles and methods of hydrostatics is needed. This will be presented in the first part of this chapter.

To describe the total dynamic behavior of the bridge in a finite element model the hydrodynamic properties of floating support must be included. This chapter will therefor also present theory and expressions for the relevant hydrodynamics. This theory is established by marine- and offshore engineers in the early 1980's [3].

2.1 Concept of Buoyancy and Stability

A floating body experience hydrostatic forces on its submerged surfaces. In third century B.C. Archimedes discovered buoyancy and what is named Archimedes' law 2:

> *A floating body displaces its own weight in the fluid in which it floats.*

Assuming the fluid has uniform specific weight a floating body experience a upward force called buoyant force F_B which is given by

$$F_B = (\gamma_{fluid}) \cdot (displaced\ volume) \tag{2.1}$$

The buoyant force acts in the centroid of the displaced volume.

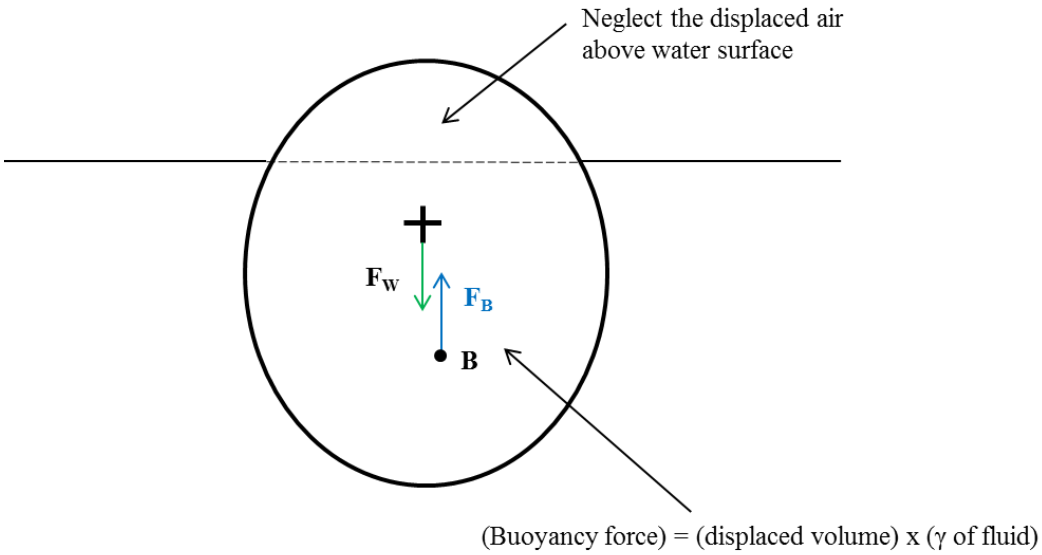

Figure 1: Buoyancy force on a floating body

Whether or not a body is floating in a stable position is checked by applying a rotation mathematically to see if the body develops a restoring moment that will return it to its original position. A general stability concept developed by naval architects can calculate the stability of floating bodies [4]. The concept assumes that the immersed body has a smooth shape (no discontinuous) near the waterline and that the body is symmetric about the tilted line.
The concept consists of the following steps:

1. When the body is in neutral buoyancy, calculate the C*enter of Gravity (CG)* and *Center of Buoyancy (CB)*.
2. Apply a small angle $\Delta\theta$ and calculate the new position of the buoyancy *B'*. The intersecting point between the vertical axis from B' and the line of symmetry (body's local y-axis) is called the *metacenter*. This point is independent of $\Delta\theta$ for small angles.
3. The *metacentric height* (*MG)* is the distance between *center of gravity* and *metacenter*. The body is stable if the *MG* is positive (e.g. *M* is above *G*)

The new position of center of buoyancy, B' can be found by mathematical derivation of the change of centroid position of the submerged volume. The deviation is based on Figure 2. $\bar{x}$ is the change of the buoyancy center and v_s is the new submerged volume given within the points *aObde*. This derivation assumes symmetry, hence the submerged wedge *Obd* is equal to the uncovered wedge *cOa*.

$$\begin{aligned}\bar{x}\, v_s &= \int_{cOdea} x\, dv + \int_{Obd} x\, dv - \int_{cOa} x\, dv = 0 + \int_{Obd} x\,(L\, dA) - \int_{cOa} x\ \mathrm{L}\,(dA) \\ &= 0 + \int_{Obd} xL\ (x\tan\theta\ dx) - \int_{cOa} xL\ (-x\tan\theta\ dx) = \tan\theta \int_{x} x^2 dA_{waterline} \\ &= I_0 \tan\theta\end{aligned} \tag{2.2}$$

Where, I_0 is the area moment of inertia of the waterline area about the axis of tilt.

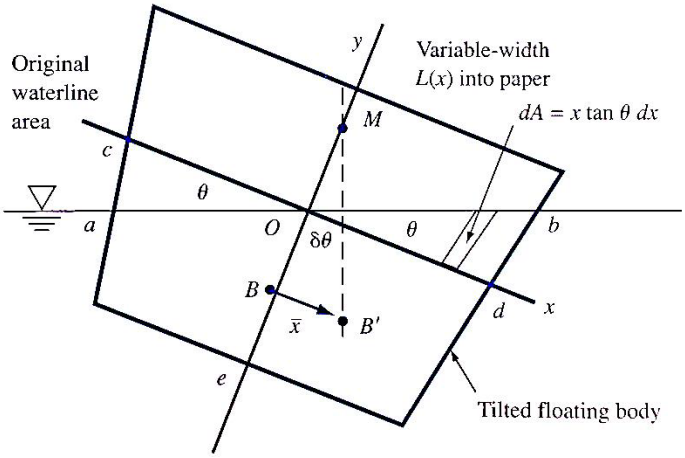

Figure 2: Center of Buoyancy for a tilted floating body [5]

Trigonometry gives the distance between metacenter and center of buoyancy (MB) as function of $\overline{x}$ and $\tan\theta$

$$MB = \frac{\overline{x}}{\tan\theta} = \frac{I_o \tan\theta / v_s}{\tan\theta} = \frac{I_0}{v_s} \tag{2.3}$$

Then the metacentric height (MG) is given introducing distance between center of gravity and center of buoyancy (GB)

$$MG = MB - GB = \frac{I_0}{V_s} - GB \tag{2.4}$$

The restoring moment the floating body can restore is given by the metacentric height and the buoyancy force. Moment equilibrium about the metacenter gives the resisting moment

$$M = F_B \cdot MG \cdot \sin\theta \tag{2.5}$$

For small rotation, i.e. $\sin\theta \approx \theta$ the relationship between moment and rotation can be assumed to be linear. This relationship is given by

$$k_\theta = \frac{M}{\theta} = \frac{F_B \cdot MG \cdot \sin\theta}{\theta} \approx F_B \cdot MG \tag{2.6}$$

Also in vertical direction a linear relationship between force and displacement can be derived. The buoyancy force is given by the submerged volume, and if assuming the cross section to

be constant the relationship between vertical load (equal to the buoyancy force) and vertical displacement (equal to extra submerged height) can be described by

$$k_z = \frac{\gamma_{fluid} \cdot \Delta v_{sub}}{\Delta z} = \frac{\gamma_{fluid} \cdot A \cdot \Delta z}{\Delta z} = \gamma_{fluid} \cdot A \tag{2.7}$$

2.2 Hydrodynamic Properties

The hydrodynamic effects of interest are the hydrodynamic added mass and hydrodynamic added damping. The hydrodynamics added mass will be derived using potential theory while for added damping the Morison equation is assumed satisfying for the purpose of this thesis.

Herein it is assumed the floating body can be described by rigid body motion. This is a valid assumption since floating body is extremely stiff compared to the hydrostatic displacements. The motion of the pontoon can be described by a single node with 6 Degree of Freedoms. The node is placed centric in the submerged volume of the body. Since this theory will be applied to a vertical cylinder, all expressions are derived especially for floating cylinders with submerged depth *d*, total depth *H* and radius *r* .

Marine and offshore engineers often refers to translations and rotations of the rigid body as *surge, heave, sway, roll, pitch* and *yaw* , but for the purpose of this thesis the motions are referred to as degree of freedom's with notation 1-6 as shown in Figure 3.

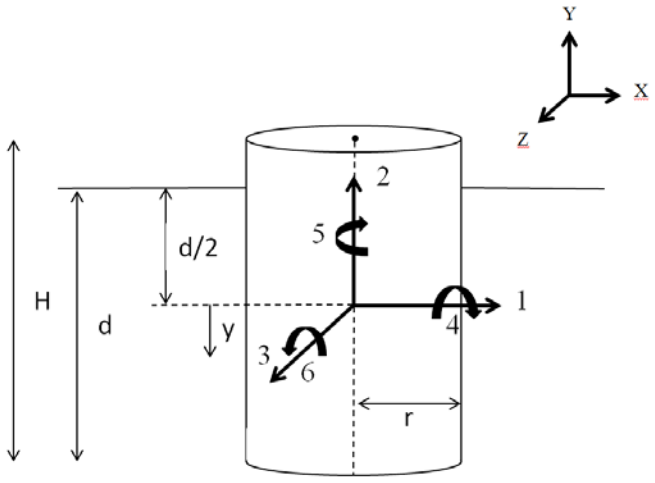

Figure 3: Floating vertical cylinder

2.2.1 Added mass

The concept of added mass originates from a body accelerating relative to the surrounding fluid to induce accelerations to the fluid. When a body accelerates so too must the fluid. Acceleration of the fluid demand forces which are utilized by the body through a pressure

distribution of the fluid on the body. Thus, more force is required to accelerate the body in a fluid than in vacuum. Since force equals mass times acceleration we can think of the additional force needed to accelerate the fluid as imaginary *added mass*, or as some mass of the fluid being attached to the body [3].

The added mass effect and hydrodynamic force acting on an sphere or cylinder can be derived analytically by using potential theory [6]. Such a derivation will carried out assuming a cylinder of radius, *R*, length, *L*, accelerating at rate $a = \partial U / \partial t = \dot{U}$. The hydrodynamic force in x-direction is obtained by integrating the pressure over the area projected in the x-direction

$$F_x = PdA_x \tag{2.8}$$

Where the projected area is given by

$$dA_x = \cos\theta dA = \cos\theta \cdot Lds = \cos\theta L \cdot Rd\theta \tag{2.9}$$

The pressure is described by the unsteady Bernoulli's equation

$$P = -\rho \frac{\partial \phi}{\partial t} + \frac{1}{2}\left|\nabla \phi\right|^2 \tag{2.10}$$

The flow around a cylinder has the given potential

$$\phi = U \frac{R^2}{r}\cos\theta \tag{2.11}$$

And the following boundary conditions yields

$$\frac{\partial \phi}{\partial t}|_{r=R} = \dot{U}\frac{R^2}{r}\cos\theta = \dot{U}R\cos\theta \tag{2.12}$$

$$\frac{1}{2}\left|\nabla \phi\right|^2 |_{r=R} = \frac{1}{2}\left|(-U\frac{R^2}{r^2}\cos\theta - U\frac{R^2}{r^2}\sin\theta)\right|^2 = \frac{1}{2}U^2 \tag{2.13}$$

Thus,

$$\begin{aligned} F_x &= \int_0^{2\pi} \left(-\rho \frac{\partial \phi}{\partial t} + \frac{1}{2} |\nabla \phi|^2 \right) \cos\theta RL d\theta \\ &= \int_0^{2\pi} \left(-\rho \dot{U} R \cos\theta + \frac{1}{2} U^2 \right) \cos\theta RL d\theta \\ &= -\rho \cdot RL \cdot \dot{U} R \underbrace{\int_0^{2\pi} \cos^2\theta d\theta}_{=2\pi} - \rho \cdot RL \cdot \frac{1}{2} U^2 \underbrace{\int_0^{2\pi} \cos\theta d\theta}_{=0} \\ &= -\rho \pi R^2 L \dot{U} \end{aligned} \tag{2.14}$$

Where $a = \dot{U}$ is the acceleration of the body and the negative sign indicates that the force is in negative direction, opposing the acceleration. Thus, the body must exert this extra force, and the superficial added mass in x-direction is then given by

$$m_{11} = \rho \pi R^2 L \tag{2.15}$$

For variable cross-sections, complex shapes and added mass in different directions the *strip method* described by [7] and [8] can be used. The method consists of dividing the body into a finite number of strips and integrating along the longitudinal direction to obtain the total hydrodynamic force. For the strip method an added mass force for a unit length of a cylinder given unit acceleration is introduced

$$a_{11} = C_a \rho \pi r^2 \tag{2.16}$$

For a circular constant radius cylinder $C_a = 1.0$ and the added mass force is obtained by integrating along the cylinder axis in the interval *-d/2* to *d/2* according to Figure 3.

$$F_{m,11} = \int_{-d/2}^{d/2} a_{11} dy \ddot{X} = \rho \pi r^2 d\ddot{X} \tag{2.17}$$

And then the added mass in x-direction is given by

$$m_{11} = \rho g p r^2 d \tag{2.18}$$

It is seen that the strip method gives the same added mass m_{11} as the analytical derivation. The strip method is also comprehensive when finding the added mass for rotational motions. For the added mass m_{66}, which is the relationship between the moment and angular acceleration about the z-axis, the tangential acceleration due to angular acceleration must be obtained. For small rotations the angular acceleration can be assumed to only have tangential acceleration in *x*-direction and the following linearization can be used

$$\ddot{x}(y) = y \cdot \ddot{\theta} \tag{2.19}$$

A strip with length *dy* will contribute to a moment about the x-axis at center of buoyancy equal to the strip force *dF* times the lever arm *y*. The total moment is obtained by integrating along the cylinder axis using the local y-axis in the interval *d/2* to *–d/2* according to Figure 3.

$$\begin{aligned} F_{m,66} &= \int_{-d/2}^{d/2} \underbrace{a_{11}\ddot{x}(y)}_{dF} \cdot \underbrace{y}_{\text{lever arm}} dy = \int_{-d/2}^{d/2} \rho\pi r^2 y\ddot{\theta} \cdot y dy \\ &= \frac{1}{12} C_a \rho\pi r^2 d^3 \cdot \ddot{\theta} \end{aligned} \tag{2.20}$$

Hence,

$$m_{66} = \frac{1}{12}\rho\pi r^2 d^3 \tag{2.21}$$

The added mass in z-direction may be given by the *flat disc approach* [3]. The added mass in z-direction when fluid is only accelerated on one side of the disc is then given by

$$m_{22} = \frac{1}{2} \cdot \frac{8}{3} \rho r^3 \tag{2.22}$$

For a circular cylinder mass force in x-direction is equal to mass force in z-direction, and mass moment about x-axis is equal to mass moment about z-axis, hence

$$\begin{aligned} m_{33} &= m_{11} \\ m_{44} &= m_{66} \end{aligned} \tag{2.23}$$

Due to vertical and horizontal symmetry all other added masses are equal to zero. And the final added mass matrix is given by

$$m_a = \begin{bmatrix} m_{11} & 0 & 0 & 0 & 0 & 0 \\ 0 & m_{22} & 0 & 0 & 0 & 0 \\ 0 & 0 & m_{33} & 0 & 0 & 0 \\ 0 & 0 & 0 & m_{44} & 0 & 0 \\ 0 & 0 & 0 & 0 & 0 & 0 \\ 0 & 0 & 0 & 0 & 0 & m_{66} \end{bmatrix} \tag{2.24}$$

2.2.2 Added damping

Two types of hydrodynamic damping forces may occur on a body oscillating on the free surface or near the surface [9] and [10].

- *Wave damping forces* due to energy dissipation in the form of surface waves by the rigid body motion.
- *Viscous damping forces* due to turbulent flow and flow separation in the lee of the body.

For a cylinder with large dimensions, e.g. a spar truss the wave damping is assumed insignificant and is therefore neglected [9]. Viscous damping is not insignificant and general damping force can be described by Morison equation and is proportional to the velocity squared [11]

$$F_D = D_F \cdot L \cdot U \left| U \right| \tag{2.25}$$

Where,

$$D_F = \frac{1}{2} \rho C_D D = \rho C_D r \tag{2.26}$$

D_f is the drag force per unit length of a circular cylinder when given unit velocity.

C_D is the drag force coefficient and for a circular cylinder $C_D = 0.6$ [9]

The added damping coefficients can be obtained similarly as the added mass, except that the force is now proportional to the velocity squared instead of acceleration normal to the cylinder axis. The deviation of the damping matrix for a vertical cylinder depends on the assumption that the coupling between circular velocities and vertical forces is insignificant. This implies that the damping forces normal to the cylinder axis and the damping moments about the horizontal axis' are only influenced by the horizontal-velocity components [11]. The added damping coefficients are obtained by the *strip method*, as for the added masses.

The damping force in x-direction is given by the integral and interval according to Figure 3

$$F_{D,11} = \int_{-d/2}^{-d/2} \underbrace{C_D \rho r \dot{X} \left| \dot{X} \right|}_{dF} dy = C_D \rho r d \cdot \dot{X} \left| \dot{X} \right| \tag{2.27}$$

Hence the added damping coefficient c_{11} is given by

$$c_{11} = C_D \rho r d \tag{2.28}$$

To calculate the damping moment about z-axis the tangential velocity is needed and same assumption as for mass forces is used. Hence the linearized x-component is given by

$$\dot{x}(y) = y \cdot \dot{\theta}_z \tag{2.29}$$

The damping moment is obtained by integrating the strip force in x-direction times the lever arm *(y)* over the interval *–d/2* to *d/2* as given by Figure 3

$$\begin{aligned} F_{D,66} &= \int_0^d \underbrace{\frac{c_{11}}{d} \dot{x}(y) \left| \dot{x}(y) \right|}_{dF} \cdot \underbrace{y}_{\text{lever arm}} dy = \int_0^d C_D \rho r \left(y\dot{\theta} \right) \left| y\dot{\theta} \right| \cdot y dy \\ &= \frac{1}{32} C_D \rho r d^4 \cdot \dot{\theta} \left| \dot{\theta} \right| \end{aligned} \tag{2.30}$$

Hence added damping coefficient c_{66} is given by

$$c_{66} = \frac{1}{32} C_D \rho r d^4 \tag{2.31}$$

For damping force in vertical direction a flat-faced cylinder is assumed with L/d ratio equal to 1, giving $C_D = 0.9$ when the force is based on the frontal area, laminar flow and Re > 10^4 [5]. Then the damping force is then given by

$$F_{D,22} = C_D \pi r^2 \dot{Y} \left| \dot{Y} \right| \tag{2.32}$$

And the added damping coefficient c_{22} is given by

$$c_{22} = C_D \pi r^2 \tag{2.33}$$

For a symmetrical circular cylinder damping force in x-direction is equal to damping force in z-direction, and damping moment about x-axis is equal to damping moment about z-axis, as for the added masses. Hence,

$$\begin{aligned} c_{33} &= c_{11} \\ c_{44} &= c_{66} \end{aligned} \tag{2.34}$$

Due to vertical and horizontal symmetry of the cylinder and by considering the centroid of the submerged body all other added damping coefficients are equal to zero. And the final added damping coefficient matrix becomes

$$c_a = \begin{bmatrix} c_{11} & 0 & 0 & 0 & 0 & 0 \\ 0 & c_{22} & 0 & 0 & 0 & 0 \\ 0 & 0 & c_{33} & 0 & 0 & 0 \\ 0 & 0 & 0 & c_{44} & 0 & 0 \\ 0 & 0 & 0 & 0 & 0 & 0 \\ 0 & 0 & 0 & 0 & 0 & c_{66} \end{bmatrix} \tag{2.35}$$

3 Preliminary Design

In this chapter the preliminary design of both the bridge design using conventional bridge design procedure and the floating support design will be carried out. It is emphasized that this is a preliminary design and details regarded insignificant for the overall structural behavior is left for further work.

3.1 Bridge Design

As explained in the introduction the preliminary design of the Sognefjord Bridge concept presented in this thesis will be based on the Hardanger Bridge. There are many parallels between the three span bridge concept and the Hardanger Bridge. Firstly, the same traffic volume and traffic load can be assumed the same as for the Hardanger Bridge. Secondly, the wind situation and wind load are in the same range in Sogn and Hardanger. Thirdly, the span length proposed to the three span suspension bridge 1230 *m* is less than 5% shorter compared to the Hardanger Bridge span 1310 *m*. Some differences and adjustments are needed, and the choices will be argumented thoroughly.

3.1.1 Geometry

The span lengths proposed to the three span suspension bridge is 1230 *m*.

The Hardanger Bridge have a stiffening girder curvature of 20,000 *m* [1] and since the Sognefjord Bridge is approximately three times as long a curvature of 60,000 *m* is suggested to avoid unnecessary elevation of the girder at midpoint. This gives an elevation 29m at midpoint compared to the endpoints.

The sag of the main cable is normally chosen as 1/10 of the span [12]. This implies well for the Hardanger Bridge where this ration is $121m/1310m \approx 0.09$ and the sag $k_m = 121m$ therefor also chosen for the Sognefjord Bridge. The height of the pylons is dependent of sag, sailing clearance, bridge girder height and hanger length at mid-point. The sailing clearance at the midpoint of the bridge is set to 75 *m*. The girder height is set to 2 *m* and the hanger has a length of 2 *m* at midspan. Hence the total height of the pylons can be chosen as 200 *m*.

A hanger spacing of approximately 20 *m* is chosen. This is chosen since the tension force in the hangers are assumed to be the same as for the Hardanger Bridge and hence the same cross

section can be used. The accurate distance is chosen as 20,1639 *m* which is resulting in 120 hangers per span and a total of 360 hangers in total.

The geometrical properties of the bridge are shown in the Figure 4.

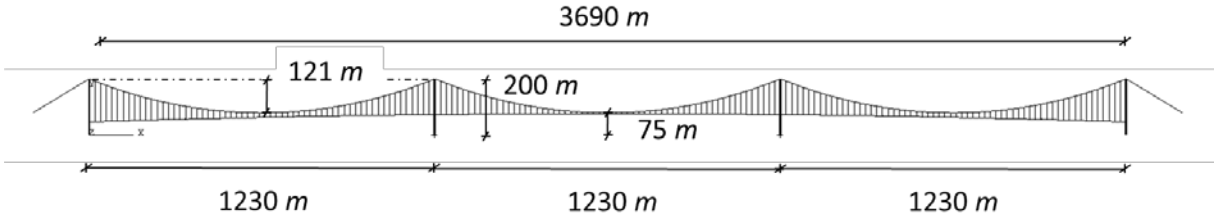

Figure 4: Bridge geometry

A coordinate system is established where the x-axis is in the longitudinal stiffening girder direction, y-axis is the vertical direction defined positive upwards and z-axis is the lateral horizontal direction.

3.1.2 Material properties

The stiffness properties and yield strengths for the different structural components are taken from the technical report [1] and is tabled in Table 1.

Table 1:Material properties for bridge elements

	Yield Strength [*Mpa*]	**Young's Modulus [*GPa*]**
Stiffening girder	*355*	*210*
Main cables	*1570*	*200*
Hangers	*1570*	*160*
Pylons	*55*	*29.764*

3.1.3 Stiffening Girder

For the Hardanger Bridge a single box stiffening girder is used. This stiffening girder is design for traffic loading given by three notional lanes and one pedestrian crossing and the same traffic and hence traffic loading can be assumed for the Sognefjord crossing. The box girder have proved to be efficient regarding aerodynamics [13]. Hence this single box girder is assumed to be a good choice for the preliminary design. The cross sectional properties are given from Technical Report [1]. The girder is 18,3 *m* wide and a height of 3,18 *m*. Placing origin centric in z-direction and bottom of stiffening girder in x-direction following shear center is obtained

$y_s = 1.759m$

$z_s = 0.155m$

The cross sectional properties for the stiffening girder about the shear center are given in Table 2.

Table 2: Cross-sectional properties for stiffening girder [2]

Cross Sectional Property	Value
A	$0.5813\ m^2$
I_Z	$0.972\ m^4$
I_Y	$16.448\ m^4$
I_T	$4.298\ m^4$

The geometry and shape of the stiffening girder is shown in Figure 5.

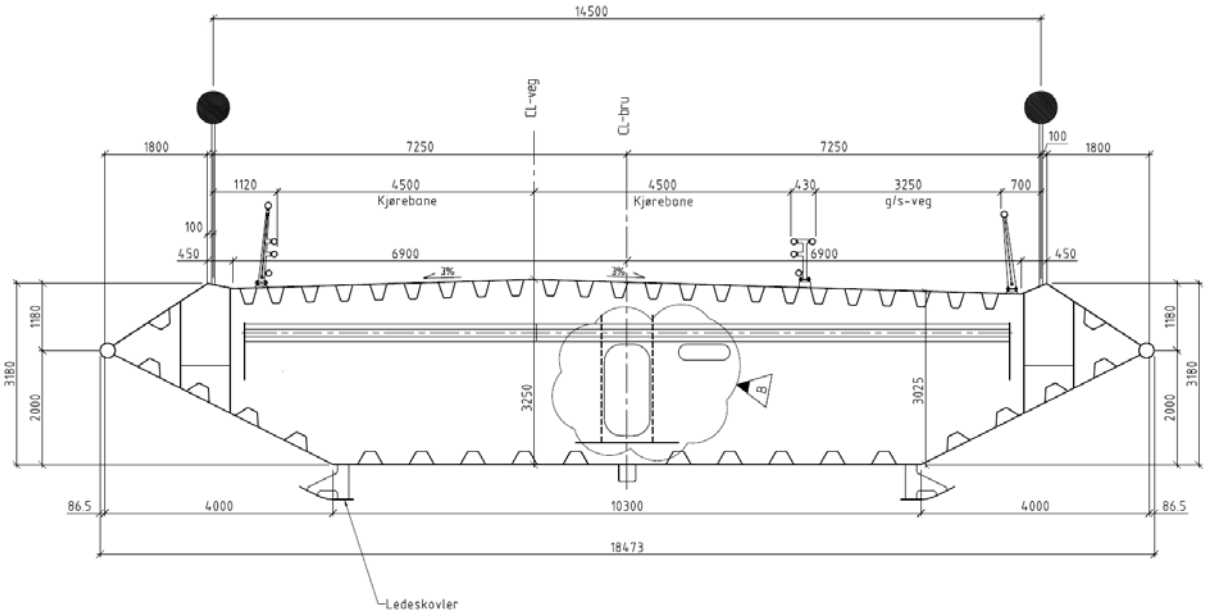

Figure 5: Stiffening girder geometry [14]

3.1.4 Main Cables

The same type of cables as for the Hardanger Bridge is assumed. These cables are made of parallel-wire strands. Each cable consist of 19 parallel wire strands, each from 528 galvanized 5.3 *mm* wires [15]. The total area of the cables are given from the Technical report $A = 0.22132m^2$ [1]. For the Sognefjord Bridge the backstay cables are designed such that the cables have the same angle on both sides of the pylons. The horizontal distance l_{bs} from the

saddle to the anchorage block is assumed to be 200 *m*, and the vertical distance h_{bs} then becomes 79 *m*.

3.1.5 Hangers

The hanger consists of a cable with a cast steel socket in each end. The cable is a locked coil cable with diameter $\varphi 70mm$ and consists of seven layers of wires. The four inner layers are parallel circular wires and the three outer layers are Z-shaped wires. The total cross-section of steel is $A = 0.0032m^2$ [1].

The hanger is attached by hanger clamps to the main cable and to the steel box girder. This connection allows free rotation in x-direction by a steel bolt.

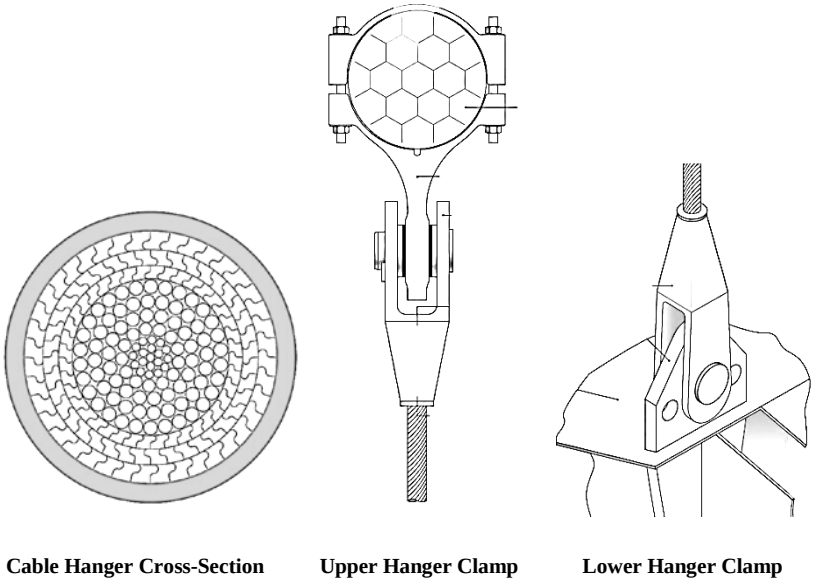

Figure 6: Hanger cross-section and hanger connection details [15]

3.1.6 Pylon

The pylon design is based on the pylons of Hardanger Bridge drawings [14]. The pylon consists of two inward leaning pylon columns and three horizontal cross beams. The columns have and inward leaning of 2.86° resulting in a horizontal offset of 10*m* for the 200*m* high columns. The pylon columns of the Hardanger Bridge have an increasing rectangular box cross-section from top to bottom. For preliminary design in this thesis three constant cross-sections have been assumed. These cross-sections are taken from the cross-sections from the Bu-side at the heights 39.1*moh*, 99.8 *moh* and 179.0 *moh* and are table in Table 3.
W is the box width in x-direction, *B* is the box breadth in z-direction, and T_B and T_W are the corresponding thickness'.

Table 3: Cross Sections Pylon Columns [3]

Cross-section name	Cross-section applied	B	W	T_B	T_W
Column 1	0-65 *m*	6.182	6.989	0.85	0.6
Column 2	65-142.5 *m*	5.199	5.252	0.85	0.6
Column 3	142.5-200	4.504	4.500	0.85	0.6

The cross beams connecting the two pylon columns together are also taken from the Bu-side of the Hardanger Bridge and dimensions are given in Table 4. *W* is the box width in x-direction, *H* is the box height in y-direction and t the thickness for all four sides.

Table 4: Cross-Sections Pylon Cross-Beam [3]

Cross-beam name	H	W	t
Cross Beam 1	6.250	7.500	0.6
Cross Beam 2	4.789	8.000	0.6
Cross Beam 3	4.000	6.000	0.6

Since the stiffening girder will pace through the pylon at different height for the end and side pylons, some adjustments are made regarding cross bema heights. For pylon 1 and 4 the bridge girder is supported by *cross beam 1*, and *cross beam 2* is placed at height 190*m*. For the mid pylons the bridge girder is supported by *cross beam 2* and *cross beam 1* is placed at height 35 *m.*

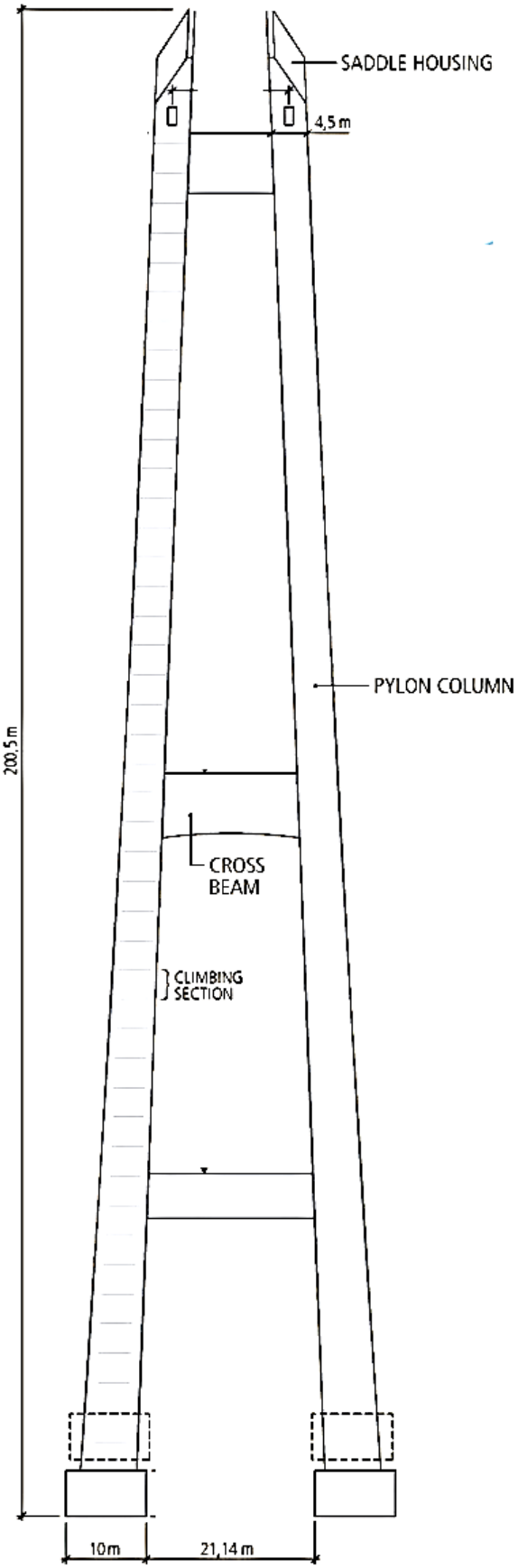

Figure 7: Pylon Geometry

3.1.7 Mass calculations

An important part of preliminary design is to determine the mass of the different structural and non-structural components. The mass calculations are based on the mass calculation carried out in the technical report of the Hardanger Bridge [1], but variations in geometry and cross sections are accounted for. The mass calculations are given in detail in Appendix A2 and the distributed masses of stiffening girder, cables and hangers are summarized in Table 5-Table 7.

Table 5: Distributed mass for stiffening girder

Description	m [kg/m]
Steel Girder	4 563
Guide Vans	114
Transverse Bulkheads	1119
Lower hanger attachment	84
Railing	183
Asphalt and wearing coarse	2 674
Electric Installation	35
Transport beam IPE120	11
Lighting Mast	5
Drain	3
Surface coating	34
TOTAL	**8 825**

Table 6: Distributed mass for cables

Description	m [kg/m]
Wires	1 737
Zink	59
Winding Wires	41
Railing	7
Polyethylene mash	7
TOTAL	**1 851**

Table 7: Distributed mass for hangers

Description	m [kg/m]
Hanger	28
Socket and clamp	37
TOTAL	**65**

3.1.8 Mass Moment of Inertia

In the finite element program the cross section of the stiffening girder will not modeled directly. The stiffening girder will be modeled as a wire and given the necessary structural properties. One important property is the mass moment of inertia (MOI) representing the moment resistance to angular acceleration. Mass moment of inertia is given by the following definition [16]

$$I = \int_m r^2 dm \tag{3.1}$$

Where *r* is the distance from the axis to the mass element *dm*. MOI about the body's center of mass also called center of gravity (CG) is given notation I_G. If I_G is known the parallel axis theorem states that the total MOI about an arbitrary parallel axis can be calculated after the following equation [16]

$$I = I_G + Mr^2 \tag{3.2}$$

Where,
r is the perpendicular distance between the two axis
M is the mass of the body

For the stiffening girder including non-structural elements the moments of mass and moments of inertia about the shear center are given in Appendix A3 and are summarized in Table 8. All masses and moments are given per unit meter.

Table 8: Mass moment of inertia (MOI) of the stiffening girder

	m [kg/m]	**m_y [m]**	**m_z [m]**	**I [kgm^2/m]**
Steel Girder	4 563	-17	8 729	139 255
Guide Vans	114	0	-68	3 779
Transverse Bulkheads	1 119	0	2 093	22 787
Lower Hanger Clamp	84	0	260	4 568
Railings	183	-13	697	6 201
Asphalt and membrane	2 674	-46	8 554	44 204
Electric Installation	35	-53	88	115
Transport Beam IPE120	11	0	22	1
Light Mast	5	34	40	454
Drain	3	0	0	147
Surface Coating	34	0	29	1 349
	8 825	**-95**	**20 444**	**222 860**

The centre of mass of the stiffening girder including non-structural parts is given by the mass and moment of mass [16]

$$z_m = \frac{\Sigma m_z}{\Sigma m} \quad \text{and} \quad y_m = \frac{\Sigma m_y}{\Sigma m} \tag{3.3}$$

Hence the center of mass is give as

$$y_m = \frac{-95}{8825} = -0.0111m \approx 0m \qquad \text{and} \qquad z_m = \frac{20444}{8825} = 2.316m \tag{3.4}$$

.

3.2 Pontoon Design

3.2.1 Concepts of floating support structures

Floating structures have been used for decades in the offshore industry. The types of floating support structures can be primarily be classified using three basic concepts: the barge, the spar and tension leg platform (TLP). The principles of these concepts are shown in Figure 8.

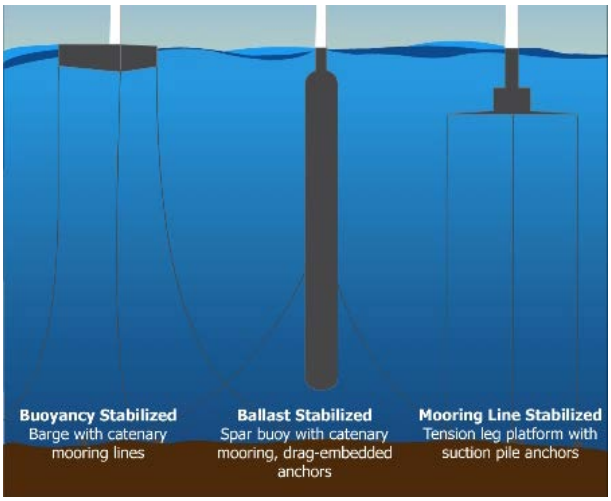

Figure 8: Concept of floating support structures

The barge concept mainly use the waterplane area to achieve static stability, usually these structures are shallow and have a large waterplane [17]. Shapes could be rectangular or cylindrical depending on the purpose of the floating support. For the barge a catenary mooring line system is normally used to achieve horizontal stiffness.

The spar is floating platform that mainly uses the relative position of the CG (Center of Gravity) with respect to the CB (Center of Buoyancy) to achieve static stability [17]. This type of concept usually consists of a single cylinder with a small radius and deep draught, but could also consist of an inner cylinder and several smaller cylinders outside. The main concept behind the spar is to lower the CG position by using ballast, to increase the lever arm and obtain stability. The ballast consists of fixed ballast and water ballast, allowing the buoyancy properties to be trimmed. The fixed ballast is usually placed at the bottom of the spar to give largest possible effect to the CG. Horizontal stiffness is normally achieved in the same way as the barge using a catenary mooring system.

The tension leg platform (TLP) is a floating platform that achieves stability by exploiting a tensioned mooring system. The platform is moored by high tensioned tethers or tendon groups at each corner of the structure. Since the tension in the tethers provides the required restoring force, the waterplane area and the distance of the CG from the CB can be designed in order to minimize the floating support structure costs.

3.2.2 The Bridge Support Concept

The floating support structure suggested in this thesis is multi-column pontoon. This concept is a combination of a barge platform and a spar platform. Hence it will have a certain draught to obtain a low CG, but also a large waterplane area to lower the position of the *metacenter* (MC). These dimensions will be calculated later on. The concept consisting of 8 outer hollow columns and a inner hollow column. One of the advantages of such a design is resistance for ship collision. Flooding of one column will not result in total collapse because buoyancy is maintained by the other columns. Ship collision is not further discussed in this thesis, but cannot be left out in a final design of the pontoon due to the large ships visiting the Sognefjord. The concept of the pontoon design is shown in Figure 9.

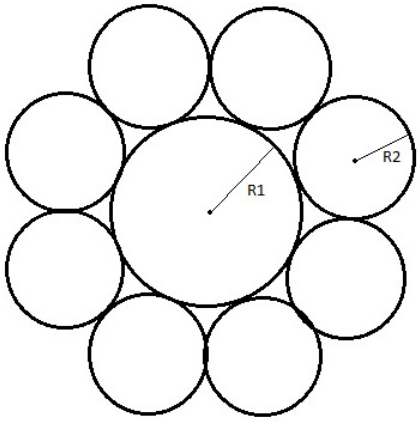

Figure 9: Bridge support structure concept: Pontoon 8+1 Cylinder

For the 8 columns to have contact both to each other and the inner column the geometrical relationship between the outer column radius and the inner column radius must be a derived. This relationship is derived in Appendix A and is given as

$$R_2 = 0.64 \cdot R_1 \tag{3.5}$$

In this thesis the pontoon hulls are suggest to be constructed in concrete. For floating structures concrete offers advantages to steel regarding maintenance, fatigue, environment and are often more cost efficient [18]. Large bending moments will occur in the columns due to the hydrostatic pressure, and stress level in the concrete will depend on column dimension, reinforcement, internal cross-bracing system and depth of the pontoon. For the purpose of this preliminary design column hull thickness $0.5m$ is assumed to be satisfying, but should be given more attention in a final design.

The purpose of this preliminary design is to find the hydrostatic forces and properties of the floating support structure. The pontoon is extremely stiff compared to the flexible and slender

suspension bridge, and therefore all properties regarding the internal behavior of the pontoon is disregarded. Connection between the columns, horizontal cross-braces inside the columns, detailed reinforcement calculations and column behavior is therefore left for further investigation. For the purpose of weight calculations and locating the *Center of Gravity* (CG) the specific weight of concrete used for the pontoon includes 5% reinforcement [17]. It is assumed specific concrete density 2500 kg / m^3 and specific steel density 7850 kg / m^3. Then the total weight density becomes

$$\rho = 0.05 \cdot 7850 + 0.95 \cdot 2500 = 2800 kg / m^3 \tag{3.6}$$

3.2.3 Pontoon Design Calculation

The principles of hydrostatics and buoyancy stability described in chapter 2 are used to create an excel spreadsheet calculating the hydrostatic properties which is given in Appendix C. The inputs for this spreadsheet are:

- Dead load from the bridge structure
- Wind load on the bridge structure
- Pontoon dimensions

The spreadsheet calculates all the hydrostatic properties, including vertical position of the pontoon and static tilt when the bridge is subjected to wind loading.

The dead loads from bridge structure are dived into pylon-, cable- and stiffening girder -dead loads. Dead load of the pylon and all its components are calculated from the preliminary design an given in Appendix A2 , while the dead load from the cable acting at pylon top and the dead load from the stiffening girder acting at the mid cross-beam is taken from the *Fixed Foundation Bridge Model* in Abaqus/ CAE. Dead load and *Center of Gravity* (CG) for these elements are summarized in table below.

Table 9: Dead load Bridge Structure

	Dead load	**Center of Gravity, CG**
	[MN]	**[m]**
Pylons	172.5	89.9
Stiffening Girder	6.4	72.3
Cables	156.6	200
TOTAL	335.5	140.9

The static wind load are calculated according to Eurocode [19] and full calculation is carried out in Appendix B. Only the horizontal lateral static mean wind load is accounted for. The stiffening girder is also subjected to lift forces and moments, but these gives restoring effects and is therefore not included in the preliminary design of the pontoon. It is assumed that the

wind load on the stiffening girder and cables distributes in way such that the lateral horizontal load from two half spans goes into the mid pylon. The wind load acting on the bridge is given in Appendix B and is summarized in Table 10.

Table 10: Reaction moment and forces in foundation when bridge is subjected to win load

	Horizontal Force	**Lever arm**	**Moment in pylon end**
	[MN]	**[m]**	**[MNm]**
Pylon Columns	2.67	100.75	269
Stiffening girder	3.94	75	295.8
Cables	1.81	85	154.5
TOTAL	8.42		719.3

Since it is of interest to find many pontoon dimensions and compare them, it is comprehensive to have as few input parameters as possible. Since the inner column radius and outer columns radius are related and the thickness for all columns are constant and equal to $0.5m$, the cross section of the pontoon can be described by one parameter. The *Total Diameter* is chosen. The depth of the pontoon is given as *Total Depth*. The fixed ballast constructed as a solid concrete plate in the bottom of the pontoon is given in as *Fixed Ballast Height*. For simplicity the cross-sectional area of the fixed ballast is assumed to be circle with diameter of the pontoon. The adjustable ballast water height is given in as W*ater Ballast Height* and is the water above the bottom plate. The area of the ballast water is the inside area of all 9 columns.

In the search for optimal pontoon dimensions there were initially three main requirements:

- Vertical hydrostatic equilibrium: Approximately distance from top of pontoon to waterline, $Z_W = 10m$.
- Buoyant Stability: positive metacentric height, MG
- Rotational hydrostatic stiffness: A maximum tiling angle, $\Theta = 5°$ when applying static wind load.

A lot of combinations of dimensions have been checked against these three considerations. Firstly a combination of pontoon diameter (D) and a pontoon height (H) was chosen, then fixed ballast was added to achieve the wanted static vertical equilibrium: $Z_W \approx 10m$. But fixed ballast is expensive and it gives unnecessarily cantilever arm, therefore a modified design combining fixed ballast and ballast water until the necessary rotational hydrostatic stiffness was achieved.

This procedure was carried out for several Diameter/Depth combinations. A minimum diameter of *40m* is required due to the distance between the pylon legs.
A selection of pontoon designs satisfying all three above criterion are given in Table 11.

Table 11: Initial pontoon designs

Design no.	D [m]	H [m]	$H_{concrete}$ [m]	H_W [m]	Z_w [m]	MG [m]	Θ [rad]	$V_{Concrete}$ [1000 m^3]
1	40	250	60	0	10	17,4	0,7	107
1	**40**	**250**	**9**	**135**	**9**	**2,8**	**4,7**	**52**
2	40	210	47	0	11	3,6	4,3	87
2	40	210	20	72	10	3,5	4,4	57
3	50	200	53	0	11	19,6	0,5	135
3	50	200	7	125	11	2	5,2	54
4	50	150	37	0	10	3	4,7	96
4	50	150	15	60	10	1,9	7,7	58
5	60	200	58	0	11	30	0,2	200
5	60	200	4	150	11	1,7	4,4	61
6	60	120	31	0	11	3,6	3,5	110
6	**60**	**120**	**12**	**54**	**10**	**2,3**	**5,4**	**61**
7	80	100	28	0	11	11	0,8	165
7	**80**	**100**	**6**	**64**	**10**	**3,2**	**2,7**	**62**
8	80	80	21	0	11	3,8	3	125
8	80	80	8	38	10	2,4	4,5	64
9	100	80	23	0	11	14,9	0,5	205
9	**100**	**80**	**2**	**61**	**10**	**2,3**	**3,1**	**49**
10	100	50	12	0	11	6,3	2	110
10	100	50	3	27	10	3,5	3,5	43

(* refers to initial design with only fixed ballast)

Four of the pontoon designs are taken to further investigation and the hydrostatic vertical stiffness and rotational stiffness are compared. These stiffness parameters are presented inTable 12.

Table 12: Hydrostatic stiffness of preliminary pontoon designs

Design no.	D [m]	H [m]	$H_{concrete}$ [m]	H_W [m]	K_y [MN / m]	$K_Θ$ [MNm / rad]
1	40	250	9	135	13	8 344
6	60	120	12	54	28	7 197
7	**80**	**100**	**6**	**64**	**50**	**14 326**
9	100	80	2	61	79	12 660

Design no. 7 is considered the best design regarding stiffness, amount of concrete needed and metacentric height. Compared to design no. 9 which has a stiffer vertical behavior the disadvantage of widening the pontoon makes the internal cross-bracing more advanced. Deisng no. 7 is therefore assumed to be the overall best design. Since the mass calculations are taken from the preliminary design it is necessary to account for some adjustments, and even a small change in dead load will affect the metacentric height. To account for such uncertainties the fixed ballast weight is increased to 10*m*. The final design dimensions are given in Table 13 and the hydrostatic properties are given in Table 14

Table 13: Pontoon dimensions of final pontoon design

Total Diameter	80 m
Radius of inner column	17.54 m
Radius of outer columns	11.23 m
Thickness columns	0.5 m
Total Height	100 m
Fixed Ballast Thickness	10 m
Water ballast height (adjustable)	64 m
Waterline Area	5 027 m^2
Concrete	81 000 m^3

Table 14: Hydrostatic properties of final pontoon design

Buoyancy Force (Dead Load)	4 501 MN
Center of Gravity, CG	-59.0 m
Metacentric height, MG	8.2 m
Clearance to waterline,	10 m
Angle in Moment Equilibrium, Θ	1,1 degree
Hydrostatic Vertical Stiffness, K_y	50 MN / m
Hydrostatic Rotational Stiffness*, K_Θ	36 903 MNm / rad*

(*rotational stiffness for pontoon and pylon)

3.2.4 Horizontal Mooring Stiffness

Due to the complexity and extreme depth of the fjord the mooring line design are left for further investigation. For this thesis the mooring lines are assumed to give horizontal linear stiffness in X and Z-direction. At NPRA Bridge Conference in 2012 Aas-Jackobsen AS and Johs. Holt AS presented horizontal stiffness parameters for three span bridge crossing the Sognefjord using floating pontoons [2]. These values will be used in this thesis and are given in Table 15.

Table 15: Horizontal mooring stiffness [2]

Horizontal Longitudinal spring stiffness, k_x	1 MN / m
Horizontal Lateral spring stiffness, k_z	2 MN / m

3.2.5 Mass Moment of Inertia

Mass moment of inertia (MOI) about the center gravity is calculated similarly as for the stiffening girder. The calculation is given in Appendix A3 and summarized in Table 16.

Table 16: Mass and inertia properties of pontoon

M	4.166 e+8	kg
I_x	3.617 e+11	kg m^2
I_y	3.351 e+11	kg m^2
I_z	3.617 e+11	kg m^2

3.2.6 Hydrodynamic Properties

By assuming the pontoon shape as a vertical circular cylinder the added mass expressions derived in chapter 2 can be used to calculated the hydrodynamic added mass in the *Center of Buoyancy*

$$M_{a,x} = M_{a,y} = \rho\pi r^2 d$$
$$M_{a,y} = \frac{4}{3}\rho r^3 \tag{3.7}$$
$$I_{a,1} = I_{a,3} = \frac{1}{12}\rho\pi r^2 d^3$$

Where, $\rho = 1000 kg/m^3$, $r = 40m$, $d = 90m$. The hydrodynamic added mass and inertia are shown in Table 17.

Table 17: Hydrodynamic added mass

M_x	4.524 e+8	kg
M_y	8.533e+7	kg
M_z	4.524 e+8	kg
$I_{a,x}$	3.054 e+11	kg m^2
$I_{a,z}$	3.054 e+11	kg m^2

By assuming the Morison Equation to be valid and the pontoon is assumed to be vertical as assumed for added mass the expressions derived in chapter XX can be used to calculate the hydrodynamic added damping in the *Center of Buoyancy*

$$\begin{aligned} C_{a,x} &= C_{a,z} = C_D{}^H \rho r d \\ C_y &= C_D{}^V \pi r^2 \\ C_{\theta_x} &= C_{\theta_z} = \frac{1}{32} C_D{}^H \rho r d^4 \end{aligned} \tag{3.8}$$

Where, $\rho = 1000 kg/m^3$, $r = 40m$, $d = 90m$, $C_D{}^H = 0.6$ is the horizontal drag coefficient on a vertical cylinder and $C_D{}^V = 0.9$ is the drag coefficient on a flat-faced cylinder. The hydrodynamic added damping are given in Table 18.

Table 18: Hydrodynamic added damping

C_X	2.16 e+6	N / (m/s)
C_Y	4.52 e+6	N / (m/s)
C_Z	2.16 e+6	N / (m/s)
$C_{\Theta x}$	4.92 e+10	Nm / (Rad/s)
$C_{\Theta z}$	4.92 e+10	Nm / (Rad/s)

4 Finite Element Modeling

In structural mechanics, advanced static and dynamic problems can be solved by using the finite element method. Abaqus/CAE is data program implementing this method to advanced as well as simple problems in a user friendly interface. Abaqus/CAE can solve both static and dynamic problems. Abaqus can handle nonlinearities as material-, geometrical- and boundary condition-nonlinearities. In this thesis material behavior and boundary conditions are modeled as linear, while the geometrical nonlinearities are included, which is absolutely necessary for suspension bridges when calculating stiffness in the cable system. The geometrical nonlinearities (stiffness) are included by specifying *NLGEOM* for all steps. The hydrodynamic damping of the pontoons will also modeled using nonlinear connectors.

Before starting to define a model in Abaqus/CAE a system of units must be chosen. Abaqus/CAE has no built in system of units and hence all input data must be specified in consistent units. SI unit system is chosen and hence the following units are used

Table 19: System of units

Quantity	**SI unit**
Length	m
Force	N
Mass	kg
Time	s
Stress	Pa (N/m)
Density	kg/m^3

The chapter is divided into two sections. In first section the three span bridge will be modeled using fixed pylon ends, and the modeled will be named *Rigid Foundation Bridge Model* (FFB-model). In section two the floating bridge will be modeled, based on the RFB-model but removing the fixities of the pylon end and adding all pontoon properties. This model is name Floating Foundation Model (FFB-model).

4.1 Rigid Foundation Model

4.1.1 Parts and Geometry

The coordinate system is defined by placing origin horizontal centric between the pylon legs of the pylon at the Lavik side and vertical position is pylon leg end. The x-axis is parallel to the girder and is positive from Lavik to Oppedal. The y-axis is the vertical axis defined positive upwards and the z-axis is the horizontal axis defined positive West.

A full step-by-step analysis of the construction phase is considered to time consuming for thesis, and therefore the bridge will modeled in its final geometry when all dead loads acts on the bridge. This geometry can taken from the preliminary design in chapter 3.1. It is important that the initial geometry is retained after the loads are applied, but this is further discussed and dealt with in the *step module.*

4.1.1.1 Cable Planes

The cables and hangers are sketched using the *Wire: Planer* option. Prior to wire planar sketching three *datum plans* in the XY-plane is created. The first datum-plane named s*tiffening-girder-datum-plane* is the centric plane and is created using *Datum Plane: Three Points* tool and the following three points: (0,0,0), (0,1,0) and (0,0,1). Then *cable-datum-plane-1* and *cable-datum-plane-2* are created using offsets 7.25*m* and -7.25*m* from s*tiffening-girder-datum-plane*. Hence the distance between the two cable datum-planes is 14.5*m*.Due to symmetry the cable planes is sketched in one of the datum plane and copied to the second datum plane.

The main cable is sketched as three identical circular arcs with length $l_m = 1230m$, sag $k_m = 121m$ and saddles 200m above origin. These three arches of the main cable are sketched using the *Through Three Points arc* tool. These points are given in Table 20.

Table 20: Points for cable arc

Arc number	First point	Second point	Third point
1	(0,200)	(1230,200)	(615,79)
2	(1230,200)	(2460,200)	(1845,79)
3	(2460,200)	(3690,200)	(3075,79)

The back stay cables are sketched as straight wires. Assuming back stay angle equal to the main cable angle $\varphi = 22.27^{\circ}$ and horizontal length $l_{bs} = 200m$ the vertical height h_{bs} becomes *82m.* The points for back stay cables are given in Table 21

Table 21: Points for back stay cables

	First point	Second point
Left Backstay	(-200,118)	(0,200)
Right Backstay	(3890,118)	(3690,200)

The outer edges of the stiffening girder (hanger attachment points) are also sketched using the arc tool in the same datum-plane. The elevation of the stiffening girder from end to mid-point is 29*m*. The shortest hanger, at midpoint, is 2*m* and hence the hanger attachment arc must go thought the midpoint 2 *m* below this point. The stiffening girder edges arc points are given in Table 22.

Table 22: Points for stiffening girder edge arc

	First point	Second point	Third point
Arc for outer edges of stiffening girder	(0,48)	(3690,48)	(1845,77)

The hangers are sketched by drawing a vertical line and using the *linear pattern* tool. Spacing 20.1639*m* is used resulting in 184 vertical lines. The four vertical lines where the pylons will are deleted and by using the *trim/extend* tool the hangers are cut at point of intersection to both the cable arc and stiffening girder edge. This results in a total of 180 hangers and 60 hangers per span. The stiffening girder edge arc is removed, since the hanger ends now represent these edge points.

The final cable plane is shown in Figure 10: Cable Plane Geometry

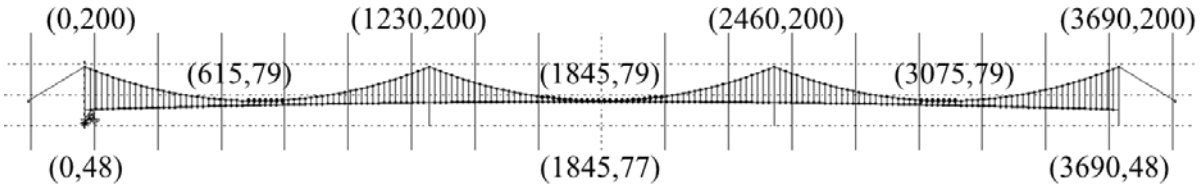

Figure 10: Cable Plane Geometry

4.1.1.2 Stiffening Girder

In the *first* datum-plane (centric) the shear centre of the stiffening girder is sketched. From preliminary design the shear centre is as located 1,759m above the bottom of the stiffening girder and approximately centric in lateral direction. From the bottom of the stiffening girder to the hanger attachments it is assumed to be 3,218*m.*Hence the vertical distance between the outer edges of the stiffening girder and the shear centre is 1.459*m*. The stiffening girder is

sketched using the same length and curve as for the outer edges of the stiffening girder, but a vertical translation of 1.459m. The stiffening girder points are given in Table 23

Table 23: Points for stiffening girder

	First point	Second point	Third point
Shear Centre line	(0,46.541)	(3690,46.541)	(1845,75.541)

The hangers are connected to the stiffening girder at every 20.1639 *m* using fictive beams. These fictive beams have practically no mass and are close to rigid, hence transferring all forces and displacements including the moments and rotation due to eccentricity. These wires cannot be created in planar sketching due to the curve of the stiffening girder and is therefore created using the *point-to-point wire* tool. The modeling technique used for the hanger-stiffening girder connection is shown in Figure 11

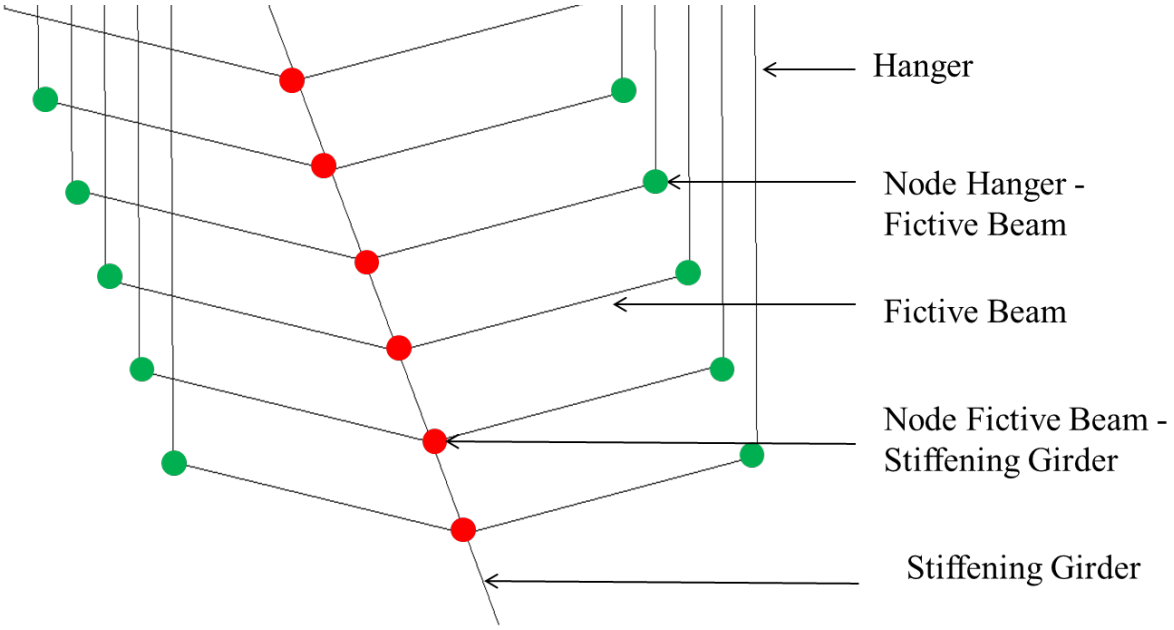

Figure 11: Stiffening girder modeling technique

4.1.1.3 Pylon

The pylons are also modeled with *Wire: Planar* using datum-planes parallel to the YZ- plane. *Pylon-datum-plane-1* have X-coordinate 0*m*, and three other datum planes are created each with offset 1230*m* from previous. Geometry is given by preliminary design and the section sketch is given in Figure 12.

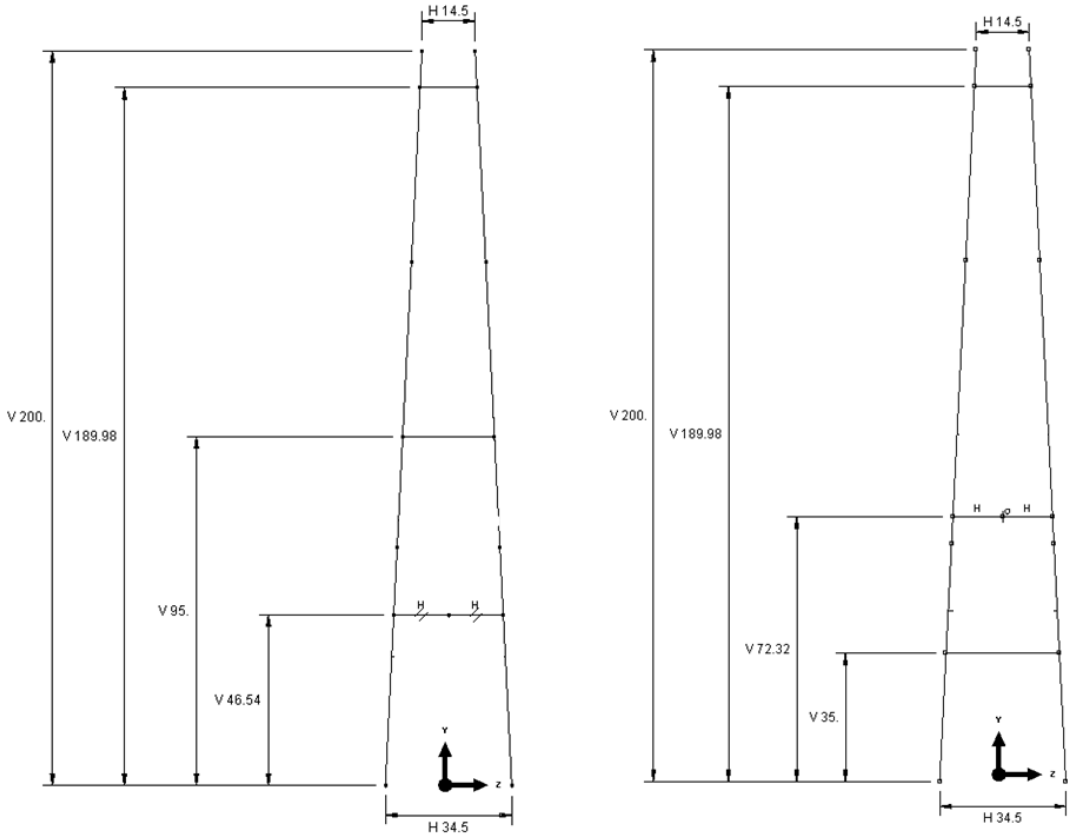

Figure 12: pylon-datum-plane-2 and 3and pylon-datum-plane-1 and 4

The final geometry of the bridge is given inFigure 13.

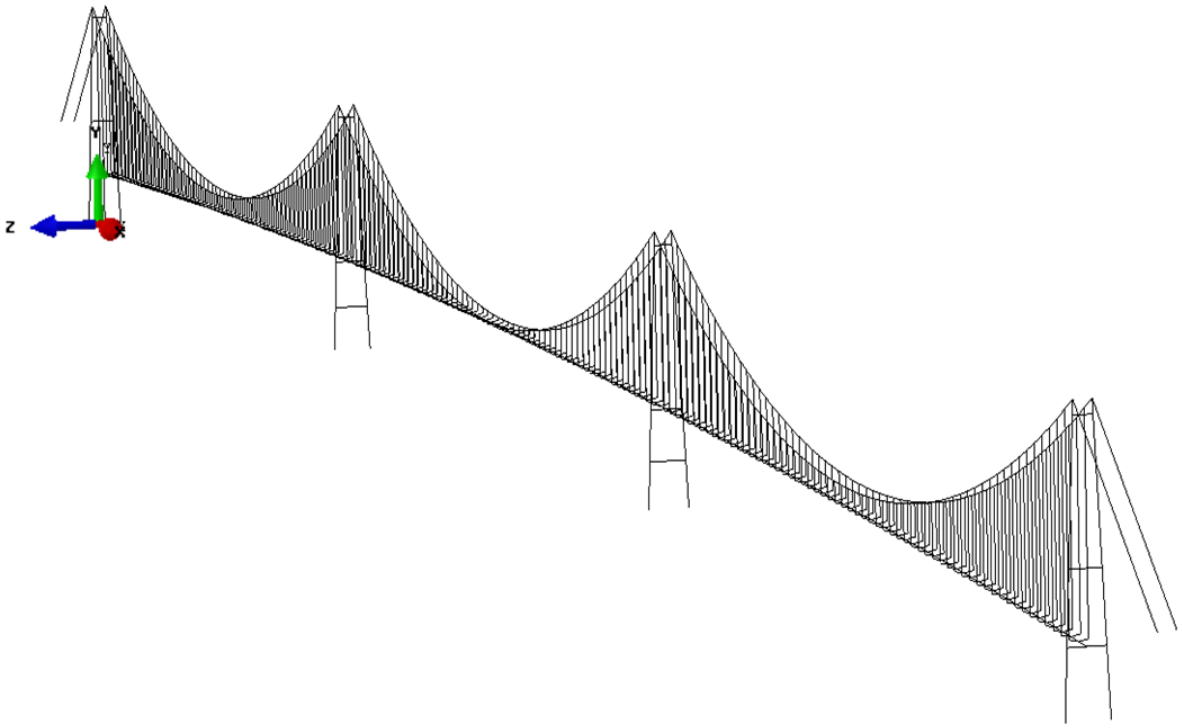

Figure 13: Bridge Geometry

4.1.2 Structural Properties

4.1.2.1 Stiffening Girder

The stiffening girder is modeled with using *Profile: generalized beam* and cross-sectional properties given from Table 2.The material properties of the stiffening girder given in Table 1 are added in the *Beam Section*. No density is because its more comprehensive to add all mass lumped to point masses, both structural and non structural

4.1.2.2 Cable

The main cable and back stay cable is modeled using *Profile: Circular*. The radius of the profile is chosen as $r = 0.26542m$ because it gives the same total cross section area $A = 0.22132m^2$ as for the 19 cable strands. This circular solid steel profile will have a much higher bending stiffness than the parallel wire strands. But since geometrical stiffness is included the initial stiffness becomes small in comparison to the geometrical stiffness. Therefore the chosen profile is assumed to give valid results. To incorporate the additional masses and weight of the cable the density of the material is higher than steel density. The total dead load per meter is used calculate modified density. This gives the following density $\rho = m / A = 1851 / 0.22132 = 8363.45kg / m^3$. It is assumed this gives satisfying results for centre of gravity and moment of inertia. The Young's modulus and Poisson's ratio is given in Table 1.

4.1.2.3 Hanger

The hangers are also given a circular profile and a radius $r = 0.03192m$ giving a cross section area $A = 0.0032m^2$ equal to the total area of the hanger wires. The density used for the hanger is set equal to steel density 7850 kg/m^3 and the weight of clamps and sockets are added as point masses in *Engineering Features*. The material properties of the hangers are given in Table 1.

4.1.2.4 Fictive beam

The fictive beams are modeled with high stiffness and low mass to avoid inertia forces and flexible behavior, but if the difference is to large *matrix singularity* may occur. The following material properties have proved to give satisfying results without *matrix singularity error*. The profile is a simple *box profile* with *b=3m, w=*3m, t*=0.5m* and the material properties give in Table 24

Table 24: Fictive beam material properties

Property	Magnitude	Unit
Young's Modulus	2e15	Pa (N/m^2)
Poisson's Ratio	0.3	-
Density	10	kg/m^3

4.1.2.5 Pylon

pylon columns and cross beams are modeled as *Box Profile* with dimensions *a, b, t_1, t_2, t_3, t_4* with explanation given in Figure 14.

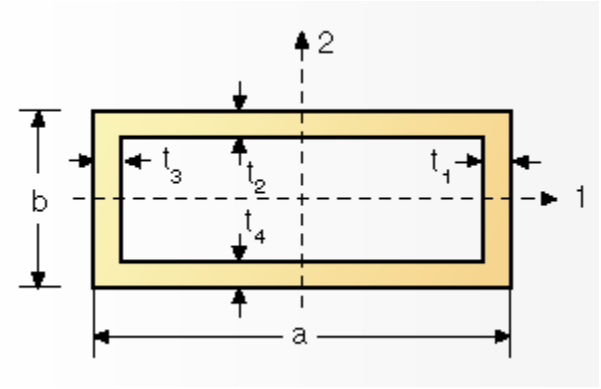

Figure 14: Dimensions for box profile

The dimensions are taken from Table 3 and Table 4 and is repeated in Table 25.

Table 25. Dimensions for pylon box profiles

Name	Position	a	b	t_1	t_2	t_3	t_4
Column 1	0-65 *m*	6.182	6.989	0.6	0.85	0.6	0.85
Cross Beam 1	35 *m* / 45.54 *m*	6.250	7.500	0.6	0.6	0.6	0.6
Column 2	65-142.5 *m*	5.199	5.252	0.6	0.85	0.6	0.85
Cross Beam 2	95 *m* / 72.32 *m*	4.789	8.000	0.6	0.6	0.6	0.6
Column 3	142.5-200	4.504	4.500	0.6	0.85	0.6	0.85
Cross Beam 3	190*m*	4.000	6.000	0.6	0.6	0.6	0.6

The pylon columns and cross beams are given material properties from Table 1. Figure 15 shows the pylon with the implemented cross sectional dimensions

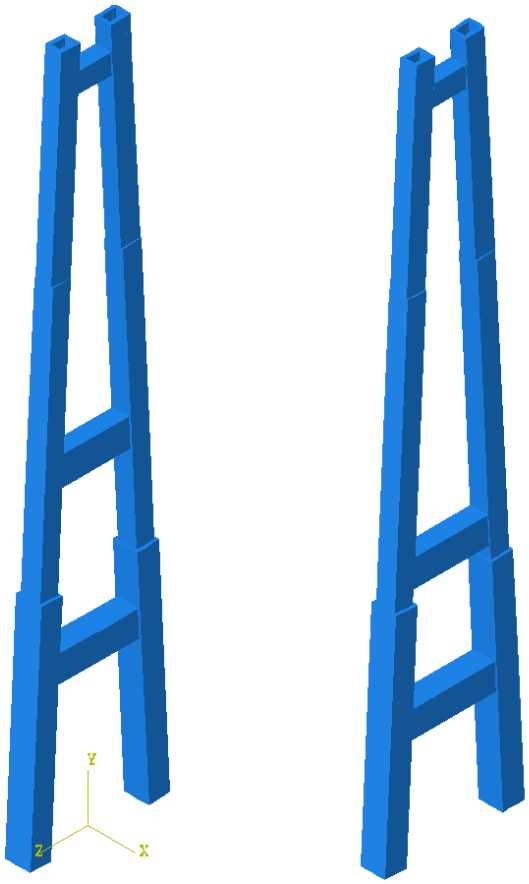

Figure 15: Mid- and side-pylon

4.1.3 Element type and meshing

All the parts in the model have been assigned 2-node cubic beam element called B33. This element is an Euler-Bernoulli element which means it does not allow transverse shear deformation; plane sections initially normal to the beam's axis remain plane and normal to the beam axis. These elements are effective for frame structures.

The chosen element sizes are given in Table 26.

Table 26: Element type and size for bridge parts

Section	Element type	Element size
Stiffening Girder	B33	20 *m*
Fictive beam	B33	One element each
Cable	B33	20 *m*
Hanger	B33	One element each
Pylon Column	B33	10 *m*
Pylon Cross Brace	B33	10 *m*

Figure below show a cut of the element mesh around one of the mid pylons.

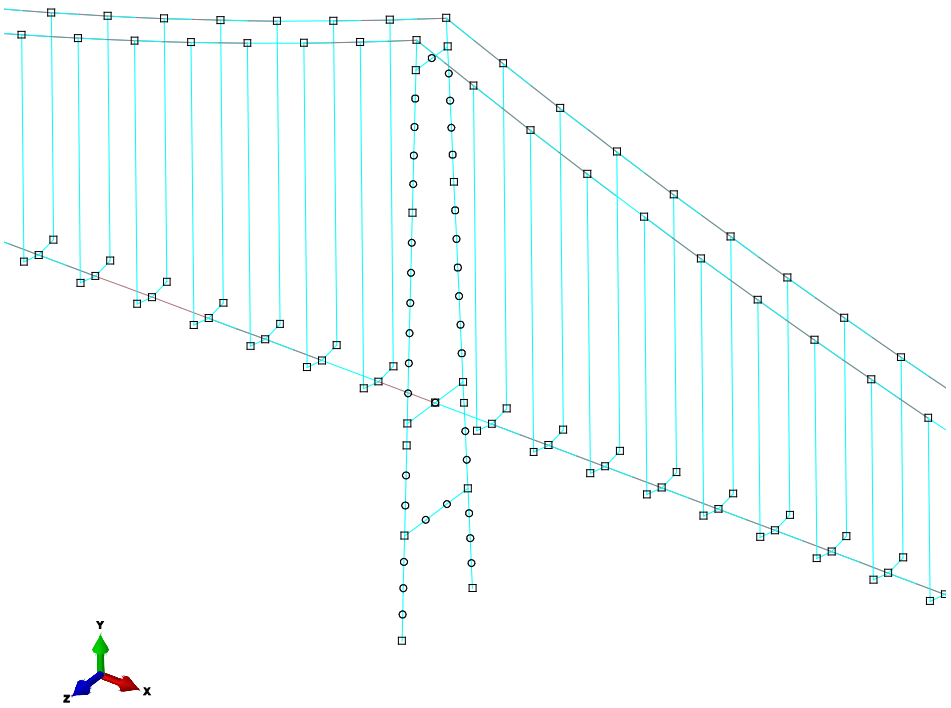

Figure 16: Element mesh

4.1.4 Engineering Features

4.1.4.1 Point Masses

Pylons and main cables are modeled with correct material density and assumed to have no additional masses. For the stiffening girder no mass is modeled, and for the hangers only the mass of the wires are modeled and not the clamps and sockets.

For the stiffening girder the mass properties are modeled as lumped masses (point masses) and moment of inertia (MOI) to the model. From Table 5 and Table 8 the distributed mass, m_x and the distributed MOI about the longitudinal axis are given. The point masses are added with distance equal to the hanger spacing in the shear centre of the stiffening girder. The point mass, *M*, is given by the distributed weight, m_x multiplied by the longitudinal spacing l_x. The total MOI about the longitudinal axis is given by distributed MOI multiplied by the longitudinal spacing. The MOI about the horizontal lateral axis and vertical axis is given by the MOI to a homogenous slender beam [20]

$$I_y = I_x = \frac{1}{12} M \cdot l_x^{\,2} = \frac{1}{12} m_x \cdot l_x^{\,3} \tag{4.1}$$

The inertia properties added to point masses are summarized in Table 27.

Table 27: Inertia properties of point masses representing stiffening girder

Property	Magnitude	Unit
M	177 946	kg
I_{11} (I_x)	4 493 727	kg m^2
I_{22} (I_y)	6 029 163	kg m^2
I_{33} (I_z)	6 029 163	kg m^2

The mass of the hanger clamps and hanger sockets are modeled as point masses in the ends of each hanger. The average mass of the clamps and sockets are 1845 *kg/hanger* resulting in 922.5*kg* added mass in all hanger ends points. The MOI for the clamps and sockets are unknown. By assuming steel density and sphere shape a rough estimate of the MOI is carried out and assumed to be valid due to the small amount of MOI. The radius is described by

$$r = \sqrt[3]{\frac{3M}{4\pi\rho}} = 0.30386m \tag{4.2}$$

and then the MOI for a sphere is given by [20]

$$I = \frac{2}{5} \cdot M \cdot r^2 = 34.07kg \cdot m^2 \tag{4.3}$$

The inertia properties for the hangers added to the each hanger end are summarized in Table 28.

Table 28: Inertia properties of point masses representing hanger clamps and sockets

Property	Magnitude	Unit
M	922.5	kg
I_{11} (I_x)	34.07	kg m^2
I_{22} (I_y)	34.07	kg m^2
I_{33} (I_z)	34.07	kg m^2

4.1.4.2 Damping Properties

Classical Rayleigh Damping is assumed and is given by the following formula

$$\mathbf{c} = a_0\mathbf{m} + a_1\mathbf{k} \tag{4.4}$$

Where,

$$a_0 = \zeta \frac{2\omega_1\omega_2}{\omega_1 + \omega_2} \qquad a_1 = \zeta \frac{2}{\omega_1 + \omega_2} \tag{4.5}$$

Here two eigen-frequencies are taken in with a give damping ratio, and then the Rayleigh-damping curve dependent of the natural frequency is obtained. It is suggest choosing the lowest eigen frequency and one of the highest frequencies within the frequency range of interest and for both frequencies use a damping ratio according to the structural behavior [21]. For welded steel and well-reinforced concrete with stress level well below yield point damping ratio $\zeta = 0.03$ can be assumed [21].

A eigen frequency analysis (performed with no damping) have shown that one of the lowest eigen frequency is 0.045 *rad/sec* and that the eigen frequencies above 2 *rad/sec* are outside the frequency range of interest. These frequencies $\omega_1 = 0.045\ rad/\sec$, $\omega_2 = 2\ rad/\sec$ and damping ratio $\zeta = 0.03$ are therefore used to calculate the coefficients for Rayleigh Damping. These coefficients are given in Table 29.

Table 29: Rayleigh coefficients implemented to all bridge materials

Rayleigh - Coefficient	Magnitude
a_0	0.00176
a_1	0.01956

The damping ratio for the *n*-th mode is then given by the Rayleigh function

$$\zeta_n(\omega_n) = \underbrace{\frac{a_0}{2}\frac{1}{\omega_n}}_{\text{mass proportional}} + \underbrace{\frac{a_1}{2}\omega_n}_{\text{stiffness proportional}} \tag{4.6}$$

4.1.5 Interaction

Since the different structural elements are made as separated parts there is initially no interaction between the different parts. The interaction tool called *tie* is simple yet effective interaction tool to tie two separate surfaces/node regions together such that there is no relative motion between them. Since the parts consists of wires it is of interest to define *node-to-node tie constraint*. A *tie constraint* constrains all translational motions, but can also be specified to constrain rotational motions.

Fictive beam - Stiffening girder interaction: As explained earlier fictive beams are used to model interaction between the outer edges of stiffening girder where the hangers are attached and the shear centre of the stiffening girder. This interaction is obviously rigid, hence all translational and rotational motion is tied.

Fictive beam - Hanger interaction: This connection consists in reality of a hanger clamp and socket connected with a steel bolt. This allows it to freely rotate around z-axis while rotation about x- and y-axis is prevented. Due to the high geometric stiffness and length of the hangers the x- rotation is assumed to have small influence on the global behavior and therefore all translational and rotational motion is tied.

Hanger - Cable interaction*:* consist of the same clamp-socket connection as for the fictive beam-hanger connection. The same argument can be used, hence all translational and rotational motion is tied

Cable - Pylon interaction*:* the pylon in constructed such that the cable is constrained in only lateral and vertical horizontal direction. In longitudinal direction the cable is not restrained but the high cable forces will result in large friction forces and in practice insignificant motion will occur in longitudinal direction. Hence all translational motion is tied.

Stiffening Girder - Pylon interaction: It is assumed that the bridge girder is rigidly connected to the cross beam and hence all translational and rotational motion is tied.

4.1.6 Boundary Condition

The boundary conditions of the FFB-model are given by:

Cable anchorage*:* The back stay anchorage consist of a splay saddle, splay chamber, anchorage block and a final anchorage plate. Such a anchorage will prevent all translational motion but allows the back stay cable to rotate. Hence all translational motion is prevented.

Side-pylon foundation*:* The pylon columns placed on the shore of the fjord is assumed to have a foundation constraining both translation and rotation to the ground, hence all translational and rotational motion is prevented.

Mid-pylon foundation: For the FFB-model the mid-pylon is assumed to have the same boundary conditions as the side-pylons. This is to later see the effect of applying a floating foundation system. Hence all translational and rotational motion is prevented.

4.1.7 Loads

4.1.7.1 Gravity Load

The only load applied to the model is dead load. This is given in as *gravity load* with $Y-component = 9.81\ m/s^2$. When applying this dead load the initial geometry will deform due to tension and strain in the cable and hangers. The deflection of the cable at midpoint is $-6.49m$. To accommodate for this deflection a fictive contraction is applied. Tthis done by applying a change in temperature, which will cause temperature strain. The cable is initially given temperature 0 *K* and as described earlier a fictive thermal expansion coefficient, $\alpha_T = 1$, is added to the cable. Several attempts have been carried out and when applying -0.00252 *K*, equal to 0.252 % strain, the deflection of the mid-point is less than 0.1m. The cable curve deviates slightly from the initial geometry but is assumed to have negligible effect.

4.1.7.2 Static Wind Load

The static wind loads acting on the bridge are modeled as line loads and concentrated moments. Assuming wind flow in negative z-direction. The horizontal load for the stiffening girder and cables are modeled as line loads and applied to the shear center of the corresponding elements. The values of these line loads are taken directly from the in *Appendix: Wind Calculations* and are given in table below.

Table 30: Static wind forces on stiffening girder and cable

	Line Load Component: 2 [N/m]	**Line Load Component: 3 [N/m]**
Stiffening girder	- 5240	- 3206
Cables	-	- 719

The static wind moment on the stiffening girder act in the shear center, but the moments have to be modeled as point moments. These moment is added to stiffening girder nodes, which have longitudinal spacing $20.1630m$, and the following point moments in the stiffening girder then becomes

$$M_1 = -1510Nm/m \cdot 20.1639m = -30447Nm \tag{4.7}$$

Static wind load on pylon legs are modeled as *line loads* but the variation in y-direction is corporate using *analytical fields*. Three analytical fields are given in describing the drag force function on the pylon as function of y-position. These functions are calculated in *Appendix: Wind Calculations* and are given table below

Table 31: Analytical functions describing the wind loads on the pylon legs

Cross Section	Analytical Field Name	Function
D_1 *(0 – 65 m*)	*Analtyical-field-1*	105.8992*log((0.1+ Y)/0.01)*log((0.1+ Y)/0.01)
D_2 (65 – 142.5 m *)*	*Analtyical-field-2*	79.5797*log((Y)/0.01)*log((Y)/0.01)
D_3 (*142.5 – 200 m*)	*Analtyical-field-3*	68.2458*log((Y)/0.01)*log((Y)/0.01)

For *analytical-field-1* as adjustment has been made to avoid numerical error.

4.1.8 Traffic Load

Traffic load in two lanes and sidewalk load is assumed to be the critical traffic load combination. Two notional lane distributed loads of 9 *kN/m* each and a distributed load on the sidewalk of 2 *kN/m* according to [22] gives the following total traffic load on the stiffening girder in the vertical direction

$$p = 9 + 9 + 2 = 20kN / m \tag{4.8}$$

The traffic load is modeled as a centric line load to the stiffening girder. A full traffic load response analysis is outside the scope of this thesis and is left for further investigation.

4.2 Floating Foundation Modeling

The design of the floating pylon foundation is given in chapter 3.2. The pontoon consists of one inner vertical cylinder and 8 outer cylinders. The thickness of the cylinders $t = 0.5m$ and the rigid connection between the inner and outer cylinders makes the pontoon extremely stiff compared to the flexural suspension bridge. Therefore the pontoon is assumed to behave as a rigid body when floating. The modeling of the pontoon in Abaqus/CAE can then be simplified and the pontoon can be modeled as a rigid beam constrained to the pylon ends. The structural properties of the pontoon can therefore be lumped and added to specific. The lumped properties which needs to be added in the pontoon are

- Buoyancy force and buoyancy stiffness
- Horizontal mooring stiffness
- Mass and inertia of the pontoon
- hydrodynamic added mass and added damping

The concept of the modeling technique is presented in Figure 17.

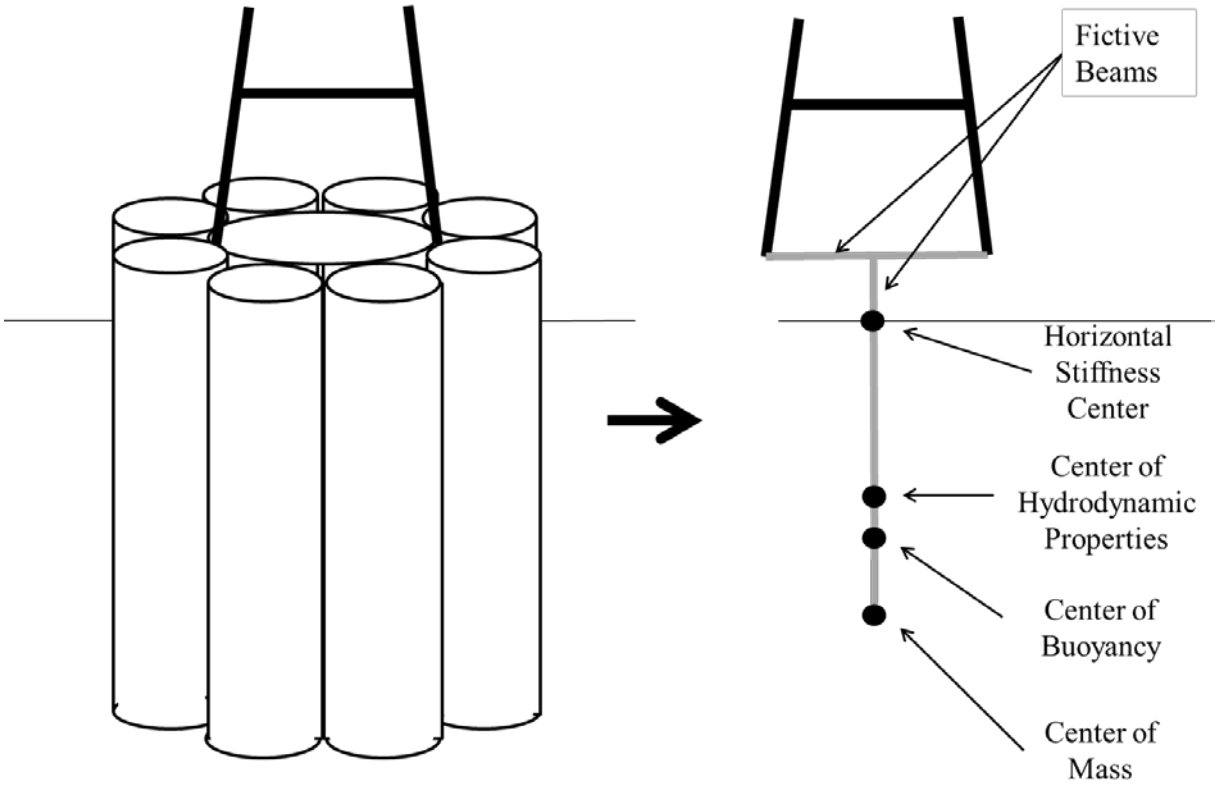

Figure 17. Pontoon modeling technique

4.2.1 Part and Geometry

The structural property points which will be modeled as nodes is given from chapter 3.2 and summarized in Table 32.

Table 32: Structural property points

Property	Y-Position [m]
Center of Horizontal Mooring Stiffness	-10 *m*
Meta Center	-50.8 *m*
Center of Buoyancy	-55 *m*
Center of Mass	-75.04*m*

The pontoons are sketched in the existing datum planes, *pylon-datum-plane-2* and *pylon-datum-plane-3*. The rigid beams are sketched using *straight wire* tool using the points in Table 33

Table 33: Wire points for rigid beam representing the pontoon

	First point	Second point
Horizontal Wire	(-17.25,0)	(17.25,0)
Vertical Wire 1	(0,0)	(0,-10)
Vertical Wire 2	(0,-10)	(-10,50.8)
Vertical Wire 3	(0,-50.8)	(0,-55)
Vertical Wire 4	(0,-55)	(0,-75.04)

The geometry of the FFB-model is shown in Figure 18

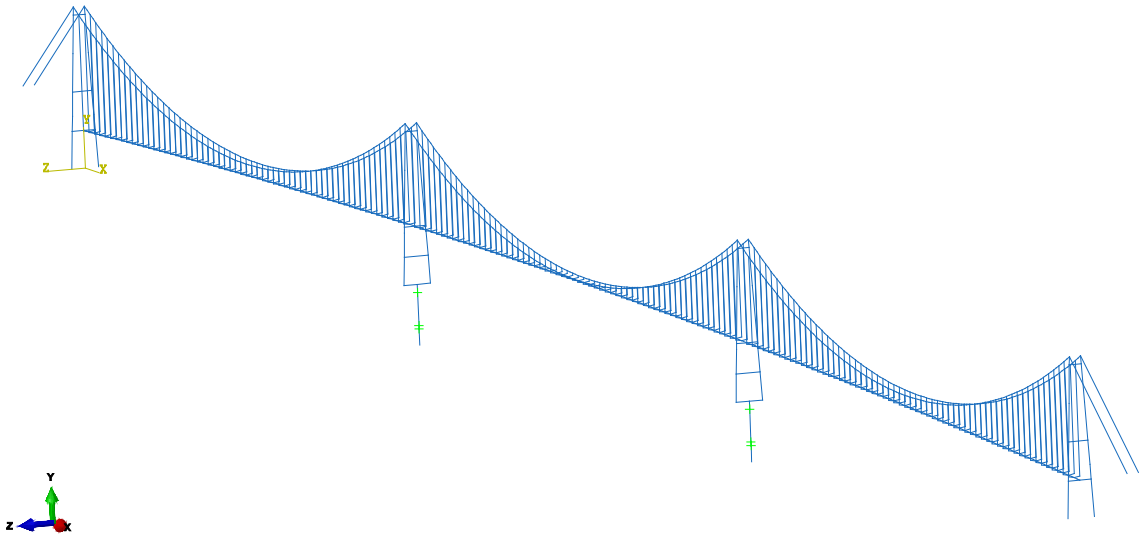

Figure 18: Floating foundation bridge model

4.2.2 Structural properties and element mesh for the rigid beam

The rigid beam part representing the pontoon is given the same dimensions and material properties as for the fictive beams used for stiffening girder, hence *b=3m* , *w*=3m, t=*0.5m* and material property as given in Table 34

Table 34: Material properties for rigid floating foundation

Property	Magnitude	Unit
Young's Modulus	2e15	Pa (N/m^2)
Poisson's Ratio	0.3	-
Density	10	kg/m^3

As for the RFB-model the rigid pontoon is assigned the 2-node cubic beam element B33. The element mesh is given by one element between the structural property points. point of interest. The element mesh for one of the pontoons are given in Figure 19.

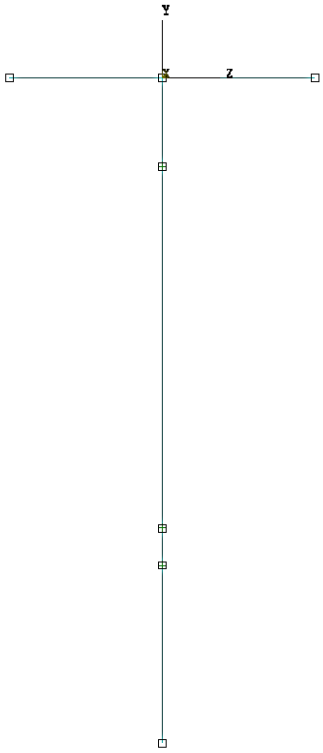

Figure 19. Element mesh of one of the pontoons

4.2.3 Mass properties

The mass and inertia properties of the pontoon are calculated in chapter 3.2 and repeated in Table 35. The inertia properties are added as a point masses in the *Center of Mass* -node in each pontoon having. These nodes have y-coordinate -75.04 *m*.

Table 35: Mass and inertia properties for each pontoon

Property	Quantity	Unit
M	4.166 e+8	kg
I_{11} (I_x)	3.617 e+11	kg m^2
I_{22} (I_y)	3.351 e+11	kg m^2
I_{33} (I_z)	3.617 e+11	kg m^2

4.2.4 Damping Properties

Same Rayleigh damping coefficients used for structural damping in RFB-model will be used for FFB-model, the values are give in Table 29 and are added to material and point masses of the pontoon.

4.2.5 Stiffness Properties

The horizontal hydrostatic stiffness given in Table 15 are modeled as *linear springs* between the *Center of Horizontal Mooring Stiffness*-nodes and fixed *attachment points* in same coordinates as the *Center of Horizontal Mooring Stiffness* -nodes. These nodes and attachment points have y-coordinate -10 *m.*

The vertical hydrostatic stiffness is given in Table 14. Same *linear spring* is used to model the stiffness. The spring is attaching the *Meta Center*–node to fixed *attachment points* in same coordinates as the *Center of Buoyancy* –node. The *Meta Center* –node and not the *Center of Buoyancy*-node is used to consider the change of buoyancy center when the pontoon rotates and the centroid of submerged volume moves. This is further explained in chapter 2.1.

The hydrostatic rotary stiffness of the pontoon is accounted for by Gravity force and Buoyancy force and the lever arm between the Center of Gravity and Meta Center, and linear rotary springs hence not needed.

4.2.6 Buoyancy Force

The initial buoyancy force in the pontoon is given by the preliminary pontoon design calculations and is given in Table 14. This buoyancy force is modeled as a *concentrated vertical forces* in both the *Meta Center* –nodes. The forces are added simultaneously as the gravity to avoid large displacements.

In the preliminary design the buoyancy force was based on simple force contributions from bridge to pontoon, and it is not assumed this force to be completely correct. Hence, in the analysis this buoyancy force was adjusted several times until the pontoon had insignificant vertical displacement . The initial and adjusted force, and corresponding vertical displacements are shown in Table 36

Table 36: Intial and adjusted buoyancy force

	Buoyancy Force	**Vertical displacement of pontoon**
Initial Buoyancy Force	4.45014 e+9 *N*	1.673 *m*
Adjusted Buoyancy Force	4.4045 e+9 *N*	0.006 *m*

4.2.7 Hydrodynamic properties

4.2.7.1 Hydrodynamic added damping

The hydrodynamic added damping is non-linear and the *linear dashpots* in Abaqus/CAE are assumed not to represent the hydrodynamic damping sufficiently. Hence, the *connector* in the interaction module can be used with the *non-linear uncoupled damping* behavior. The damping behavior must be given in as vector with damping force and corresponding velocity. The general damping force - velocity relationship is given by Eq. (2.25) and the hydrodynamic damping coefficients for all directions are given in Table 18. For the three translational directions the damping -velocity vectors are given in the interval [-5 , 5] *m/s* and $\Delta v_i = 0.01 m/s$ .For the two rotational directions the damping-velocity vectors are given in the interval [-0.1, 0.1] *rad/s* and $\Delta v_i = 0.0001 m/s$.

The *added damping connectors* are attaching the *Center of Buoyancy*-node to fixed attachment points in same coordinates as the *Center of Buoyancy*-nodes. These nodes and attachment points have y-coordinate -55 *m.*

4.2.7.2 Hydrodynamic added mass

The added hydrodynamic added mass is given in as point masses in the *Center of Buoyancy* - nodes. These nodes have y-coordinate -55 *m.* The hydrodynamic added mass and inertia properties for the pontoon are given in Table 17.

Added hydrodynamic mass is only associated with acceleration of the floating pontoon. Since Abaqus/CAE have problems excluding point mass from gravity loading, a concentrated force equalizing the mass in vertical direction is added to the model in the *Center of Buoyancy* – nodes. These two forces are given by

$$F_G = -g \cdot M_{22} = -(-9.81) \cdot 8.533e+7 = 8.371e+8N \tag{4.9}$$

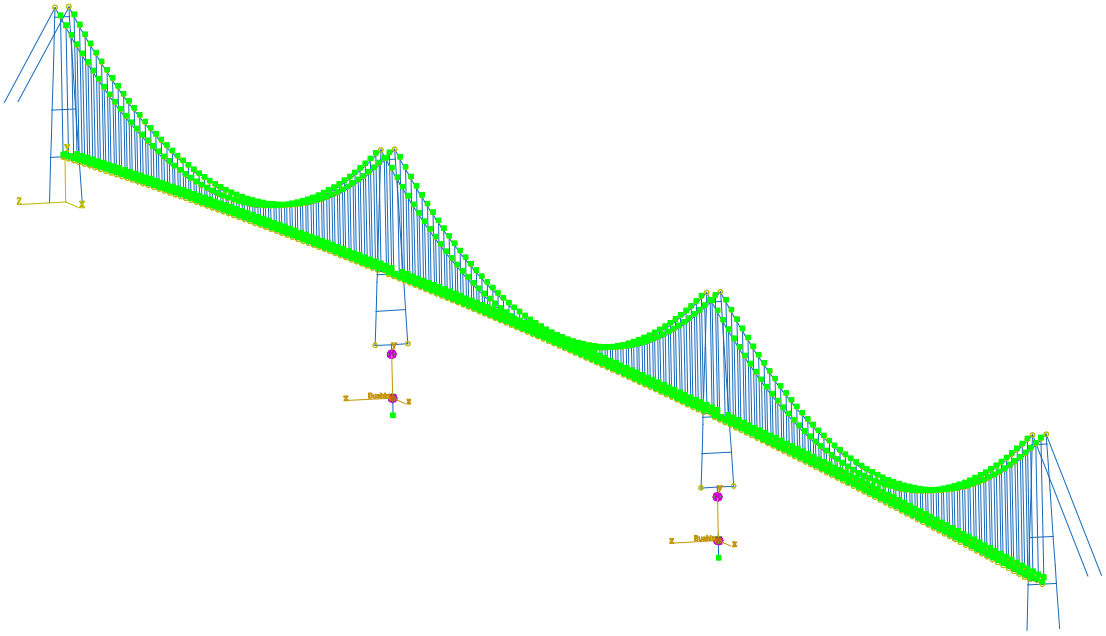

Figure 20: Final Bridge model.
Blue lines: elements, Green dots: Point masses, Purple dots: springs, Orange Arrows: Damping Connectors

5 Results and Discussion

In this chapter all results of the numerical analysis will be presented. The static mean wind and traffic analysis will be presented in the first chapters. The dynamic properties from the eigen-value analysis in terms of natural frequencies and the corresponding mode shapes will be presented in section 3. The effective modal mass for the floating foundation bridge model will be given in section 4. The effective damping ratios from the complex eigen-value analysis will be compared to the Rayleigh damping and the hydrodynamic damping effect on the damping ratios will be presented. I the final section the results from non-linear dynamic time-domain response simulations will be presented and compared to the linear interpreted effective damping ratios in section 4.

5.1 Static mean wind load

The static mean wind analysis are applied to stiffening girder, pylon and cables according to Table 30, Table 31 and Eq. (4.7). The displacement of the bridge is shown in Figure 21. Scale factor 1:10 is used to illustrate the deflections better. The pontoons have vertical displacement -0.13 *m*, horizontal lateral displacement - 1.99 *m* and rotation 1.3 ° about the longitudinal axis (x-axis). The pylon-top displaces - 6.98 *m* in later horizontal direction. The mid-point of the stiffening girder at mid-span displaces - 8.81 *m* in lateral horizontal direction.

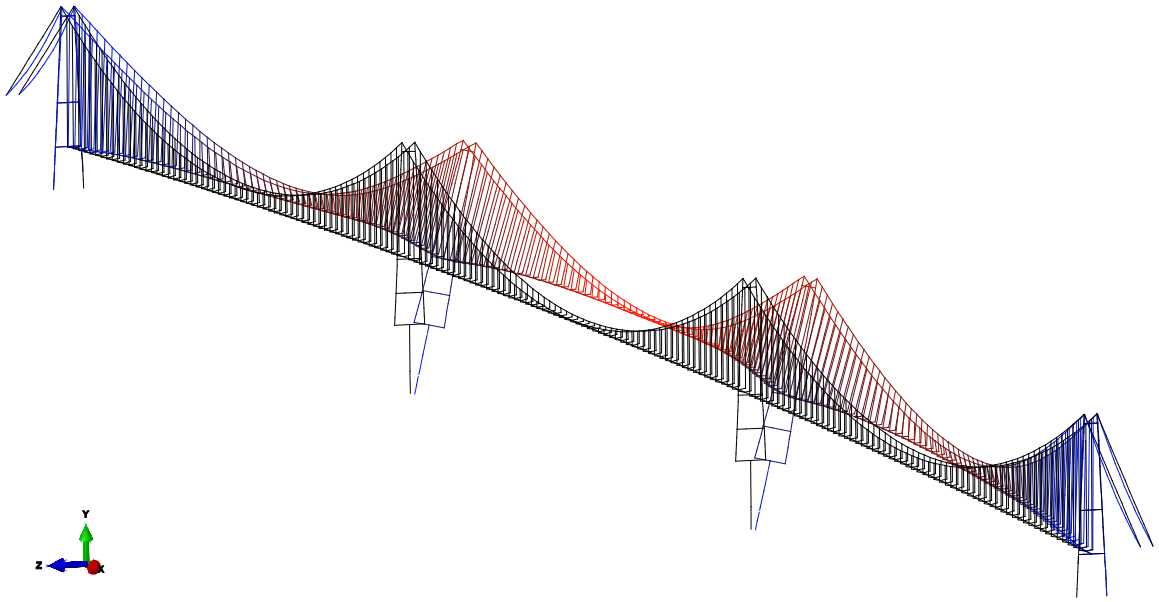

Figure 21: Static mean wind displacements

The lateral displacement and rotation of the pontoon results in a rigid body lateral displacement of - 6.52 *m* at pylon top. Hence the bending in the pylons only gives a lateral displacement of - 0.46 *m*. A bending deflection less than 0.5 *m* in lateral direction is assumed acceptable for the pylon.

For the stiffening girder the pontoon movement results in a rigid body lateral displacement at the cross beam -3.63 *m*, hence the deflection in the stiffening girder due to bending is - 5.18 *m*. Compared to the L/200 requirement giving 6.6 *m*, the deflection of the stiffening girder is not acceptable if displacement of the pylon and pontoon is included. Validity cannot be given without further investigation of regulations and general serviceability criterion.

5.2 Traffic load

For the traffic load three combinations are carried checked:

- Traffic load in all spans
- Traffic load in one side-span
- Traffic load in mid-span

The three cases with corresponding maximum vertical deflection of stiffening girder, bending of pylon and pontoon displacement are given in the three next sections.

5.2.1 Traffic Load, All Spans

The deflection of the bridge due to traffic load in all spans is shown in Figure 22. The vertical displacement of the stiffening girder in mid-span at mid-point is - 1.42 *m.* the vertical displacement of the pontoon is - 0.46 *m*. Due to symmetry in loading the rotation of the pontoon and pylon is insignificant.

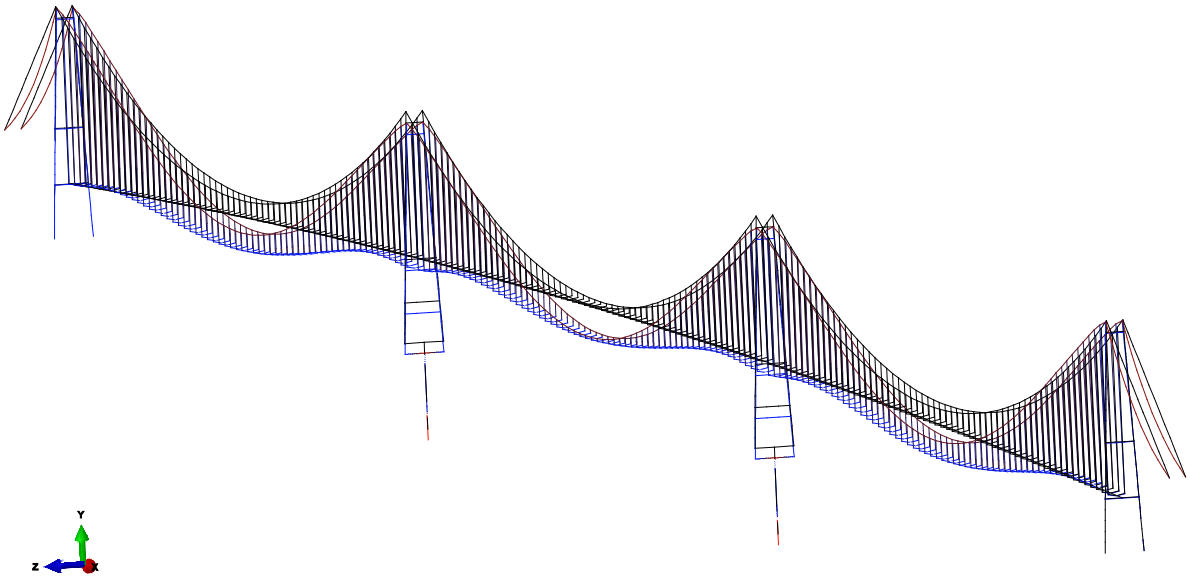

Figure 22: Traffic load deflection, all spans

This load case is the load resulting in largest vertical displacement in the pontoons. A displacement of - 0.46 *m* is regarded well within the acceptable limit, and hence the vertical hydrostatic stiffness is assumed satisfactory for the static traffic load.

The relatively small deflection of the bending girder is due to symmetric loading and the most of the load is taken as tension forces in the cables.

5.2.2 Traffic Load, Side-span

The deflection of the bridge due to traffic load in one side-span is shown in Figure 23. The maximum vertical displacement of the stiffening girder in the side span is - 5.04 *m*. The adjacent pontoon rotates 0.39° about the lateral axis (z-axis) and the vertical movement is - 0.25 *m*. The pylon deflects - 2.61 *m* in longitudinal direction and has a rotation at top equal to 1.3°.

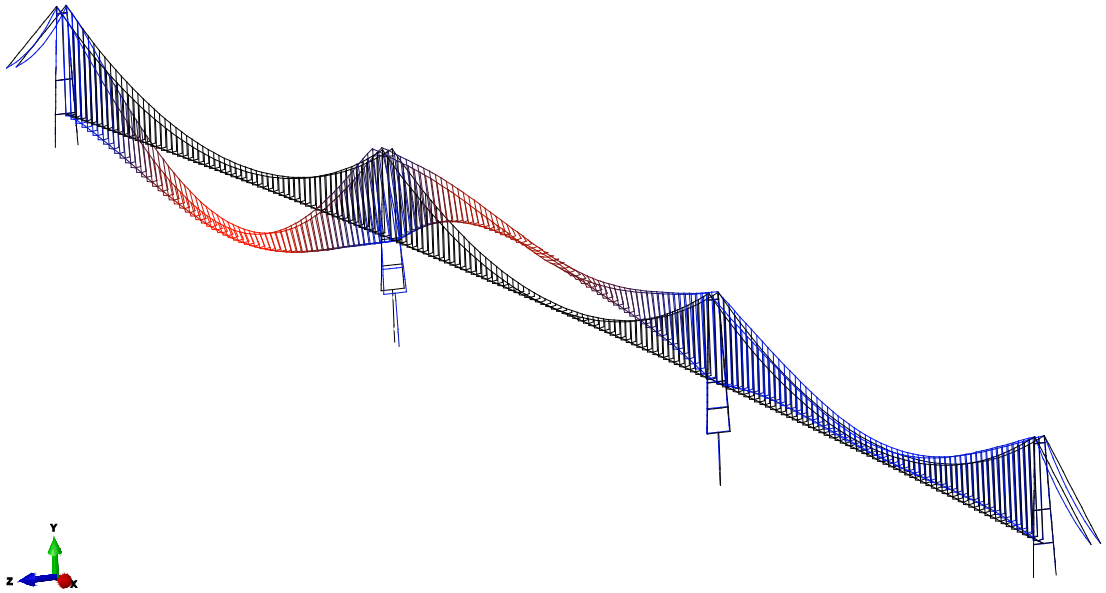

Figure 23: Traffic load deflection, side-span

The large difference in vertical deflection compared to the first load case is caused by the asymmetric loading about the pylon. This results in deviation in cables forces and rotation of the pontoon and bending of the pylon occurs. This longitudinal displacement at pylon top increases the sag of the cables and hence more vertical load have to be carried by the stiffening girder and results in large vertical deflections in the stiffening girder.

5.2.3 Traffic Load, Mid-span

The deflection of the bridge due to traffic load in mid-spans is shown in Figure 24. The maximum deflection in the stiffening girder in midspan is -9.75 *m*. The pontoons rotate 0.36° about the lateral axis (z-axis) and moves -0.25 *m* vertically. The pylon top displaces -2.4 *m*.

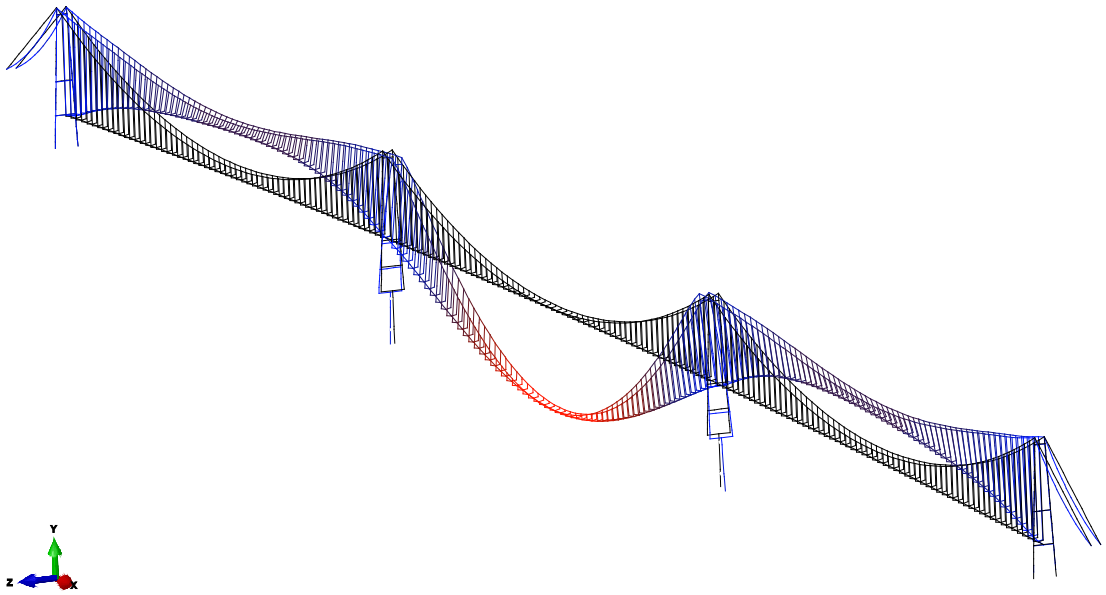

Figure 24: Traffic laod deflection, mid-span

The same force distribution as explained for the side-span load case is seen here. Now both pylons are subjected to asymmetric loading and both pylons tilt towards the mid-span. The sag is increased even more and large deflections occurs in the mid-span. It is also seen that the tilt of the pylon decrease the sat at the side-spans and vertical positive defelctions occur in these-side spans.

The bending of the pylons is larger in this load case compared to previous load case. The pontoon rotation results in 1.24 *m* longitudinal displacement, and hence the longitudinal displacement due to bending of the pylon is 1.16*m*. This is more than twice the displacement in lateral direction compared to wind load.

The large deflection at mid-span is close to 10 *m*, and is larger than normal deflection requirements, and validity cannot be given without further investigation of regulations and general serviceability criterion.

5.3 Natural Frequencies and Mode Shapes

The natural frequencies and corresponding mode shapes were extracted from Abaqus/CAE for both the *Rigid Foundation Bridge Model* (RFB-model) and the *Floating Foundation Bridge Model* (FFB-model). The modes, referring to both the frequency and corresponding mode shape, are named after ascending order of the natural frequency. Initially the first 50 modes for the *Rigid Foundation Bridge* Model were extracted, and are referred to as f*ixed* b*ridge mode shapes*. All these 50 mode shapes where found among the 62 first eigen values of the FFB-model. The 12 unique mode shapes of the FFB are referred to as *pontoon mode shapes*.

For the fixed bridge modes it is comprehensive to describe the mode shape in terms of the components in motion, the shape itself and the symmetrical behavior. The modes are given capital letters describing the element and component in motion. The following categories have been used

- H: Stiffening girder in horizontal (lateral) motion
- V: Stiffening girder in vertical motion
- C: Cable planes in horizontal (lateral) motion
- T: Stiffening girder in torsional (rotation about longitudinal axis) motion

The components are given a number describing the number of waves in each span or number of peak amplitudes. Since the bridge consists of three spans and the different modes having different motion in different spans the mode description also includes which of the spans who are in motion. The following classes are used

- All: All three spans are in motion
- Side: Side-span motions are relatively large compared to mid-span
- Mid: Mid-span motion is relatively large compared to side-span

For the pontoon mode shapes the translational and rotational components of the pontoon sufficiently describes the mode shapes since the pontoons moves as rigid bodies.

Both for the fixed bridge modes shapes and the pontoon mode shapes the description includes if the mode is either symmetric or asymmetric, which tells how the bridge spans and pontoons moves relatively to each other about the midpoint.

pontoon mode shapes and fixed bridge mode shapes and the with its corresponding natural frequencies are presented in the two following sections.

5.3.1 Pontoon Mode Shapes

Mode 1-10, 23 and 28 have considerable motion in the pontoons. They are considered the most interesting and therefore all 12 mode shapes with corresponding natural frequencies are shown in Figure 25 and Figure 26. The mode shape descriptions and natural frequencies of these modes are given in Table 37.

Table 37: Natural frequencies and mode shape description of the hydrodynamic modes.

Mode nr.	**Natural Frequency [rad/s]**	**Mode Shape Description**		
		Translational Motion	Rotational Motion	Symmetry
1	0.0454	Z	Θ_X	S
2	0.0461	Z	Θ_X	A
3	0.0792	X	Θ_Z	S
4	0.0802	X and Y	Θ_Z	A
5	0.1828		Θ_X	S
6	0.2229		Θ_X	A
7	0.2621		Θ_Y	S
8	0.2860	Z	Θ_X and Θ_Y	A
9	0.3064	Y		S
10	0.3090	Y		A
23	0.9821		Θ_Z	A
28	1.2555		Θ_Z	S

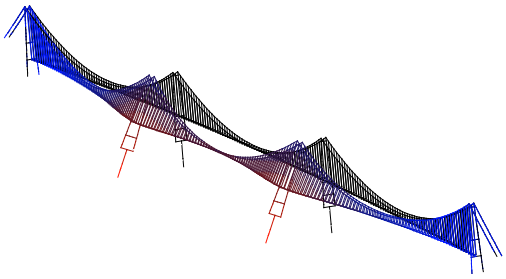

Mode Shape 1 ($\omega = 0.0454 rad/s$)

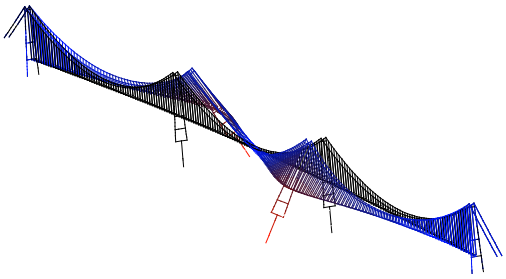

Mode Shape 2 ($\omega = 0.0461 rad/s$)

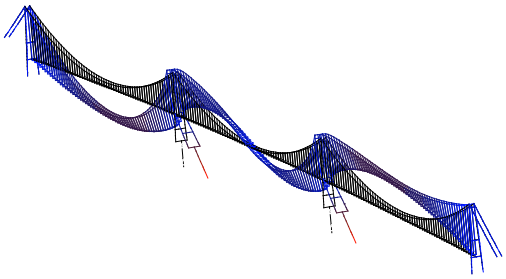

Mode Shape 3 ($\omega = 0.0787 rad/s$)

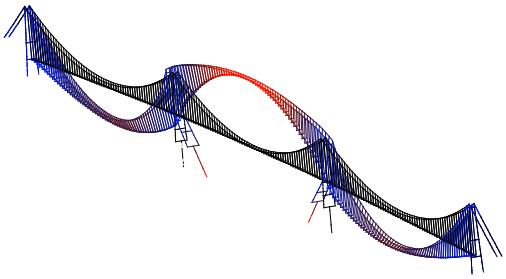

Mode Shape 4 ($\omega = 0.0802 rad/s$)

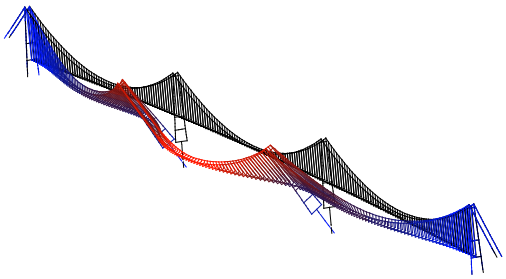

Mode Shape 5 ($\omega = 0.1828 rad/s$)

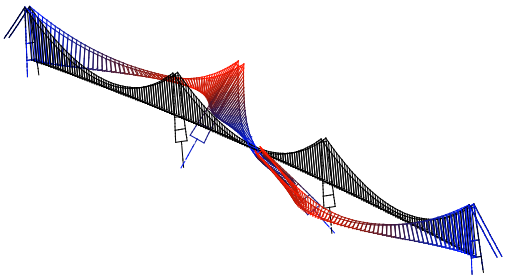

Mode Shape 6 ($\omega = 0.2228 rad/s$)

Figure 25. Mode Shape 1-6 for Floating Foundation Bridge Model

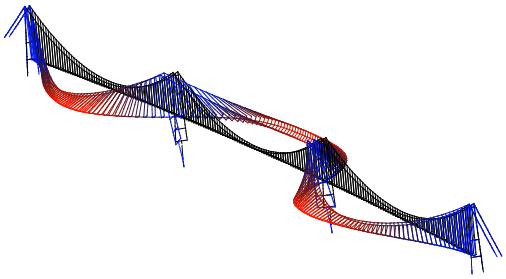

Mode Shape 7 ($\omega = 0.2620 rad/s$)

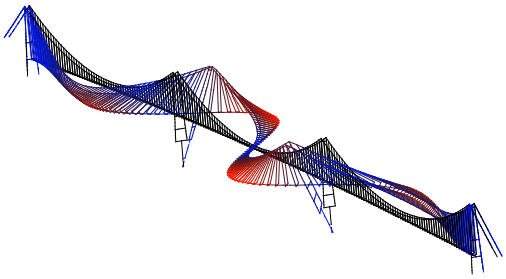

Mode Shape 8 ($\omega = 0.2859 rad/s$)

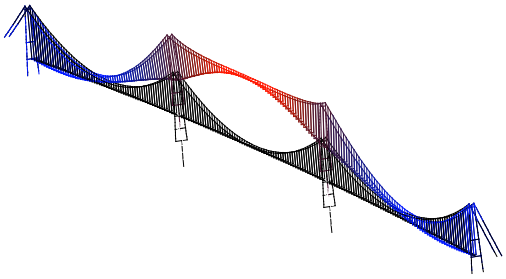

Mode Shape 9 ($\omega = 0.3064 rad/s$)

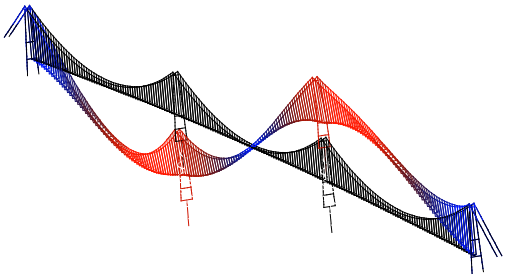

Mode Shape 10 ($\omega = 0.3090 rad/s$)

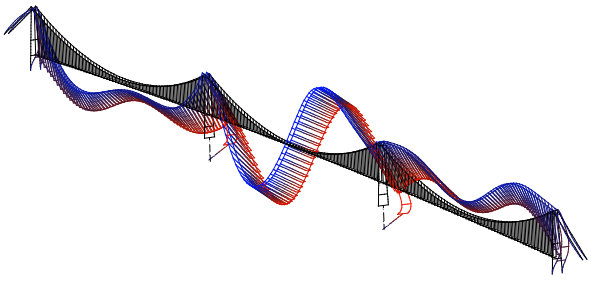

Mode Shape 23 ($\omega = 0.9821 rad/s$)

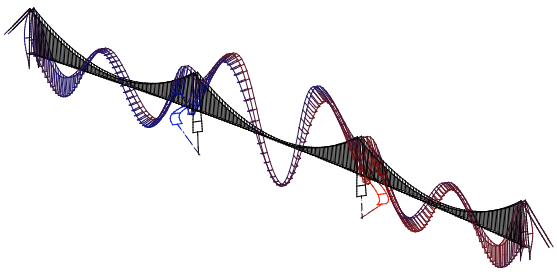

Mode Shape 28 ($\omega = 1.2554 rad/s$)

Figure 26: Mode Shape 7-10, 23 and 28 for Floating Foundation Bridge Model

Mode 1 and 2 are the two horizontal modes. These horizontal modes are coupled to pontoon rotation about the x-axis, and hence the bridge girder experiences a coupling of both horizontal bending and torsional twisting. This coupling occurs due to the eccentricity between the *Center of Horizontal Mooring Stiffness* and *Center of Mass*. The first horizontal mode is symmetrical and the second horizontal mode asymmetrical resulting in corresponding half sine wave and full sine wave in both bending and twisting. There deviation in natural frequency is less than 1 % and natural frequencies are 0.0454 *rad/s* and 0.0461 *rad/s.*

Mode 3 and 4 have the main motion in the rotation about the z-axis. The pontoons in mode 3 have rotation symmetrically while the vertical translation is asymmetrically. The bridge girder makes a full sine wave in mid-span and half waves in the side-spans. Mode 4 has rotation in opposite directions resulting in symmetry about midpoint. The natural frequencies are 0.0792 *rad/s* and 0.0802 *rad/s*. The deviation is less than 2 %, and they are well separated from mode 2 and mode 5.

Mode 5 and 6 have rotation about the x-axis in *Center of Mass* of the pontoons, hence horizontal displacements occurs in the stiffening girder. The shape of the girder is similar as in mode 1 and 2, but the torsional twist is in the opposite direction meaning pylon top moves more than the bridge girder. The natural frequency for these mode are 0.1828 *rad/s* and 0.229 *rad/s*, and deviation is 18 %. These modes are well separated from mode 4, but the natural frequency for mode 7 only 18 % above mode 4.

Mode 7 and 8 have the main motion in rotation about z-axis, but both modes are coupled to a considerable rotation about x-axis in the *Center of Mass*. Due to rotation about the z-axis large horizontal bending displacement occurs in stiffening girder. The natural frequencies for these modes are 0.2621 *rad/s* and 0.2860 *rad/s*, and the deviation is 8 %. Both mode 6 and 9 are generally close to these modes frequency wise.

Mode 9 and 10 are the two vertical modes. In mode 9 the pontoons moves symmetrical and the three span bridge girder makes a half sine wave. Mode 10 is asymmetric, hence the pontoons moves in different directions. The natural frequency for these modes are 0.3064 *rad/s* and 0.3090 *rad/s* hence the deviation in is 1 %.This implies that the extra stiffness from full wave bending of stiffening girder is insignificant.

Mode 23 and 28 are found among the vertical fixed bridge modes with three half waves. Mode 23 have three vertical waves (V3) in the side spans and two vertical waves (V2) in the midspan causing large bending and rotation of the lower part of the pylon legs and the pontoons rotate symmetrically about the z-axis. Mode 28 have three vertical waves (V3) in side spans and three vertical waves (V3) in midspan, also causing large bending and rotation of the pylon and the pontoons rotates asymmetrically about the z-axis. These modes have very similar motion in all four pylons and the two pontoons, but the stiffening girder bending gives some deviation of natural frequency. The natural frequencies are 09821 *rad/s* and 1.2555 *rad/s*

5.3.2 Fixed Bridge Modes

The 50 fixed bridge modes will be presented in the following section. Since the *FFB-Model* is the main model of interest the modes are presented after the natural frequencies from this model. The mode number from the RFB-model having same mode shape is given in last column. The table of these modes is given in Table 38.

Table 38: Natural frequencies and mode shape description of the bridge modes.

Mode no. FFB	Natural Frequency FFB [rad/s]	Bridge Mode Desciption	Span in Motion	Symmetry	Mode no. RFB
11	0.3798	V1	All	S	3
12	0.4160	H1	All	S	1
13	0.4232	H1	Side	A	2
14	0.4682	H1	All	S	4
15	0.5067	V1 and V2	All	A	5
16	0.7022	V2	Side	A	7
17	0.7023	V2	Side	S	6
18	0.7589	V1 and V2	mid	A	8
19	0.8337	H2	All	A	9
20	0.8600	H2	Side	A	10
21	0.9199	H2	All	A	11
22	0.9515	V3	All	S	12
24	1.0337	V3	All	S	13
25	1.0489	V3	Side	A	14
26	1.1931	C1	One Side Span	-	15
27	1.1931	C1	One Side Span	-	16
29	1.3007	C1 (H1, T1)	Side	S	17
30	1.3015	C1 (H1, T1)	Side	A	18
31	1.4088	V4	All	A	19
32	1.4106	V4	Side	S	20
33	1.4156	V4	Mid	A	21
34	1.4427	C2	One Side Span	-	22
35	1.4427	C2	One Side Span	-	23
36	1.4535	V4	All	S	24
37	1.4578	H3	All	S	25
38	1.4874	C2 (H2, T2)	Side	A	26
39	1.4952	C2 (H2, T2)	Side	S	27
40	1.5371	H3	Side	A	28
41	1.5558	C2	Mid	S	29
42	1.5764	C2	Mid	A	30
43	1.6015	H3	All	S	31

44	1.6482	C2 (H2, T2)	Mid	A	32
45	1.6672	C2 (H2, T2)	Mid	S	33
46	1.8014	V5	Side	A	34
47	1.8088	V5	All	S	35
48	1.8664	V5	All	S	36
49	2.0092	C3	One Side Span	-	37
50	2.0092	C3	One Side Span	-	38
51	2.0459	C3 (H3, T3)	Side	A	39
52	2.0468	C3 (H3, T3)	Side	A	40
53	2.2235	V6	All	A	41
54	2.2273	V6	Side	S	42
55	2.2378	V6	Mid	A	43
56	2.3221	H4	All	A	44
57	2.3877	T1 Mid, H4 Sid	All	S	45
58	2.4160	T1 Mid	Mid	S	47
59	2.4514	H4	All	A	46
60	2.5059	V7	All	A	48
61	2.5236	C4	One Side Span	-	49
62	2.5236	C4	One Side Span	-	50

5.3.2.1 Vertical modes

All the vertical modes of the fixed bridge modes are uncoupled from horizontal and torsional components. Except from mode 23 and 28, all vertical modes are uncoupled from any significant pontoon motion or horizontal stiffening girder component. Generally the increase in frequency for the vertical modes is related to the bending in terms of number of half waves in each span. Mode 15 and 18 have combinations of V1 and V2, while mode 16 and 17 have a V2 shape in all spans. The natural frequencies for these four modes are in the range 0.51-0.76 rad/s. For higher order modes V3 (mode 22, 24-25), V4 (31-33,36), V5(46-48) and V6 (53-55) the natural frequencies are concentrate around 1 rad/s, 1.4 *rad/s*, 1.8 *rad/s* and 2.2 *rad/s*. Since 62 modes where extracted only one of the three seventh vertical waves (V7) are presented, this mode had natural frequency 2.5 *rad/s*.

Generally it can be seen that modes which have waves asymmetric about one of the pylons, hence creating large moments have a coupled rotation about the x-axis of the pylon. This is the case for mode 11, 15 and 53.

5.3.2.2 Horizontal Modes

Mode 12, 13, 14 are the three first horizontal modes. These modes are coupled to a rotation about the x-axis in the pontoons.. For these modes the difference in between cable motion and bridge girder motion is insignificant, hence the torsional twisting in the bridge girder is small.

Mode 19, 20 and 21 are the three modes with two half waves in each span. The difference between cable motion and bridge girder motion are more prominent and a significant torsional twisting component of the bridge girder is coupled to all these modes.

The three mode shapes with three half waves are 37, 40 and 43. All these modes have large deviation between cable motion and bridge girder motion, hence the coupled torsional twisting component of the bridge girder is considerably larger than in the other horizontal modes.

5.3.2.3 Cable Modes

When cables displaces in different directions, no stiffening girder components are coupled to the mode. This is the case for mode 26 and 27 (C1) , 34, 35, 41 and 42 (C2), 49 and 50 (C3), and 61 and 62 (C4). All these modes have only motion in side-span cables, except mode 41 and 42 which have motion only in mid-span cables. These mid-span cable modes have 8% higher natural frequencies than the equivalent side-span modes. This is because the mid-span has shorter hangers and hence the stiffness is increased.

5.3.2.4 Coupling Cable and Torsional Component

When cables oscillates in phase (same direction) torsional twisting of the bridge girder is coupled to the mode. Also horizontal motion in the stiffening girder is coupled but this component is insignificant. These coupled cable modes are found only few modes after the uncoupled cable modes, hence the frequency is slightly higher. Mode 29 and 30 are the side-span coupled half wave modes, 38, 39, 44 and 45 are the side-span and mid-span coupled two half wave modes, while 51 and 52 are the mid-span coupled three half wave modes. The frequencies of these coupled cable modes are 3-10 % higher than the corresponding uncoupled cable modes.

5.3.2.5 Torsional Modes

Among the first 62 modes included only one torsional mode is found. Mode 57 have torsional twisting and no lateral cable motion or lateral girder motion is coupled to the mode. This mode have natural frequency 2.3877 *rad/s*.

5.4 Effective Modal Mass

The mode shapes and natural frequencies presented in previous section only shows the relative displacement of each mode but it tells nothing about the response. An effective method of understanding the mode influence on response is studying the *effective modal mass*. The effective modal mass is representing the effective mass participating in each mode in e certain direction. Large effective modal mass (in comparison to the total effective mass) contributes significantly to the response [21].

The total effective mass is found summing all the effective modal masses. In reality a finite element model have as many modes as it have degrees of freedom. In the initial analysis 62 eigenvalue where extracted, and to compare the contribution from these modes, these modes are compared to an analysis extracting 1000 eigenvalues. Table 39 shows this comparison. As it can be seen the 62 first eigenvalues contributes between 97.3 - 99.7 % to total 1000 modes depending on direction. For the purpose of this study the 62 first modes are assumed to be representing the total effective modal mass sufficiently.

Table 39: Total Effective Mass for 62 eigen values and 1000 eigen values

Eigenvalues included	**Total Effective Mass**			
	X-direction [*kg*]	**Y-direction [*kg*]**	**Z-direction [*kg*]**	**X-rotation [kgm^2]**
62	1.800 E+09	1.082 E+09	1.817 E+09	9.459 E+12
1000	1.849 E+09	1.085 E+09	1.850 E+09	9.656 E+12
Contribution	97.35 %	99.71 %	98.23 %	97.96 %

The effective modal mass for 62 first modes for the X, Y, Z and Θ_x direction from the FFB-model is shown in Figure 27 - Figure 30. Since most of the modes have an insignificant effective modal mass only modes with effective modal mass above 1000 *kg* for the translational directions and 1 000 000 $kg\ m^2$ for the rotational direction. 63 modes included)

All figures are shown in y-logarithmic plot to separate the effective modal masses better.

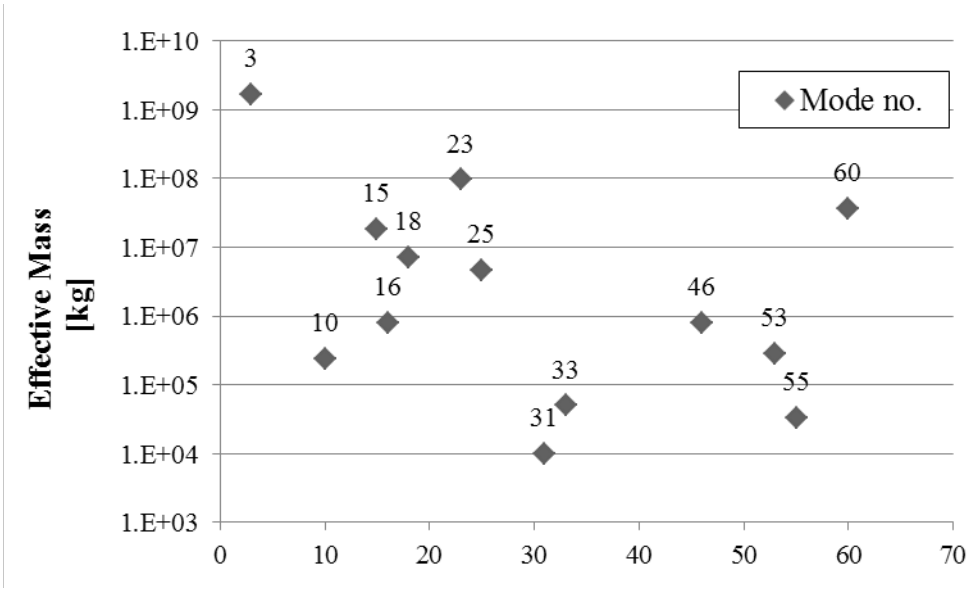

Figure 27: Effective modal mass contribution, x-direction

Figure 27 shows the effective modal mass in longitudinal direction. Mode 3 and 23 contributes 96 % percent of the total effective mass. The large contribution in mode 3 is due to the symmetric pontoon motion in x-direction. Mode 2 has very similar shape but is asymmetric and the mass in motion cancel each other out, and the effective modal mass for mode 2 is close to zero. Mode shape 23 has the second largest effective mass in x-direction due to longitudinal motion of all four pylons.

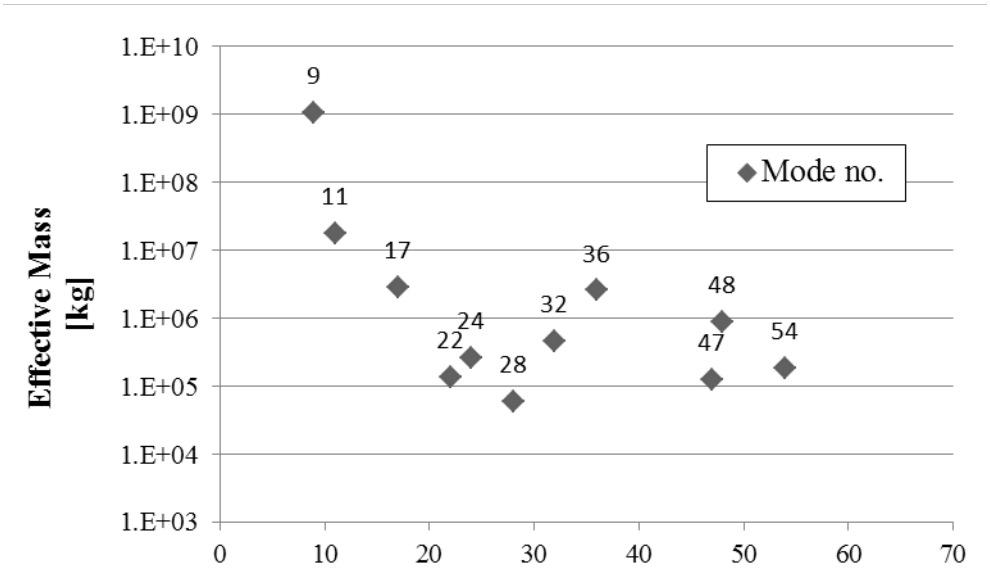

Figure 28: Effective modal mass contribution, y-direction

Figure 28 shows the effective modal mass in vertical direction. Mode 9 contributes to 98 % of the total effective mass due to both mid pylons and pontoons in symmetrical vertical motion. Mode 11, 17 and 36 have also a significant effective modal mass. These modes contributes because the majority of the spans swings in phase, this can best be illustrated by the mode shape of mode 36.

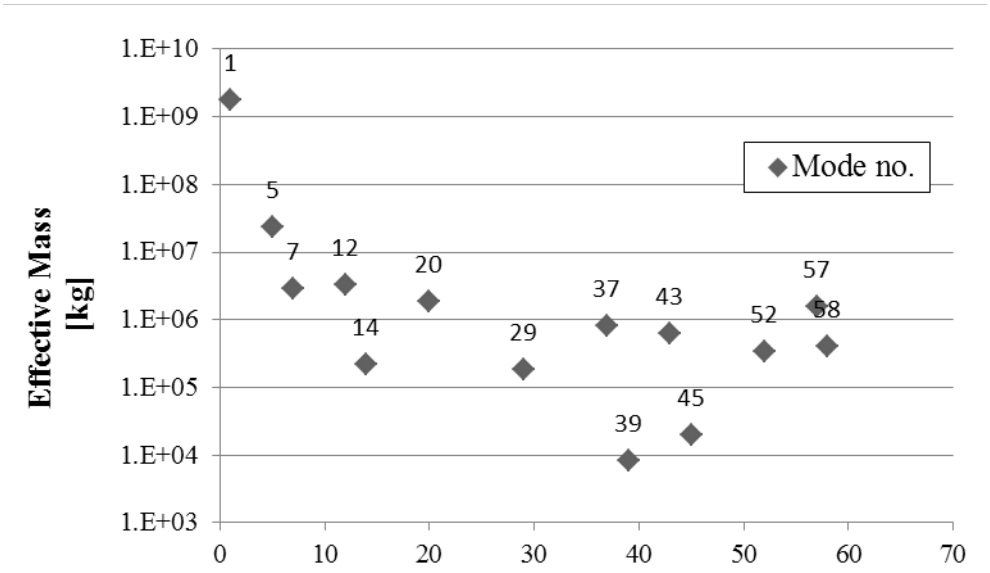

Figure 29: Effective modal mass contribution, z-direction

Figure 29 shows the effective modal mass in horizontal lateral direction. The same can be seen in this direction as in the vertical direction. Mode including pontoon motion in phase, in this case mode 1, contributes to most of the total effective mass. Mode 3 alone contributes alone with 96 % of the total effective mass. Mode 5 has the second largest contribution with 1.3 % of the total effective mass.

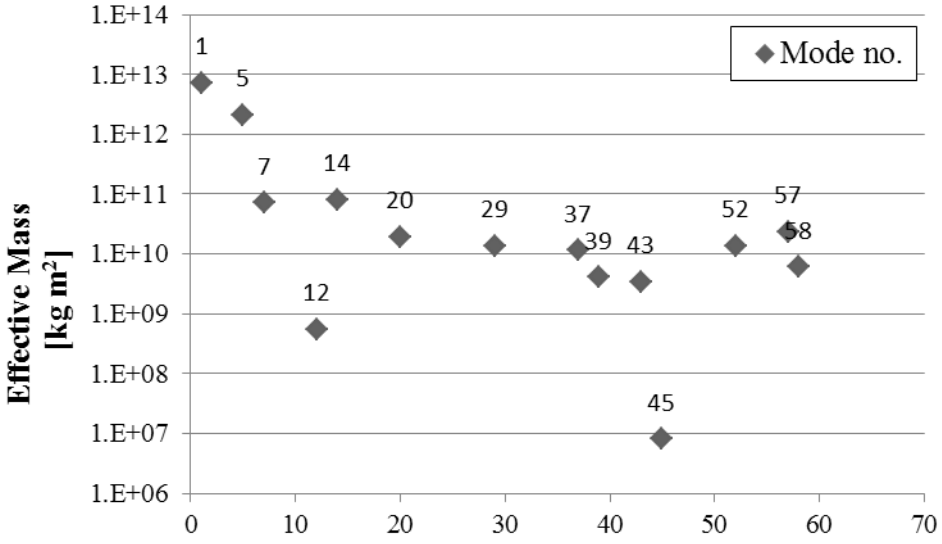

Figure 30: Effective modal mass contribution, x-rotation

Figure 30 shows the effective modal mass in x-rotation. As for the lateral horizontal direction mode 1 contributes most with 74 % but also mode 5 have considerable contribution with 22 %, both these modes are in-phase rotation of the pontoons and hence large masses rotates about the x-axis. Mode 7 and 14 have the third largest contribution and these modes have a significant coupling of rotation in the pontoons due to horizontal motion in the stiffening girder.

5.5 Damping Ratio

From a linear perturbation and complex frequency analysis in Abaqus/CAE the effective damping ratios are extracted. These effective modal damping ratios are compared to the classical Rayleigh mass- and stiffness dependent damping ratios and the total Rayleigh-damping ratio as function of natural frequency. This comparison is shown in Figure 31.

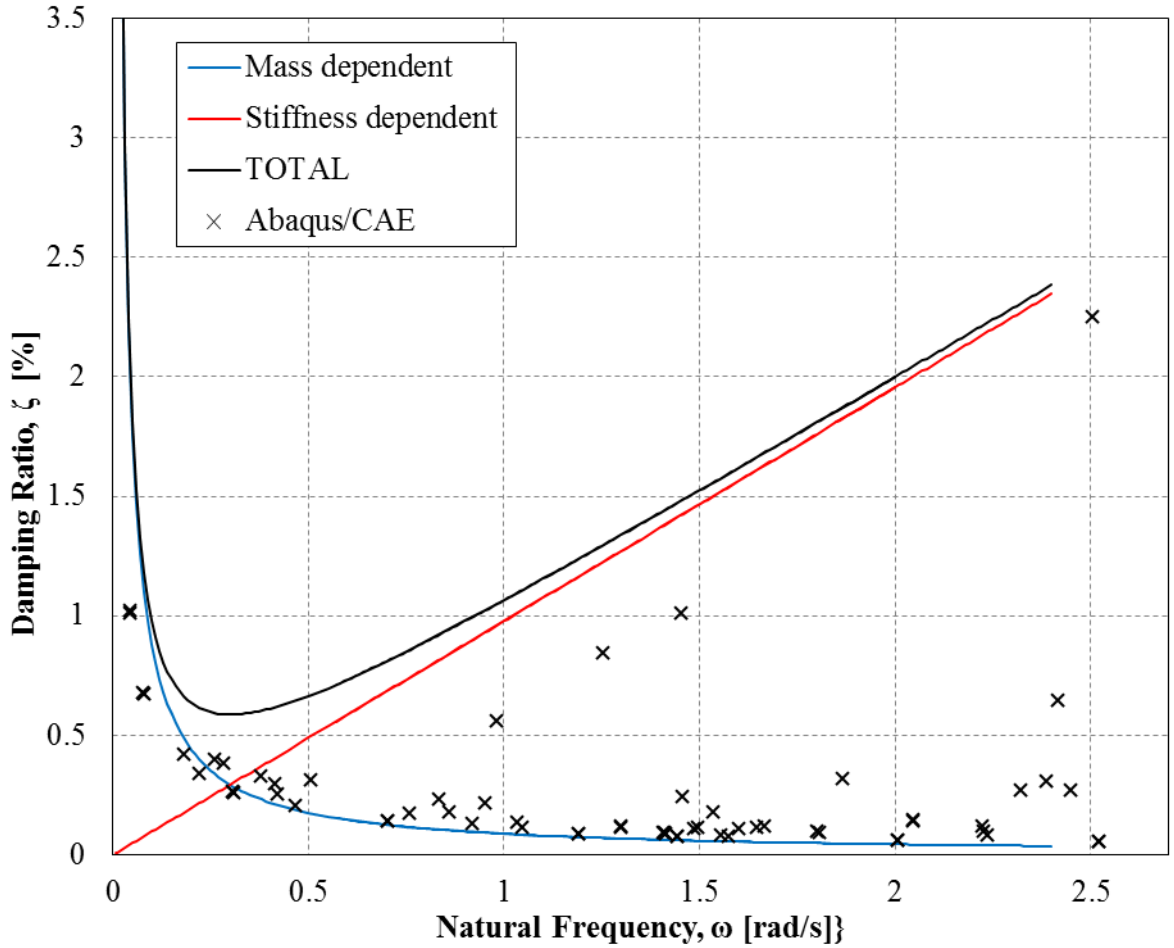

Figure 31: Effective damping ratio for FFB-model

The majority of the modes in Abaqus/CAE have damping ratio between 0.1% and 0.4%.Mode 1, 2 and 3 have considerable higher effective damping ratio with 1%, 1.01% and 0.67%. another exception of the low values are modes 23, 28, 36 and 60 with 0.55%, 0.84%, 1.00% and 2.25%.

Comparing the damping ratios for the modes to the Classical Rayleigh damping it is clearly that the effective damping ratios from Abaqus/CAE is close to independent from the Rayleigh stiffness coefficient added to the model, with exception of mode 23, 28, 36 and 60 showing a linear increase similar to the stiffness dependent Rayleigh damping.
The reason for Abaqus/CAE underestimating most of the damping ratios compared to the Rayleigh–damping is the fact that Abaqus/CAE uses only the initial stiffness matrix when calculating the stiffness contribution to the damping ratio, and not the total contribtion from

both initial and geometric stiffness amtrix. For a suspension bridge the contribution from the geometrical stiffness is significant whci way the low damping ratios is observed in figure.

It is of interest to see the effect of the hydrodynamic damping on the effective modal damping ratio. A model excluding the hydrodynamic damping connectors is created and the results from the analysis are compared to the existing model where the hydrodynamic damping is included. The results are shown in Table 40.

Table 40: Natural Frequency and Effective damping ratio, including and excluding hydrodynamic damping.

Mode no.	**Natural Frequency**	**Effective DampingRatio [%]**		**Increased Damping Ratio**
	[rad/s]	**Excluding H. Damping**	**Including H. Damping**	**[%]**
1	0.045	0.9885	1.0145	2.63
2	0.046	0.9785	1.0035	2.55
3	0.079	0.6310	0.6715	6.42
4	0.080	0.6260	0.6650	6.23
5	0.183	0.4080	0.4115	0.86
6	0.223	0.3300	0.3335	1.06
7	0.262	0.3895	0.3895	0.00
8	0.286	0.3750	0.3750	0.00
9	0.306	0.2430	0.2565	5.56
10	0.309	0.2400	0.2540	5.83
23	0.982	0.5525	0.5545	0.36
28	1.255	0.8355	0.8375	0.24

The damping ratio is increased with almost 3 % for mode 1 and mode 2, while for mode 3, 4, 9 and 10 the damping ratio is increased in the range of 6 %. Damping ratio for mode 5 - 8, 23 and 28 are almost unaffected.

Mode 3, 4, 9 and 10 are the only modes with significant motion in longitudinal and vertical direction of the pontoons. Hence it is be concluded that the hydrodynamic damping is significantly increased for these motions in the complex frequency analysis .

Mode 1 and 2 are the only mode with lateral motion in the pontoons. The increase is still significant but less than for the motion mentioned in previous paragraph.

Mode 7 and 8 have the pontoon motion in rotation about the lateral axis, since no hydrodynamic damping existing in this rotation zero increase in damping ratio was expected.

5.6 Dynamic Response to Concentrated Force

In this section the effect of damping will be tested in a time-domain response simulation. The most interesting pontoon motions are the X-direction, Y-direction, Z-direction and X-rotation (rotation about x-axis). In total 4 simulations are carried out, in each an initial static displacement in one of the directions are modeled and a then a dynamic step analysis the oscillations from the force is removed to the energy is dissipated and the initial position is obtained. The static force applied and corresponding static displacement for each simulation are given in Table 41.

Table 41: Dynamic Simulations

Analysis Name	Force direction	Force applied	Static displacement
DynSimX	X	- 1 e6 N	- 0.56 m
DynSimY	Y	- 2 e8 N	- 2.76761 m
DynSimZ	Z	- 2 e6 N	- 2.18 m
DynSimRX	Θ_X	2 e9 Nm	0.0025 Rad (0.143°)

A *dynamic, implicit* step are used to simulate the oscillations. Firstly the force is removed instantaneously (from 100 % to 0% in 0.1s) and then the bridge oscillates freely. The time-increment in the simulations are set to automatic, but a maximum time increment of 10 s is chosen.

For each directional simulation the displacement and hydrodynamic damping force in the corresponding direction is extracted from the Abaqus/CAE. These displacements and damping forces are show in Figure 32 -Figure 39

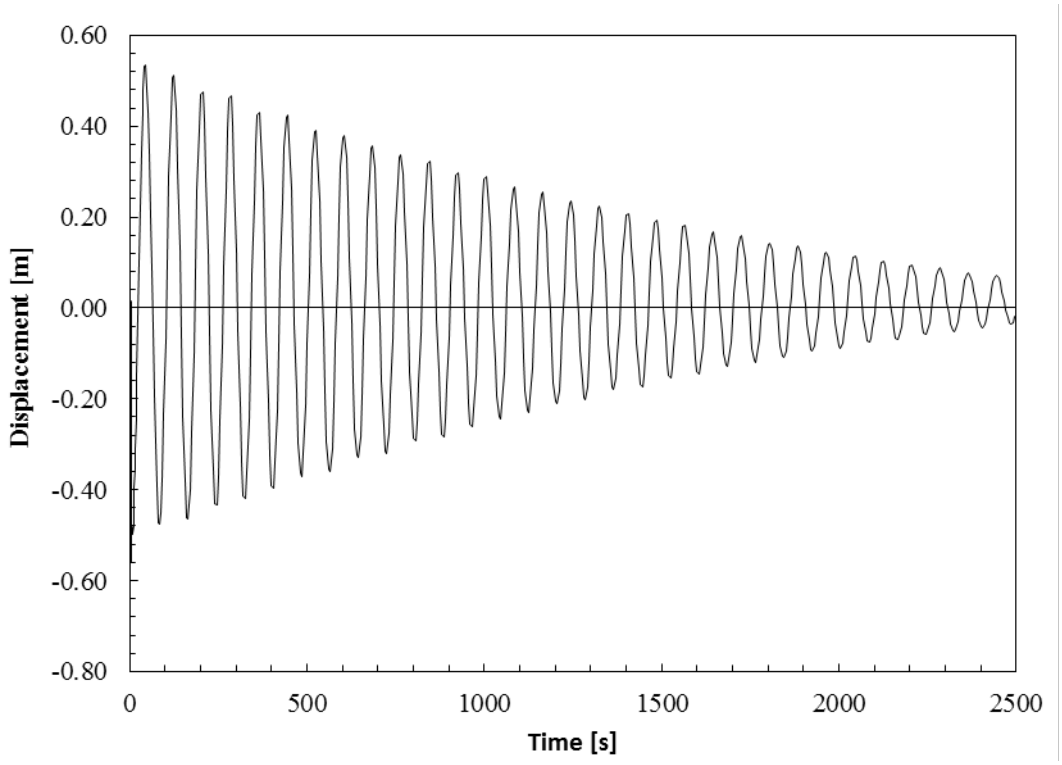

Figure 32: Dynamic response in X-direction in pontoon

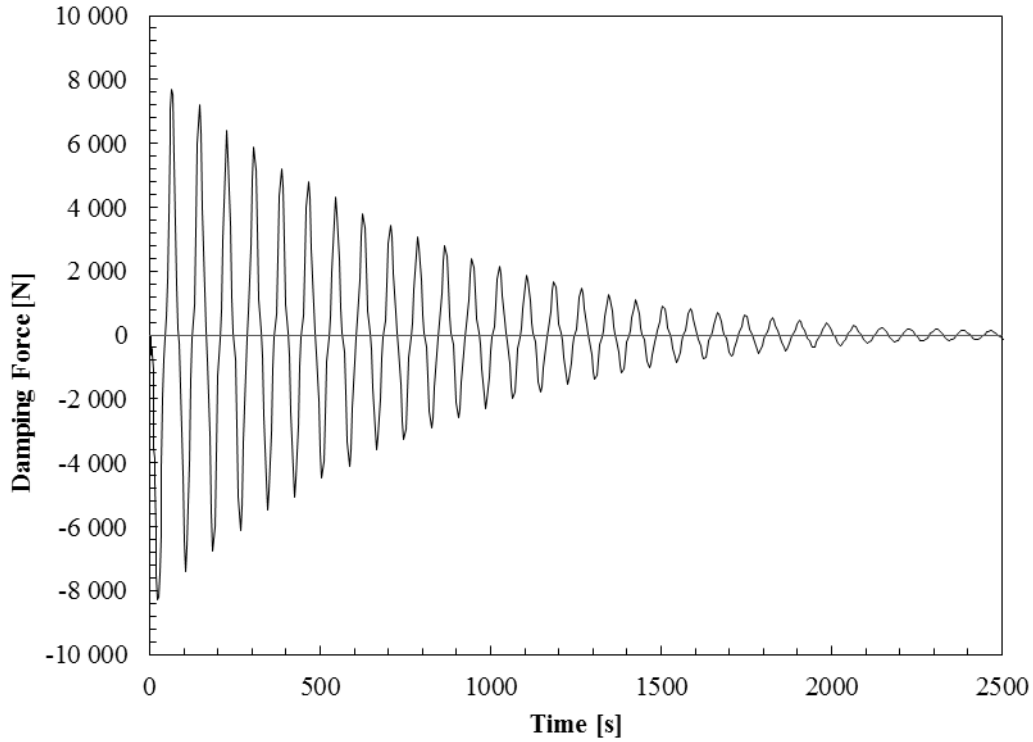

Figure 33: Hydrodynamic damping force in X-direction in pontoon

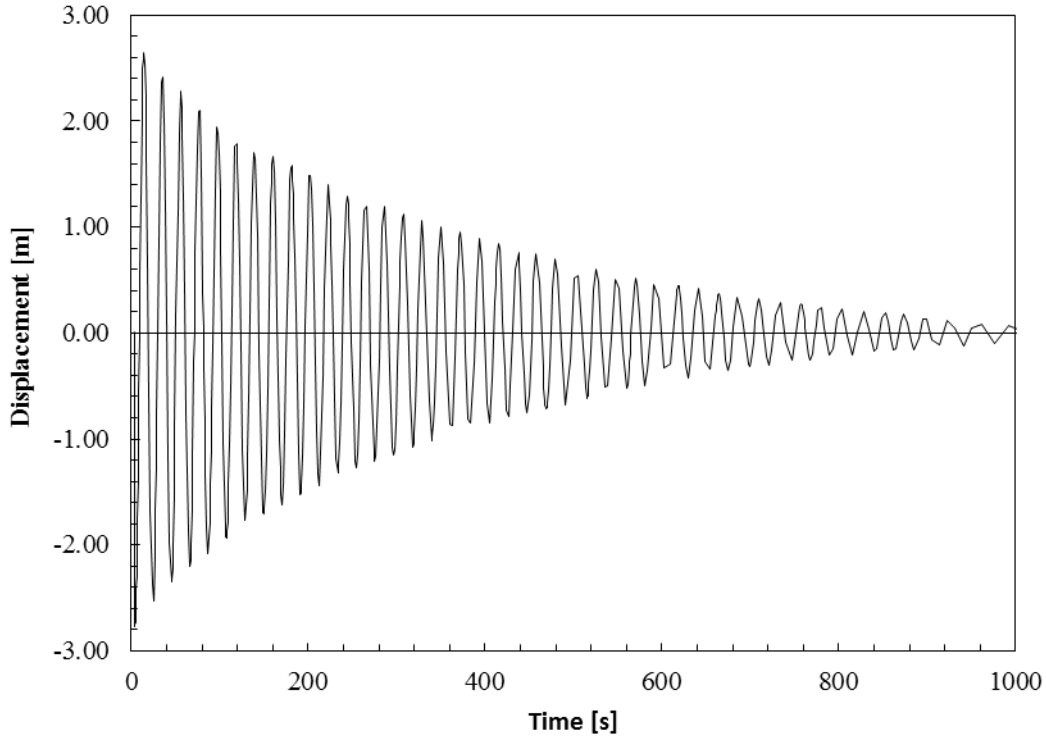

Figure 34: Dynamic response in Y-direction in pontoon

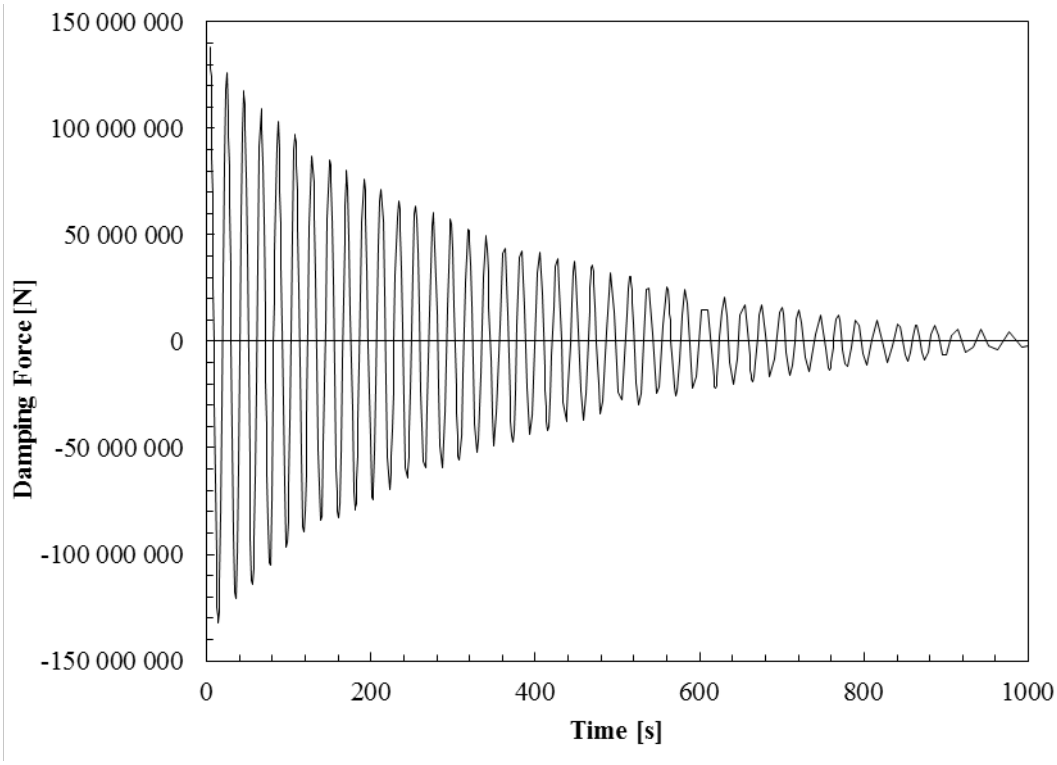

Figure 35: Hydrodynamic damping force in Y-direction in pontoon

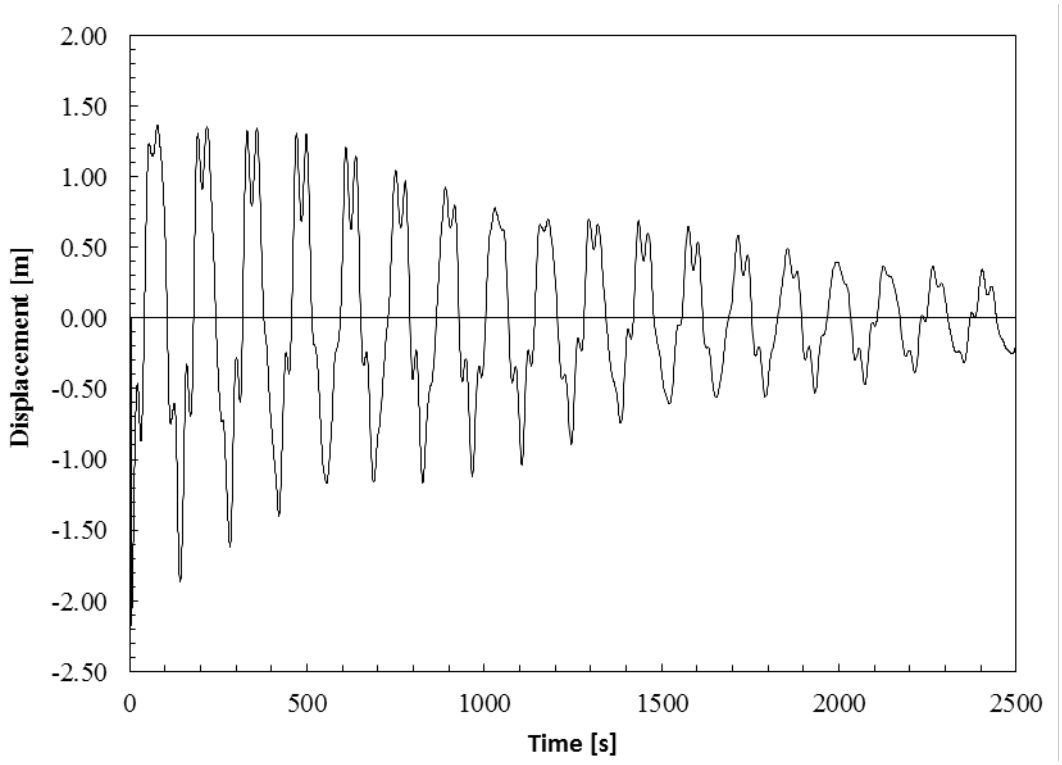

Figure 36: Dynamic response in Z-direction in pontoon

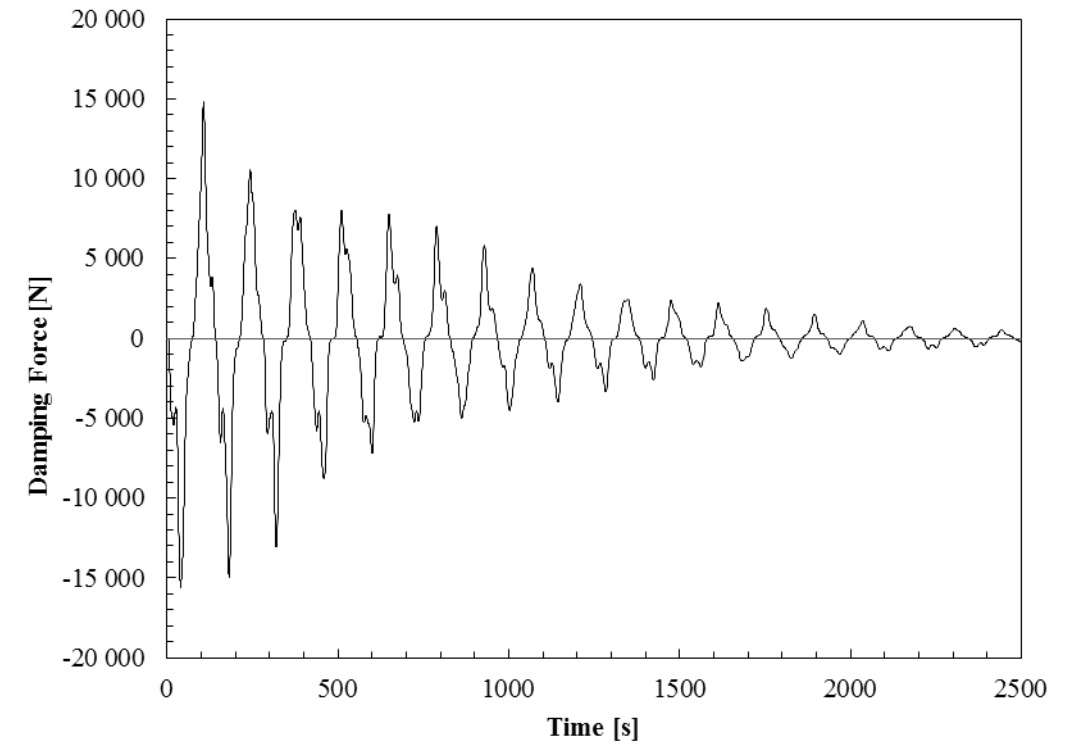

Figure 37: Hydrodynamic damping force in Z-direction in pontoon

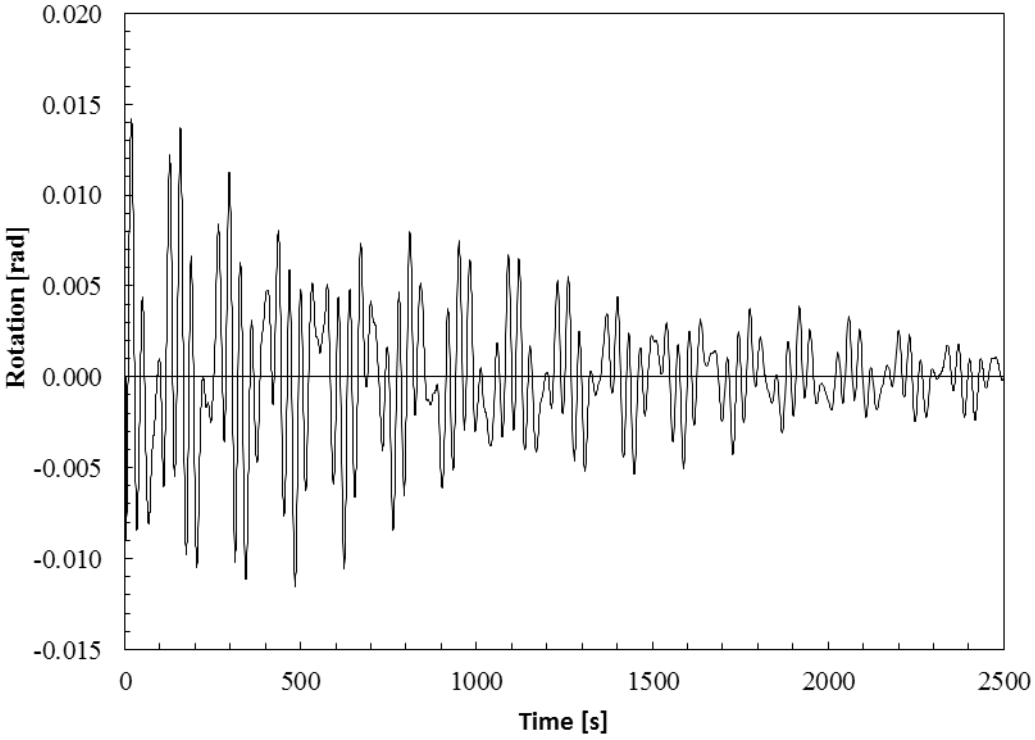

Figure 38: Dynamic response in X-rotation in pontoon

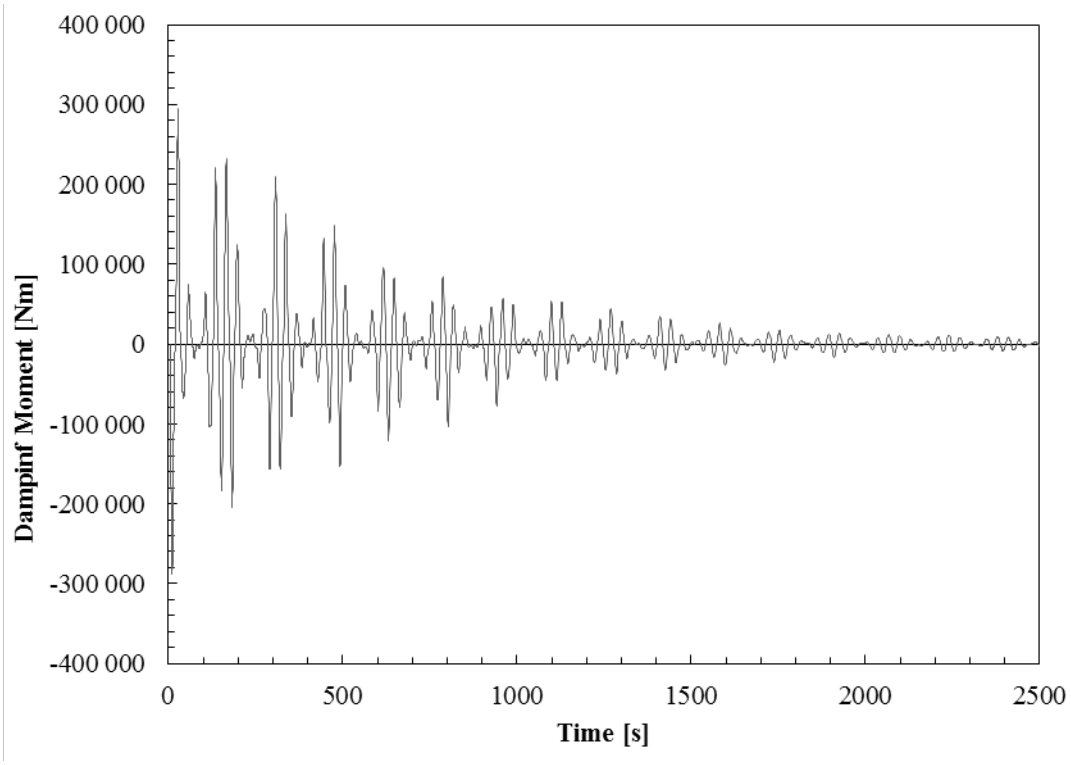

Figure 39: Hydrodynamic damping force in X-rotation in pontoon

For the x-displacement simulation it can be seen that the system oscillates with only one frequency. The amplitude slowly decreases from 0.53*m* at the first peak to 0.05*m* at the 31st peak. The time between these 30 oscillations is 2393.5 *s*, giving an average period of 79.8 *s* or a circular frequency of 0.0736 *rad/s*. This corresponds well the natural frequency of mode 3 which has circular frequency 0.0787 *rad/s*. The global oscillation is also similar tot the mode shape 3. Since the oscillation only have one mode the logarithmic decrement and damping ratio can be found using the following equation [23]

$$\xi = \frac{1}{\sqrt{1+\left(\frac{2\pi}{1/n\ln(x_i / x_{i+n})}\right)^2}} \tag{5.1}$$

Where x_i and x_{i+n} are two peak values with distance *n* periods.

Between two adjacent peaks the damping ratio varies from 0.21% and 1.84% , while the average damping ratio for all 30 oscillations are 1.17%. The variation in damping ratio could be caused by the large time-increment, and thus the real maximum could be situated between two time-increments. By comparing to the linear perturbation the damping ratio for mode 3 is 0.67%, almost half the damping ratio.

Figure 33 show the damping force in x-direction due to dynamic response in x-direction. The maximum force decreases from 7679 *N* at first peak to 150 *N* in the last peak. By assuming maximum velocity given by natural frequency times the maximum amplitude and damping coefficient, the theoretical maximum damping forces implies well with the forces from the figure.

For the y-displacement oscillation shown in Figure 34 it is seen that also here only one mode contribute to the oscillation. The amplitude at first peak is 2.59m while for the 43rd peak has decreased to 0.12m. The average increment for the oscillation is 0.073 and the average damping ratio is then given as 1.17 %. The period of the oscillation is 21.6 s or circular frequency 0.2902rad/s which implies well with mode 9 both in frequency and global motion. Mode 9 has damping ratio 0.254 % which means the damping ratio from the logarithmic decrement is more than 4 times as high.

Figure 35 shows vertical damping force. These forces are much higher than forces in the other directions. The maximum force for one of the first peak is 126 MN, this corresponds to a velocity of more than 5 *m/s*. Using same approach to verify the damping force, natural frequency and maximum displacement gives a maximum damping force equal to 2.55MN and the deviation is enormous. From this it is concluded that the hydrodynamic damping force is not represented correctly.

For the z-displacement simulation it can be seen that the response oscillates with two frequencies. The lowest frequency have an average period 139*s* or circular frequency 0.0452 *rad/s*. This corresponds very well with mode 1 which has circular frequency 0.0454 *rad/s*. The amplitude of this response-component is harder to find than for the two others, but a maximums occur at 3rd 10th and 17th peak. These corresponding amplitudes are 1.33*m*, 0.69*m*

and 0.36*m*. Using the decrement damping equation the damping ratio from 3rd to 17th peak the average damping ratio becomes 1.59%. The effective damping ratio for mode 4 given from complex frequency is 1.00% and hence the deviation is significantly smaller than for the other simulations.

In Figure 37 the hydrodynamic damping force as function of time in z-direction is shown. The curve is similar to the displacement curve. The maximum force is -15.3 *kN* at 38*s* and the force oscillations decreases to the last maximum force 0.1 *kN* at 2470 *s*. using the same method to verify the hydrodynamic damping force it is seen that the calculated damping force is 9 *kN*, implies not perfectly but better than for the y-direction.

For the x-rotation simulation the response seems to have local peaks at every 32*s* giving a circular frequency 0.1954 *rad/s*, This corresponds to frequency between mode 5 0.1828*rad/s* and mode 6 0.2229*rad/s*. It is difficult to see any patterns in the amplitude of these local peaks meaning several components are part of the total response. Even though a pattern is hard to see, generally the amplitudes decrease. One of the first maximum rotations is 0.0139 *rad* at t=18s, while the maximum rotation at approximately t=2000*s* are decreased to 0.0033 *rad*. By assuming this decrease over 61 oscillations (hence period 32*s*) the damping ratio becomes 0.38 %. The complex frequency analysis damping ratio in mode 5 is 0.41 % is very close to the damping ratio found in the dynamic simulation, but the uncertainties are high.

Figure 35shows the hydrodynamic damping moment in x-rotation. The highest moment 300 *kNm* occurs at at early stage and one of the last peak moments are 7.8 *kN*. The same method as used earlier gives a maximum damping moment of 318 000 Nm whvi corresponds very well to the maximum damping from the figure.

Generally it can be concluded that the damping ratios for the time-history analysis gives a higher damping ratio than the complex frequency analysis. The oscillation frequencies corresponded well to the natural frequencies for the modes witch had mode shapes similar to the initial disturbance. The maximum damping force from the figures implies quiet well considering the simple assumption using natural frequency, amplitude and damping coefficients, except from the X-direction simulation where the maximum forces in the figure is almost 50 times as high. Hence the hydrodynamic in this direction is not implemented ass wanted.

6 Conclusion

The purpose of this thesis was to investigate the concept of a multi-span suspension bridge with floating towers. Firstly a preliminary design was carried out, resulting in three spans of 1230 *m* each, cable sag 121 *m* and pylon height 200 *m*. The multi-column pontoons were design using hydrostatic principles and static mean wind load, and given total diameter 80 *m*, total depth 100 *m* and minimum 6 *m* concrete for fixed ballast. The hydrodynamic added mass and added damping was calculated according to expressions derived in chapter 2, assuming potential theory and Morison equation. A finite element model was created using the geometry and structural properties from preliminary design.

Static mean wind analysis gave pontoon rotation 1.3°. The total lateral displacement of the stiffening girder at mid span was 8.81*m*, where 3.63 *m* are contributions from pontoon displacement and rotation. Less deflection can be obtained by increasing hydrostatic rotational stiffness, lateral mooring stiffness or cross sectional bending stiffness of the girder.

For the traffic load, mid-span loading gave largest vertical displacement in stiffening girder. The pontoons had a rotation of 0.36°, resulting in 1.25 *m* longitudinal displacement at top, while bending of pylon columns are resulting in 1.14 *m* longitudinal displacement. The total vertical displacement becomes -9.75 *m*. Both stiffer pylon structure and increased hydrostatic rotational stiffness would improve the behavior for this loading.

The eigen-value analysis showed that the floating foundation bridge model had extra 10 eigen modes, all with natural frequencies below the 50 eigen modes associated with the rigid floating foundation model. From these 10 pontoon motion modes 5 different types of pontoon motion are represented with frequencies well separated. The 1^{st} mode (lateral translation) had natural period 138 *s* and the 10^{th} mode (lateral rotation) had natural period 20 *s*. The first mode uncoupled from pontoon motion is the vertical half sine wave shape in the girder with corresponding natural period 16.5 *s*. The first horizontal half sine wave shape have natural period 15.1 *s* . First cable mode coupled to torsion have natural period 4.8 *s* while the first uncoupled torsional mode have natural period 2.63 *s*. In general all the vertical modes are uncoupled, while for horizontal modes the torsional degree of coupling increases with number of half sine waves.

Regarding contributions to a future dynamic wind response calculation, the 10 pontoon motion modes with extremely low natural frequencies will be largely excited by the strong wind fluctuations. From a general wind velocity spectrum [24], it is seen that the major content are at low frequencies hence low natural frequency modes will contribute considerably more than high frequency modes.

Another important method to describe the mode's contribution to response is the effective modal mass. From the results is can be concluded that the large effective modal masses are

related to the symmetric motion in the pontoons. For x-directional modal mass a pontoon x-rotational mode (mode 3) has the largest contribution, while for the y-directional modal mass it is the first vertical pontoon motion mode (mode 9) having the largest cotribution. For both z-directional and x-rotational modal mass it is the first lateral pontoon motion (mode 1) having the largest contribution.

The complex frequency analysis shows that the effective damping ratio decreases rapidly for the first 5 modes. Mode 1 has an effective damping ratio equal to 1.01%, while the damping ratio for mode 6 and is in the range of 0.3 %. It is a exception of a few modes where all bridge components in x-directional motion. Compared to classical Rayleigh damping the complex frequency analysis have a more mass dependent damping. It can also be concluded that complex frequency analysis increase the effective damping ratio by approximately 6 % for translational modes when hydrodynamic damping is added, but increase the damping ratio insignificantly for rotational modes.

The time-domain dynamic analysis showed a distinct energy dissipation in all simulations. The hydrodynamic damping force was correctly implemented to three of simulations, but for X-direction the force was unreasonably high. For the X-component simulation the bridge motion and frequency corresponded well with mode 3. The effective damping ratio given by the average decrement gave a damping ratio 1.17 % compared to the 0.67 % for complex frequency analysis. For the Y-component simulation mode 9 was recognized and decrement method gave same average damping ratio as for the X-component, while complex frequency gave damping ratio 0.25 %. It was observed that for the Z-component and X-rotational component simulations several modes were contributing, still damping ratio in the same range as for the complex frequency analysis were found. For all time-domain simulations the highest frequencies and maximum displacement were found and by using the hydrodynamic coefficients the maximum hydrodynamic force could be compared to the maximum force in the figures. For all direction except X-direction the damping force was in the same range as the figured showed.

Generally it can be concluded that effective damping ratio from the complex frequency analysis does not describe the non-linear hydrodynamic damping correctly. Still it seen a increase of 6 % for translational pontoon modes which illustrate that the linear interpretation in the complex frequency analysis tries to incorporate the hydrodynamic damping. The damping seen in the time-domain simulations are probably more correct since 3 of the 4 damping forces were behaving as wanted.

7 Further Work

Recommendations and important aspects for future work:

- Regarding the pylon design a pylon tower optimized for a multi-span bridge and increased bending stiffness about lateral axis would greatly improve the structural behavior when subjected to traffic loading. Steel truss structures for the bridge pylons could be investigated because it would lower the weight of the pylons considerably which is favorable for hydrostatic stability and behavior, and hence smaller pontoon dimensions are required to achieve stability.

- Different pontoon shapes and dimensions could be investigated more thoroughly. A numerical *fluid-structure-interaction* program would describe the hydrodynamic effects more precisely and these effects can be added directly to a finite element program.

- Design and investigation of structural behavior of mooring system and horizontal stiffness for the floating foundation.

- Dynamic time-domain analysis or frequency domain analysis for both wind and waves to investigate the dynamic response of the bridge.

Appendix A: Preliminary Design

A1: Geometry Calculations

The lengths of the cables and girder are calculated by calculating the length of a circular sector. A equation describing this relationship is given by

$$b = 2\pi R \frac{\theta}{360} \tag{1.1}$$

Where,
b is the length of the sector
R is the radius of the circle
θ is the angle of the sector

The angle of the cable of girder sector is given by

$$\theta = 2\arcsin\left(\frac{L/2}{R}\right) \tag{1.2}$$

Where,
L is the horizontal projection of the sector

For the cable only the sag and span length is defined. A simple matlab script calculates the radius when three points are given. By using (0,0), (615,-121) and (1230,0). For the girder the radius is given and the horizontal length (projection) is given. The results are tabled below.

	Horizontal Length	Sag/ Elevation	Radius	Sector Angle	Sector Length
Cable	1230 *m*	121 *m*	1 623,4 *m*	44,5346 °	1261,50 *m*
Girder	1230 *m*	29 *m*	58 700 *m*	3,6023 °	3690,61 *m*

A2. Mass Calculations

Stiffening Girder

1. *Stiffening Girder*

$\rho = 7850 kg / m^3$

$A = 0.5813 m^2$

$m = 0.5813 \cdot 7850 = 4563 kg / m$

2. *Guide Vans*

Guide vane $A = 0.00585 m^2 / m$ per guide vane

Attachement plate $A = 0.0014 m^2 / m$ per guide vane

Steel density: $\rho = 7850 kg / m^2$

$m = 2 \cdot (0.0085 + 0.0014) \cdot 7850 = 114 kg / m$

3. *Transverse Bulkheads*

Transverse bulkheads $m = 1110 kg / m$

Stiffeners $m = 103 kg / m$

Stiffeners around access point $m = 15 kg / m$

Access point (reduced mass) $m = -28 kg / m$

Cable duct (reduced mass) $m = -6 kg / m$

Clearance trapezoidal stiffeners $m = -75 kg / m$

$m = 1119 kg / m$

4. *Lower hanger attachment*

Average attachment weight $m = 842 kg$

$m = 860 \cdot 360 / 3680 = 84 kg / m$

5. *Railing*

$m = 183 kg / m$

6. *Asphfalt and wearing course*

According to Norwegian Handbooks weight of asphalt should be chosen as $2 kN / m^2$. Outside the wearing course a 12mm membrane of density $2000 kg / m^3$ is placed.

Asphalt: $m = 12.9 \cdot 2000 / 9.81 = 2630 kg / m$

Membrane $m = 0.012 \cdot 1.83 \cdot 2000 = 44 kg / m$

$m = 2674 kg / m$

7. *Electric Installation*

$m = 35 kg / m$

8. Transport beam IPE120

$m = 11kg/m$

9. Lamp post

Lamp post of 10*m* height , spacing 40*m*

$m = 5kg/m$

10. Drain

Two drains every 20 *m*.Weight per drain 30*kg*.

$m = 30 \cdot 2/20 = 3kg/m$

11. Surface coating

Zink, layer $100\mu m$, density $7100kg/m^3$

Paint, layer $255\mu m$, density $900kg/m^3$

Areal $A = 36.4m^2/m$

$m = 36.4 \cdot (0.00001 \cdot 7100 + 0.000255 \cdot 900) = 34.2kg/m$

Description	**m [kg/m]**
Steel Girder	4563
Guide Vans	114
Transverse Bulkheads	1119
Lower hanger attachment	84
Railing	183
Asphfalt and wearing course	2674
Electric Installation	35
Transport beam IPE120	11
Lighting Mast	5
Drain	3
Surface coating	34
TOTAL	**8825**

Main Cables

From Abaqus/CAE the length of the main cables geometry are found by a *General Query: Mass Properties*. $M_{initial} = 14774300kg$. $L = M_{initial}/(\rho \cdot A) = 8504m$. Subtracting the length of backs stay cables gives $L = 8504 - 4 \cdot 233.75 = 7569m$

1. Wires

$A = 0.22132m^2$

$m = 7850 \cdot 0.22132 = 1737kg/m$

2. Zink

Assume $50\mu m$ Zink layer, density $7100kg/m^3$

Areal of the 10032 wires ($\phi 5.3mm$): $A = \pi \cdot 0.0053 \cdot 10032 = 167m^2$

$m = 167 \cdot 0.00005 \cdot 7100 = 59 kg / m$

3. Winding Wire

Winding wire ($\phi 3.5 mm$)

Diameter of cable without w.w. $D = 609 mm$

Diameter of cable with w.w. $D = 609 + 2 \cdot 3.5 = 616 mm$

$m = \pi \cdot (0.308^2 - 0.3045^2) \cdot 7850 \cdot \pi / 4 = 41 kg / m$

4. Railing

Wire $\phi 25$ $m = 6 kg / m$

Post incl. attachment $m = 1 kg / m$

$m = 7 kg / m$

5. Polyethylene mash

Double layer protection of cables. Density $1.71 kg / m^2$

$m = \pi \cdot 0.616 \cdot 2 \cdot 1.71 = 7 kg / m$

Description	**m [kg/m]**
Wires	1737
Zink	59
Winding Wires	41
Railing	7
Polyethylene mash	7
TOTAL	**1851**

Hangers

From Abaqus/CAE the length of the hangers geometry are found by a *General Query: Mass Properties*.

$M_{initial} = 452388 kg$. $L = M_{initial} / (\rho \cdot A) = 18003 m$.

1. Steel hanger

$m = 28 kg / m$

2. Average mass of socket and clamp

$M = (52320 + 6968 + 15119 + 165360) / 130 = 239767 / 130 = 1845 kg / hanger$

$m = 1845 \cdot 360 / 18003 = 36,89 kg / m$

Description	**m [kg/m]**
Hanger	28
Socket and clamp	37
TOTAL	**65**

Pontoon

Density concrete: $\rho_c = 2500\ kg/m^3$

Density Ballast Water: $\rho_w = 1000\ kg/m^3$

	Cross-Section [m^2]	Length [m]	Weight [kg]	Center of gravity [m]	Mx [kgm]
1 x Inner Cylinder	55,12	90	12 402 000	-45	-558 090 000
8 x Outer Cylinder	35,27	90	63 486 000	-45	-2 856 870 000
1 x Bottom Plate	5027	10	125 675 000	- 95	-11 939 125 000
Ballast Water	4135	52	215 020 000	-74	-15911480000

Total mass:

$M = 416\ 583\ 000\ kg$

Center of gravity:

$y_m = 75,05m$

A3: Mass moment of inertia (MOI)

MOI Stiffening Girder

The mass moment of inertia for the stiffening girder including the non-structural elements are taken from technical report, NPRA [1] The MOI is calculated from the girders shear center using the following equation

$$I_M = I_G + I_2 = \frac{1}{12} ml^2 + mr^2 \tag{1.3}$$

Where,
L is the length of the part
m is the mass of the part
$r = \sqrt{(x - x_s)^2 + (y - y_s)^2}$, the distance from the parts centre of gravity to the shear centre

The following shear centre has been assumed:

$x_s = 0.155m$ and $y_s = 1.759m$

	M [kg/m]	m_x [m]	m_y [m]	I [kgm^2/m]
Steel Girder	4 563	-17	8 729	139 255
Guide Vans	114	0	-68	3779
Transvere Bulkheads	1 119	0	2 093	22787
Lower Hanger Clamp	84	0	260	4568
Railings	183	-13	697	6201
Asphalt and membrane	2 674	-46	8 554	44 204
Electric Instaltion	35	-53	88	115
Transport Beam IPE120	11	0	22	1
Light Mast	5	34	40	454
Drain	3	0	0	147
Surface Coating	34	0	29	1 349
	8 825	-95	20 444	222 860

Centre of gravity

$$X_m = \frac{\Sigma m_x}{\Sigma m} = \frac{-95}{8825} = -0.0111m \approx 0m$$

$$Y_M = \frac{\Sigma m_y}{\Sigma m} = \frac{20444}{8825} = 2.316m$$

Modeling point masses

The non structural masses of the girder will be modelled as point masses distributed at each hanger e.g. with distance 20.1639m. The total moment of inertia (MOI) abouth the longitudinal axis, $I_{M,11}$ is found by multiplying the distributed value by the distance of each mass. The total MOI about the vertical and horizontal lateral axis, I_y and I_z is given by the inertia to a homogenous slender beam $I_y = I_z = \frac{1}{12} M \cdot l_x^{\,2} = \frac{1}{12} m_x \cdot l_x^{\,3}$. The values of these MOI's are calculated below

$I_{M,11} = 20.1639 \cdot 222860 = 4493727 kgm^2$

$withoutGirder: 1\ 685\ 802\ \text{kgm}^2$

$I_{M,22} = I_{M,33} = \frac{1}{12} \cdot 8825 \cdot 20.1639^3 = 6029163\ \text{kgm}^2$

$withoutGirder: 2911761$

MOI pontoon

MOI for pontoon is calculated about center of mass. For the hollow concrete cylinders the following equations have been used [20]

$$I_{X,G} = I_{X,G} + I_{X,2} = \left(\frac{1}{12}ML^2 + \frac{1}{2}MR^2\right) + \left(Mr_z^{\,2}\right)$$
$$I_{Z,G} = I_{Z,G} + I_{Z,2} = \left(\frac{1}{12}ML^2 + \frac{1}{2}MR^2\right) + \left(Mr_x^{\,2}\right) \quad (1.4)$$

(1.5)

$$I_y = I_{y,G} + I_{y,2} = MR^2 + Mr_y^{\,2} \quad (1.6)$$

For the ballast water and ballast fixed weight a solid circular cross-section is assumed and hence the following equations can be used

$$I_{X,G} = I_{X,G} + I_{X,2} = \left(\frac{1}{12}ML^2 + \frac{1}{4}MR^2\right) + \left(Mr_z^{\,2}\right) \quad (1.7)$$

$$I_{Z,G} = I_{Z,G} + I_{Z,2} = \left(\frac{1}{12}ML^2 + \frac{1}{4}MR^2\right) + \left(Mr_x^{\,2}\right) \quad (1.8)$$

$$I_y = I_{y,G} + I_{y,2} = MR^2 + Mr_y^{\,2} \quad (1.9)$$

	Mass, M [kg]	radius,R [m]	Length, L [m]	Parallell axis disatance, Ry [m]	Parallell axis disatance, Rz [m]	Ix tot [kg m^2]	Iy tot [kg m^2]
inner cylinder	12402000	17,54	90	-30,05	0	2,15E+10	3,82E+09
4 x outer cylinder (each)	7935750	11,23	90	-30,05	11,01	1,30E+10	1,96E+09
4 x outer cylinder (each)	7935750	11,23	90	-30,05	26,58	1,30E+10	6,61E+09
Bottom Plate	125 675 000	40	10	19,95	0	1,01E+11	6,28E+09
Water Ballast	215 020 000	40	52	-1,05	0	1,35E+11	2,91E+11

Moment of inertia:

Ix tot	3,617E+11	kgm^2
Iy tot	3,351E+11	kgm^2
Iz tot	3,617E+11	kgm^2

If solid homogenous cylinder assumed:

Ix	4,478E+11	kgm^2
Iy	1,687E+12	kgm^2

Appendix B: Static Wind Calculations

This appendix gives the calculations for determining the static wind loads acting on the bridge. The wind velocity pressure is given by Bernouuli's equation and wind loads are given by

The necessary mean wind velocity is calculated according to European Standard [XX] which is based on metrological records over years of observation.

Mean Wind Velocity

The reference wind velocity 10*m* above ground dependent on the location and geography $v_{b,0}$ is *28 m/*s for region where the bridge will be located [Ytre Oppedal, Municipality of Gulen, Sogn og Fjordane, Norway]. The reference mean wind velocity 10*m* above ground is given by

$$v_b = c_{dir} \cdot c_{season} \cdot c_{alt} \cdot c_{prob} \cdot v_{b,0} \tag{2.1}$$

Where,
c_{dir} is the direction factor. Equal to 1.0 normal to the bridge axis.
c_{season} is the season factor. Equal to 1.0 for permanent structures.
c_{prob} is the probability factor used when other return periods then 50 years is used, if 50 years return period is used it is equal to 1.0.
c_{alt} is the level factor. Set equal to 1.0

Hence,

$$v_b = v_{b,0} = 28\ m/s \tag{2.2}$$

The mean wind velocity $v_m(z)$ at an arbitrary vertical distance above ground depends on the terrain roughness factor, orography and the reference wind velocity v_b. The expression is given by

$$v_m(z) = v_b \cdot c_r(z) c_0(z) \tag{2.3}$$

Where, $c_0(z)$ is the orography factor and can be set equal to 1.0. The roughness factor is given by

$$c_r(z) = k_r \cdot \ln\left(\frac{z}{z_0}\right) \tag{2.4}$$

Where, k_r is the terrain roughness factor and z_o is often called the roughness length. These parameters have the following values

$k_r = 0{,}17$
$z_0 = 0{,}01m$

Hence the mean wind velocity is given by the following expression

$$v_m(z) = 4.76 \cdot \ln\left(\frac{z}{0{,}01}\right)\ m/s \qquad \text{z} \geq 2\text{m} \tag{2.5}$$

And $v_m(z \leq 2m) = 25.22m/s$.

Static wind load

The static wind load is based on the mean wind velocity pressure given by Bernoulli's equation

$$q(z) = \frac{1}{2}\rho \cdot v_m(z)^2 \tag{2.6}$$

Stiffening Girder

The forces acting on the stiffening girder due to the wind pressure in main flow direction, assuming the effect of rotation can be disregarded, can be described by three uncoupled components

$$\begin{aligned} F_D &= C_D \cdot q \cdot H \cdot L \\ F_L &= C_L \cdot q \cdot H \cdot L \\ F_M &= C_M \cdot q \cdot B^2 \cdot L \end{aligned} \tag{2.7}$$

Where,
C_D, C_L C_M is the drag coefficients given by wind tunnels tests or CFD-calculations.
H is the projected height of the stiffening girder perpendicular to the flow direction.
L is the length of the stiffening girder perpendicular to the flow direction.

B is the width of stiffening girder parallel to the flow direction.

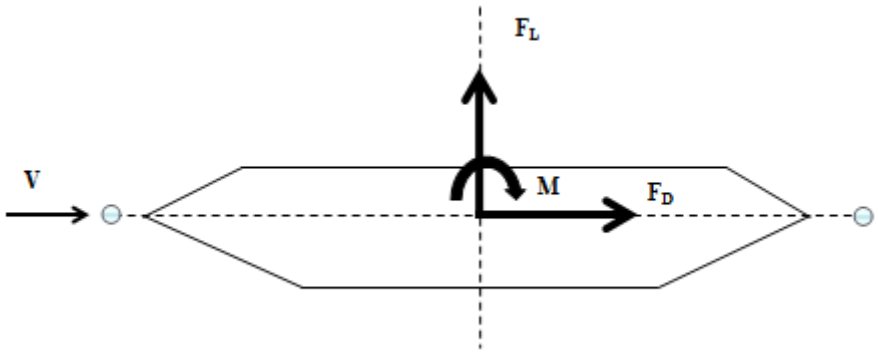

Drag force acting on stiffening girder

The stiffening girder of the bridge is assumed to have the same geometry and aerodynamic properties as the stiffening girder of the Hardanger Bridge. Hence values from the technical report [XX] can be used.

Parameter	Values
Height, H	3.33 m
Width, B	18.3 m
Drag coefficient, C_D*	0.854
Drag coefficient, C_L	-0.254
Drag coefficient, C_M	0.004

*Increased by 6% to accommodate the drag forces acting on the hangers, lower hanger clamps and lower hanger sockets.

Cross-sectional properties of stiffening girder

It is assumed that the average height of the stiffening is 75m above ground and that the corresponding mean wind velocity $v_m = 42.5\ m/s$ gives valid results for all heights of the stiffening girder, due to small changes of mean wind velocities at such height above ground. The forces acting on the stiffening girder per meter (L=1m) is summarized in table below

Force Direction	Values
Vertical Force, F_D	3206 N/m
Horizontal Force, F_L	-5240 N/m
Rotational Moment, M	1510 N/m

Distributed drag force on stiffening girder

Cables

The cables will only experience static drag force parallel to the flow direction, and no lift or moment forces due to symmetry of the cross section. The drag force is given by

$$F_D = C_D \cdot q \cdot D \cdot L \tag{2.8}$$

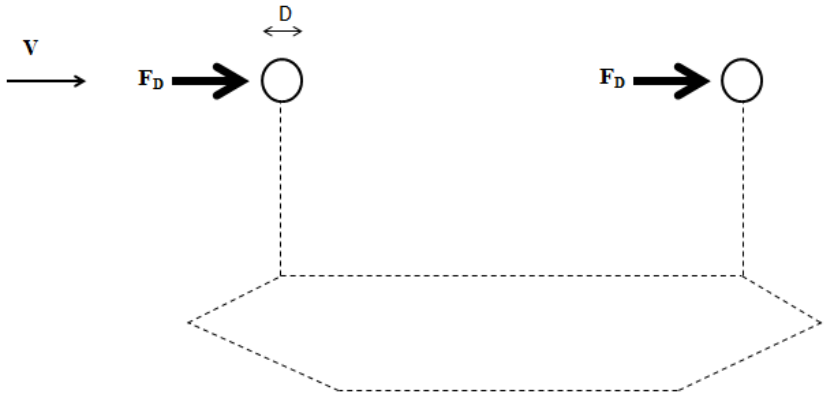

Drag force acting on cables

As for the Stiffening girder, the cables are assumed have the same geometrical and aerodynamic properties as the cables for the Hardanger . The technical report [XX] gives a drag coefficient of 0.92 including drag contribution from the hanger cables, upper hanger sockets and upper hanger clamps. To be on the conservative side drag coefficient 1.0 is assumed. With cable plane spacing 14.5 *m* no lee-effect is considered, hence calculating full drag force on both cables. The diameter *D* of the cable is 0.62 *m*.

Mean wind velocity changes only 8 % from lowest to heights cable point. Hence, it is assumed that the mean wind velocity at the centroid of the cable will give satisfying global results. The average height above ground is 85 *m* (given by *Querry: Centroid* in Abaqus/CAE) and the corresponding mean wind velocity becomes $v_m = 43.1\ m/s$ for the cables. The drag force acting on each cable per meter cable (L=1m) is given in table below.

Force Direction	Values
Vertical Force, F_D	719 N/m

Distributed Drag force on cable

Pylon

The pylon legs will experience static drag force parallel to the flow direction. Eventhough there is a slight inclination it is assumed no lift force on the pylon legs. Symmetrical cross-section gives no moment forces. There is assumed no wind force on the cross-brace beams, due to beam orientation parallel to wind flow. Same as for Cables, there is assumed no lee-effect on the second pylon leg. The drag force is given by

$$F_D = C_D \cdot q \cdot H \cdot L \tag{2.9}$$

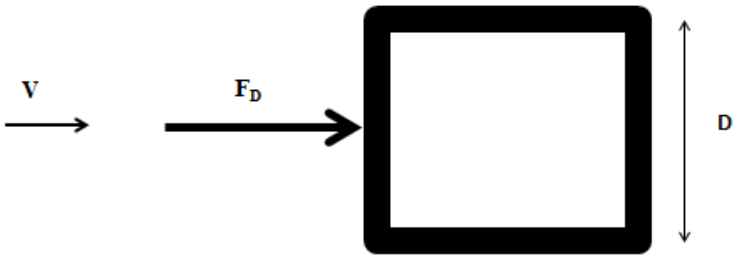

Drag force acting on pylon leg

The cross-sectional properties of the pylon legs are taken from Preliminary Design. The drag coefficient used for the pylon legs is be 1.07 assuming cube shape and Re > 10^4. [5] The proeprties of the pylon legs are given in table below.

Properties	**Value**
D *(0 – 65 m*)	6.989 *m*
D (65 – 142.5 m *)*	5.252 *m*
D (*142.5 – 200 m*)	4.500 *m*
C_D	1.07

Cross-sectional properties of pylon leg

For the pylon the change of mean wind velocity can not be neglected. The height above ground varies from 0- 200*m*. The pylon also have different cross-sectional properties at different heights. To accommodate for this a excel spreadsheet calculate the drag force per meter at every 2nd meter. The drag force as function of postion above ground is given in figure XX.

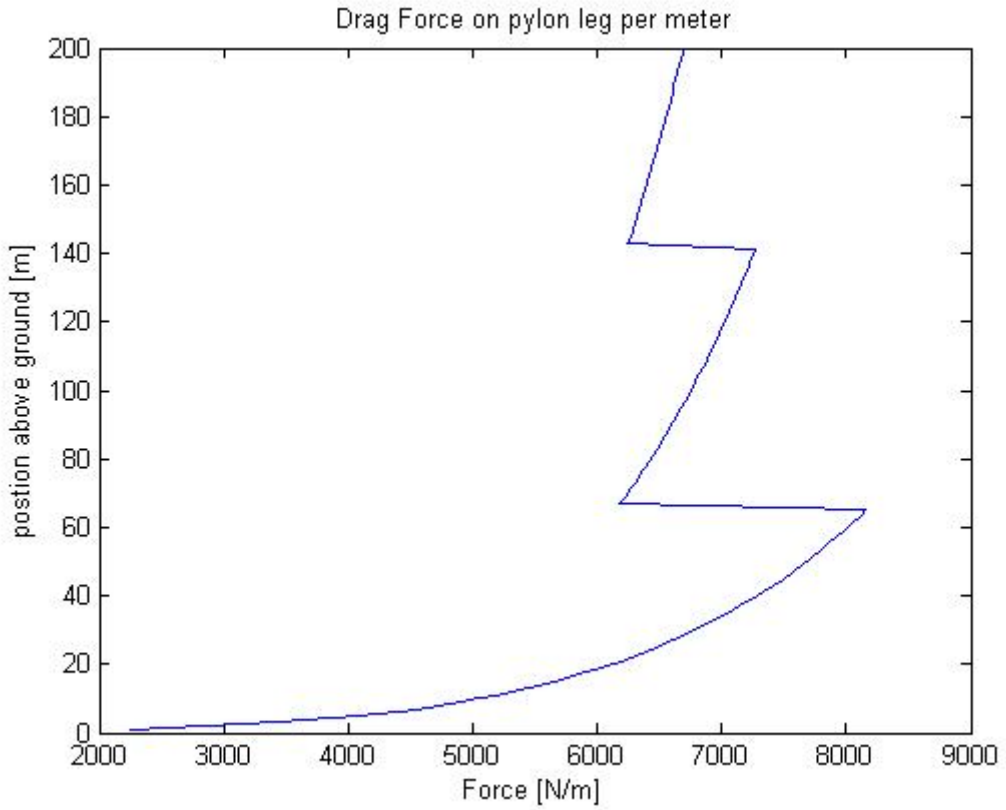

Drag force distribution on pylon leg in vertical direction

The drag force on the pylon leg can be described by the following function

$$q(z) = a \cdot \left(\ln \frac{z}{b} \right)^2 \tag{2.10}$$

Where a changes for bottom (*a1*), mid (*a2)* and top section (*a3*). *b* stays unchanged.

Constant name	Constant value
a1	105.8992
a2	79.5797
a3	68.2458
b	0.01

Constants for description of drag force on pylon

Horizontal force and moment in mid pylon foundation, spans on both sides, due to wind loading are calculated assuming drag force contribution from all elements from two half spans. For stiffening girder and cables an average lever arm and distributed load is assumed, while for the pylon legs a integration along the pylon axis is carried out. Table below shows the contribution from each structural element

Structural Element	**Distributed Load [*N/m*], *[*N m*]**	**Length *m*]**	**Lever arm [*m*]**	**Horizontal Force in Foundation [*MN*]**	**Moment in Foundation [*MNm*]**
Stiffening girder, F_D	3206	1230	75	3.94	295.8
Cables	719	2 x 261.5	85	1.81	154.5
Pylon Legs	-	2 x 200	100.75	2.67	269.0
TOTAL				8.42	719.3

Static Wind Reaction Forces on Pylon Foundation.

Appendix C: Pootoon Design

Wind loading	From Appendix B		
Pylon	134	268	MNm
Bridge Deck	298	257	MNm
Cable	78	156	MNm

Dead loads			
Cables, Top	from Abaqus	156.56	MN
		200	m
Bridge Deck	from Abaqus	6.4	MN
		72.3	m
Pylon		172.5	MN
		89.9	m

Pontoon Properties		
Total Diameter	80	m
Radius, Inner Cylinder	17.54	m
Radius, Outher Cylinders	11.23	m
Thickness, Inner	0.5	m
Thickness, Outer	0.5	m
Total Depth	100	m
Fixed Ballast Height	10	m
Water Ballast Height	64	m
Density water	10	kN/m3
Concrete Density	25	kN/m3

Pontoon Properties	Area [m2]	Weight [MN]	Center of gravity
Inner Cylinder	55.1	124	-45
Outer Cylinde (per cylinder)	35.3	79	-45
Bottom plate	5027	1257	-95
Ballast Water	4135	2150	-74

Submerged Properties		
A,s, submerged (assume cirle =r1+r2)	5027	m2
Io,s, submerged areal	2010619	m4

Vertical dead loads	Force		x	mx
Cable forces	156.56	MN	200	31312
Bridgedeck	6.4	MN	72.3	462.72

Tower	173	MN	89.9	15508
pontoon outer	635	MN	-45	-28572
pontoon inner	124	MN	-45	-5580
pontoon bottom plate	1257	MN	-95	-119381
pontoon ballast (use A,s)	2150	MN	-74	-159131
TOTAL	**4501**	**MN**		**-265381**

BUOYANCY STABILITY CHECK (no wind)		
G, Center of gravity	**-59.0**	**m**
V,sub	450146	m3
Pontoon under water	89.55	m
	90	%
Distance from pontoon to waterline	**10**	**m**
F,B=rho*(displace volume)=Body Weight		
B, Center of buoyancy	**-55.2**	**m**
GB, Distance between COG and COB	-3.7	m
MB, Io/Vsub	4.5	m
M, metacenter	-50.8	m
Metacentric height	**8.2**	**m**

MOMENT EQUILIBRIUM		
Mw, Wind moment	681	Nm
Sin Theta	0.0185	
THETA	0.0185	rad
	1.1	**degress**

Concret Needed		
Inner Cylinder	4960	m3
Outer Cylinders	25397	m3
Bottom Plate	50265	m3
	81	***1000 (m3)**

Appendix D: Mode Shapes: Floating Foundation Model

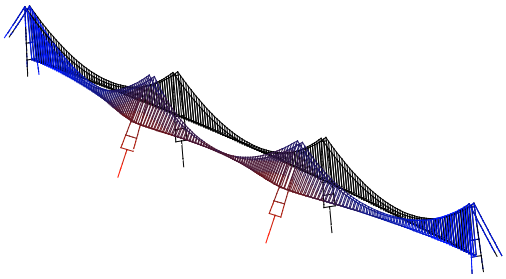

Mode Shape 1

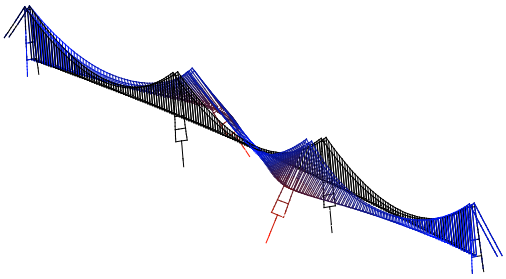

Mode Shape 2

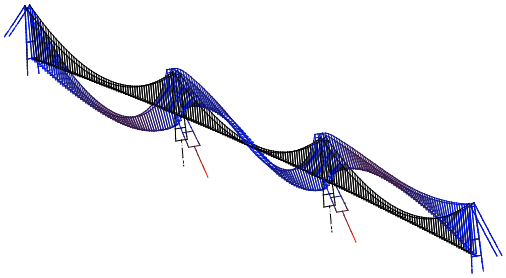

Mode Shape 3

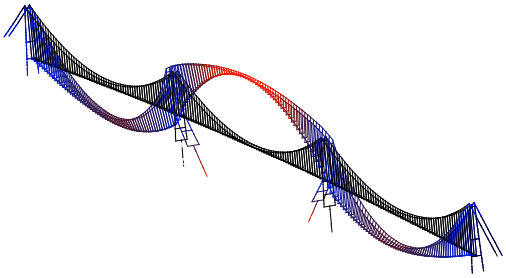

Mode Shape 4

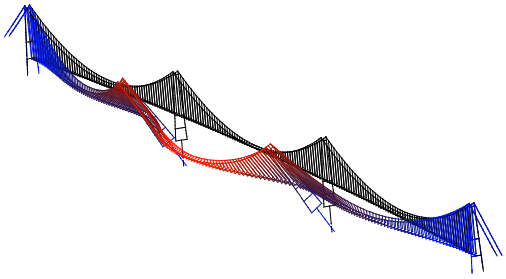

Mode Shape 5

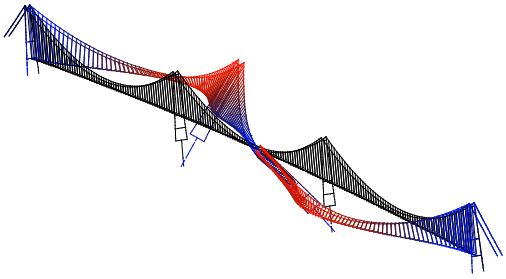

Mode Shape 6

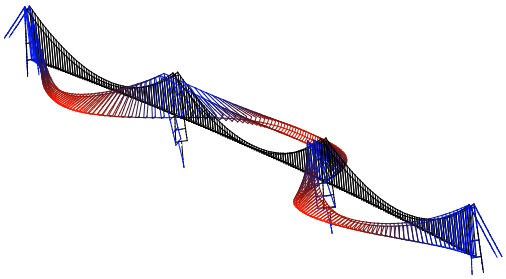

Mode Shape 7

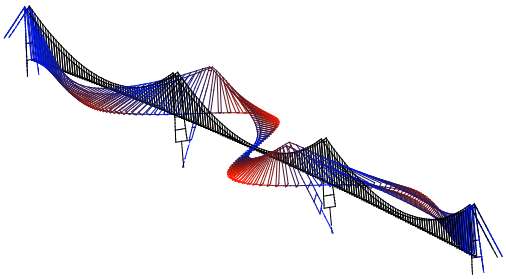

Mode Shape 8

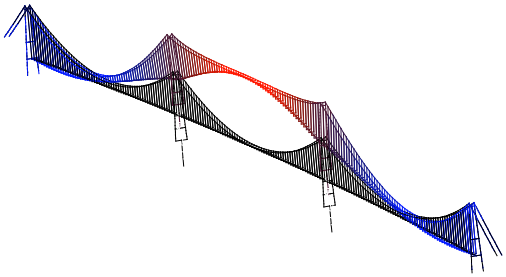

Mode Shape 9

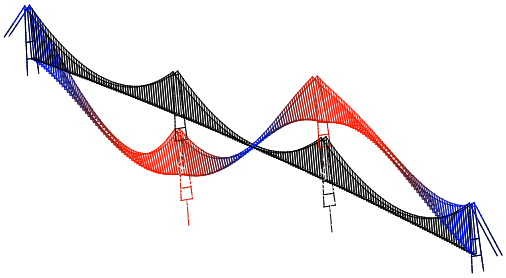

Mode Shape 10

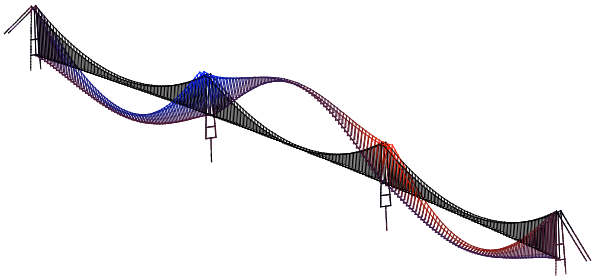

Mode Shape 11

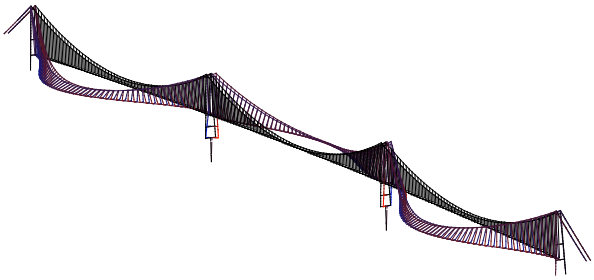

Mode Shape 12

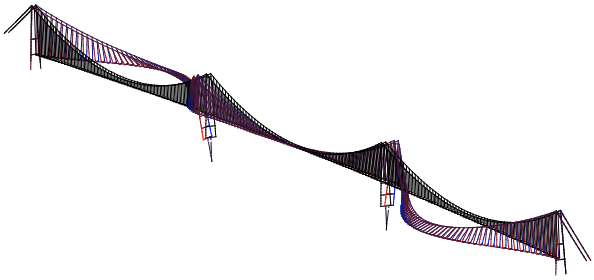

Mode Shape 13

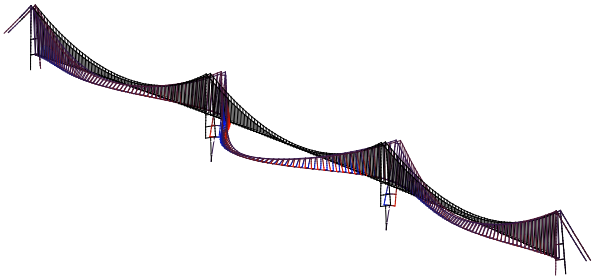

Mode Shape 14

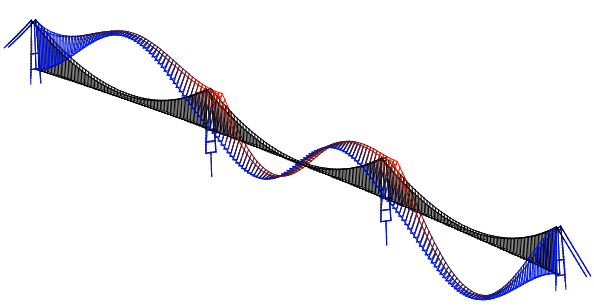

Mode Shape 15

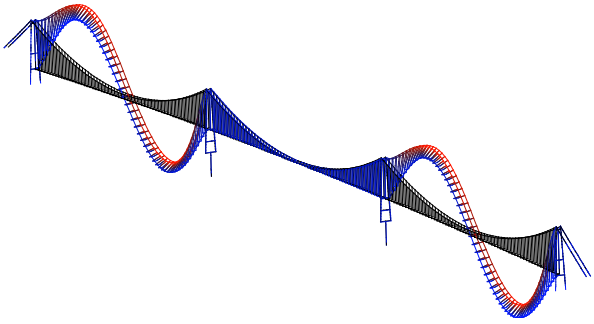

Mode Shape 16

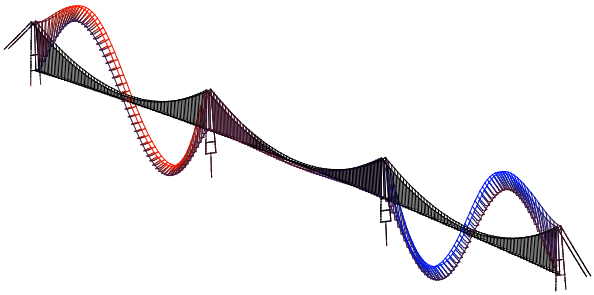

Mode Shape 17

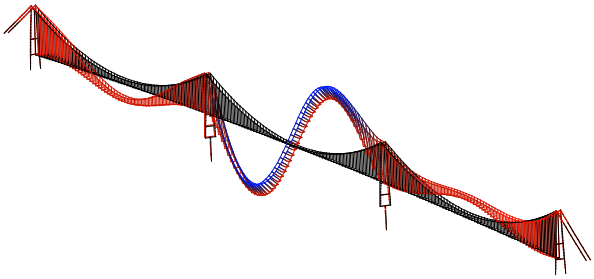

Mode Shape 18

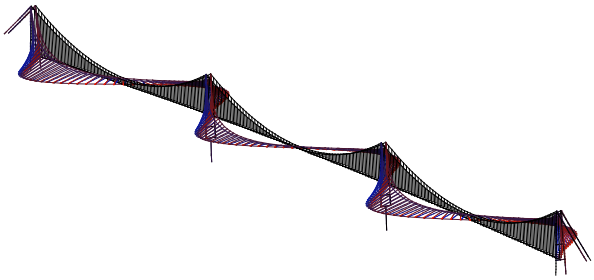

Mode Shape 19

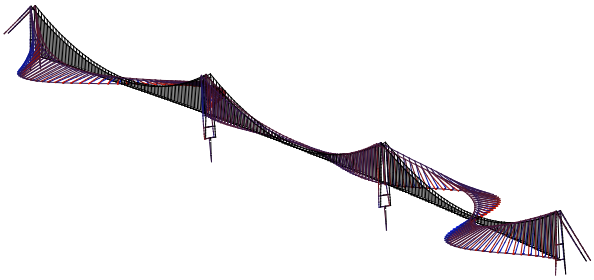

Mode Shape 20

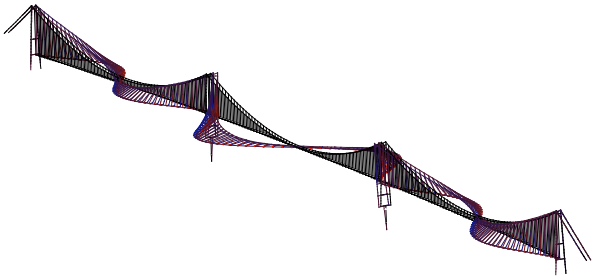

Mode Shape 21

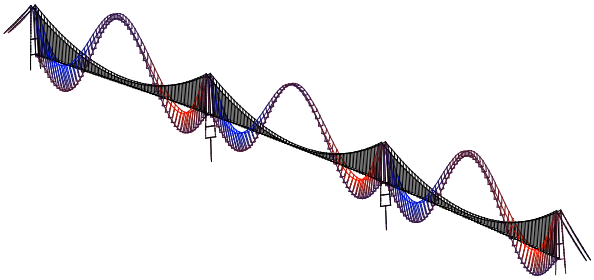

Mode Shape 22

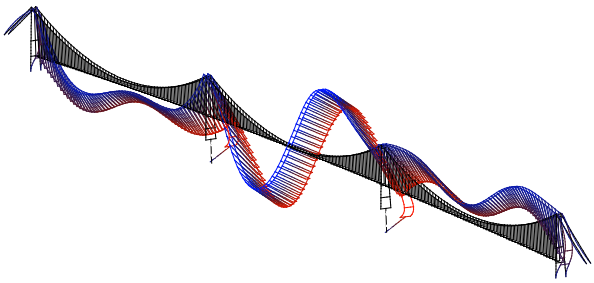

Mode Shape 23

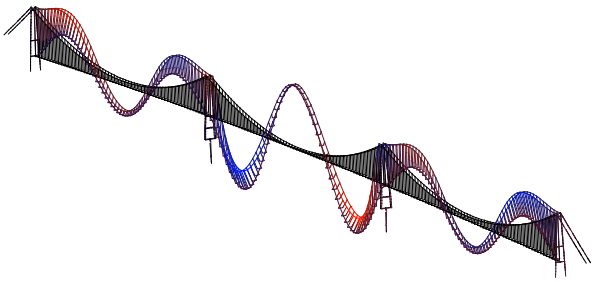

Mode Shape 24

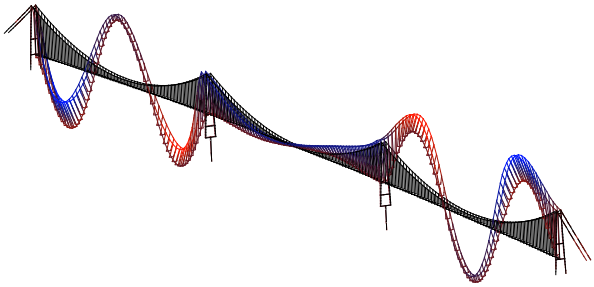

Mode Shape 25

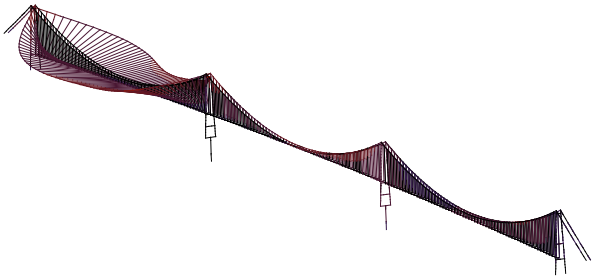

Mode Shape 26

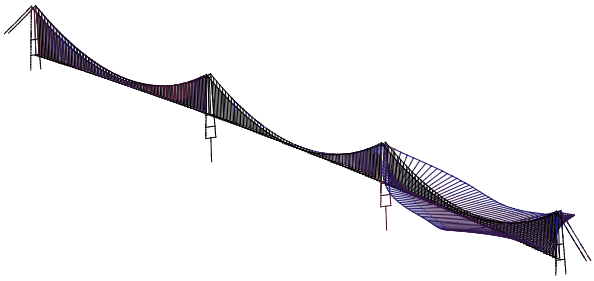

Mode Shape 27

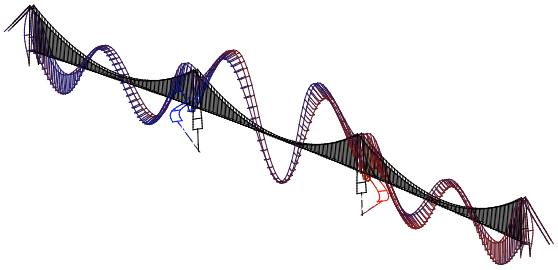

Mode Shape 28

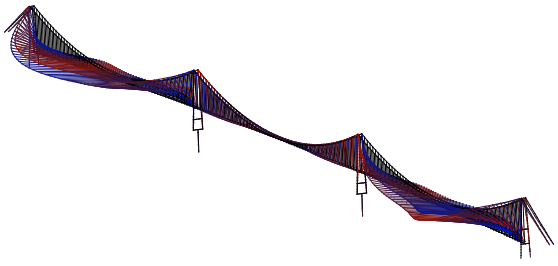

Mode Shape 29

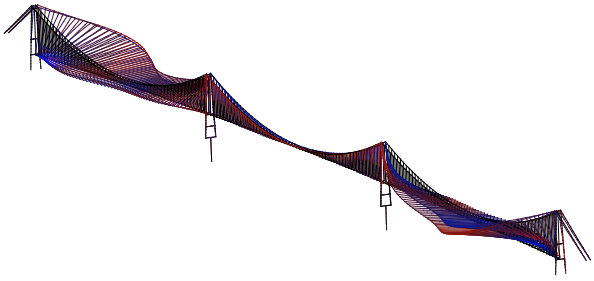

Mode Shape 30

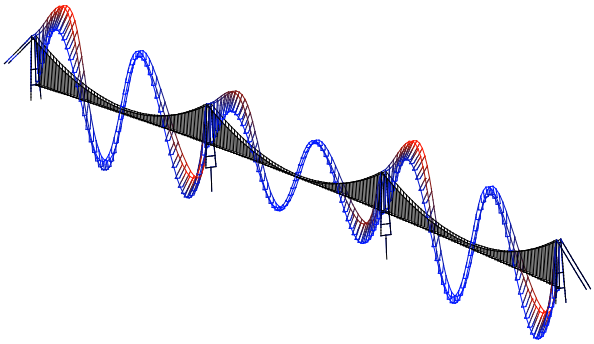

Mode Shape 31

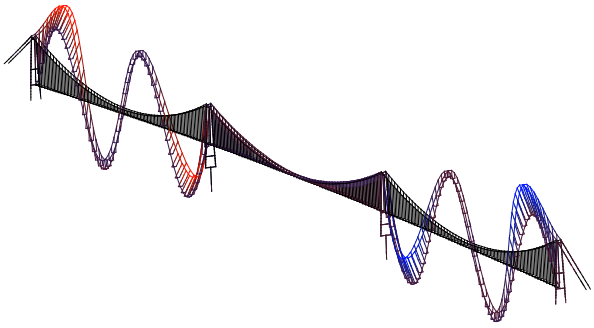

Mode Shape 32

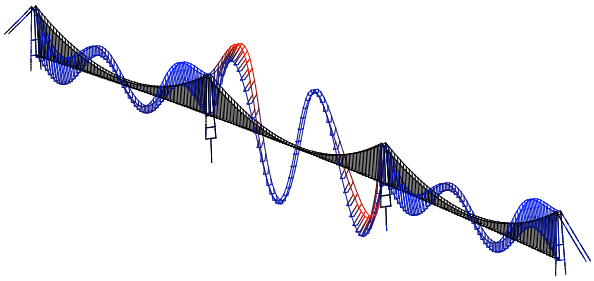

Mode Shape 33

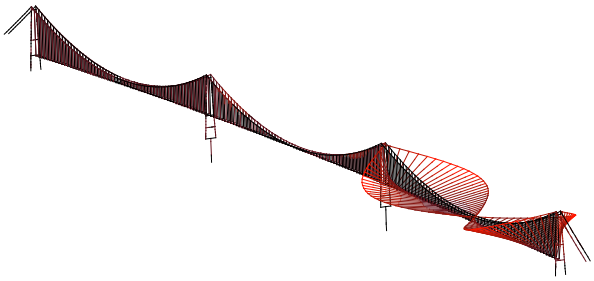

Mode Shape 34

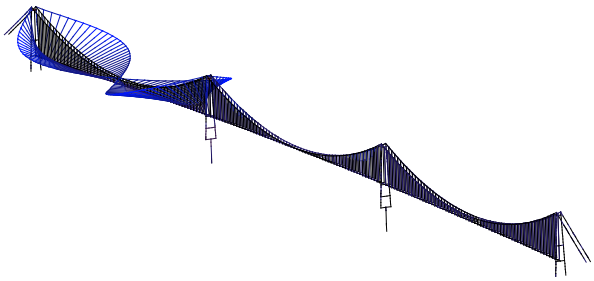

Mode Shape 35

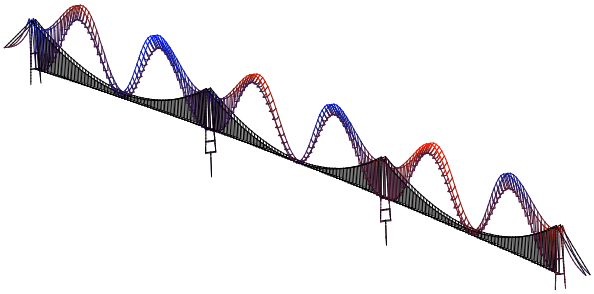

Mode Shape 36

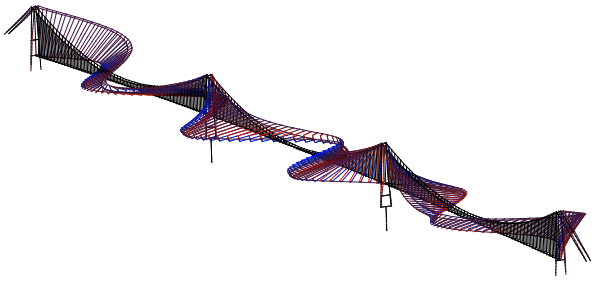

Mode Shape 37

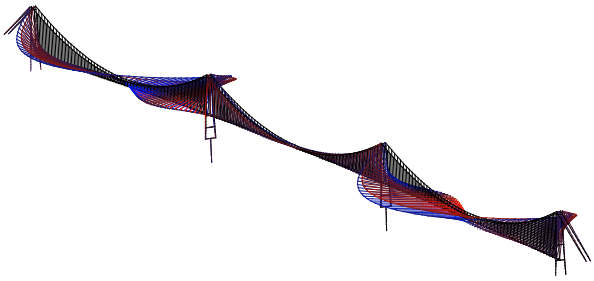

Mode Shape 38

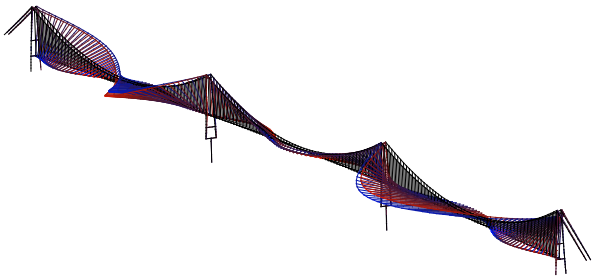

Mode Shape 39

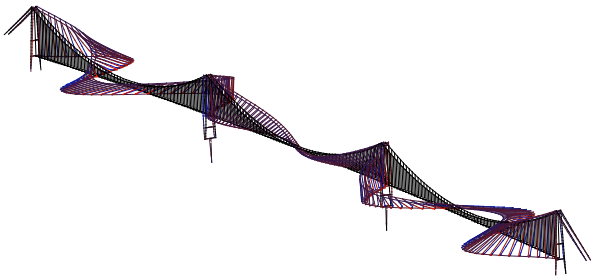

Mode Shape 40

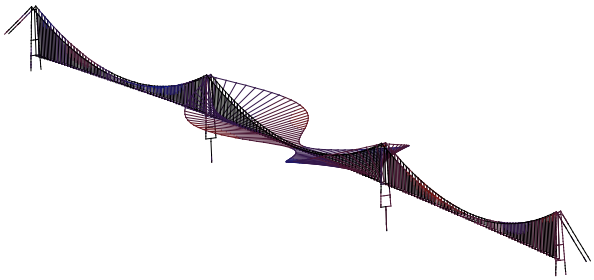

Mode Shape 41

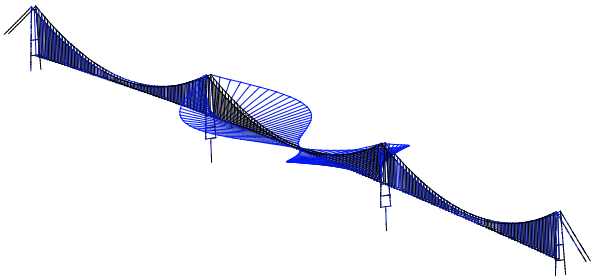

Mode Shape 42

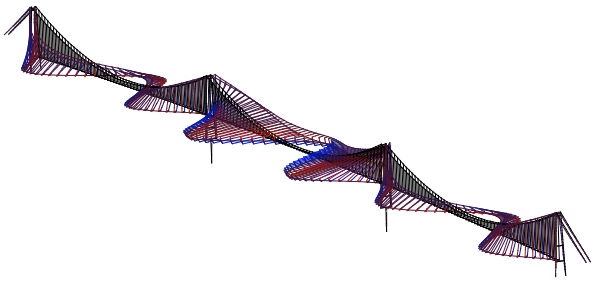

Mode Shape 43

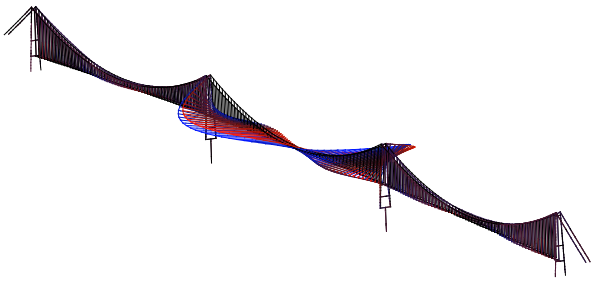

Mode Shape 44

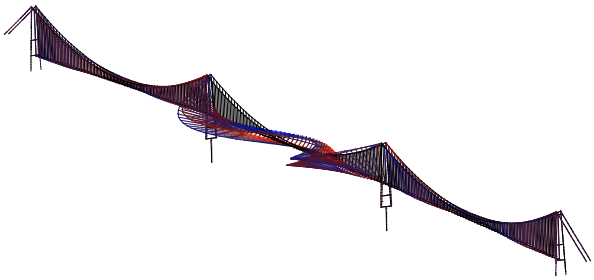

Mode Shape 45

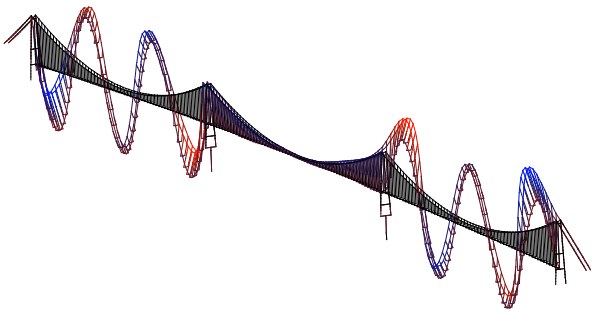

Mode Shape 46

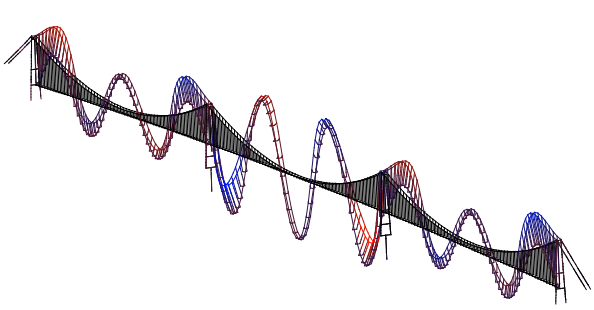

Mode Shape 47

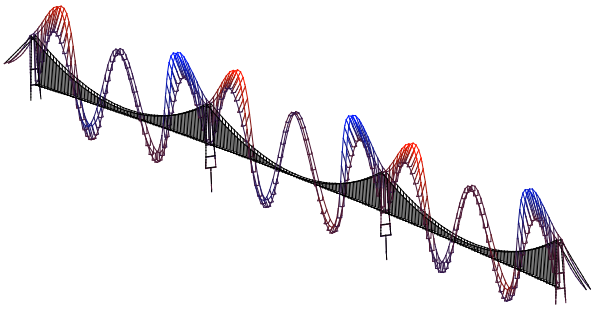

Mode Shape 48

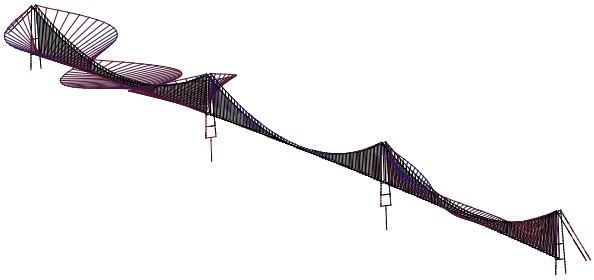

Mode Shape 49

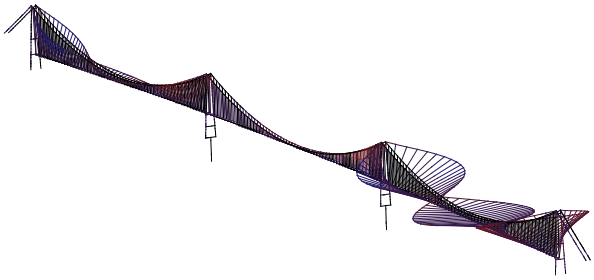

Mode Shape 50

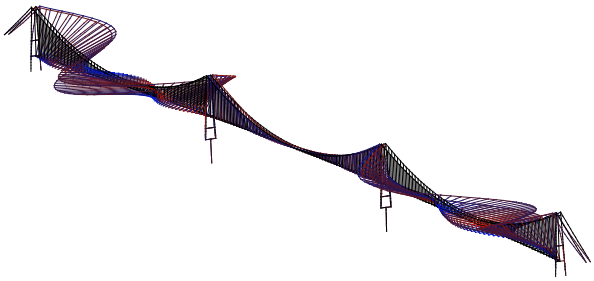

Mode Shape 51

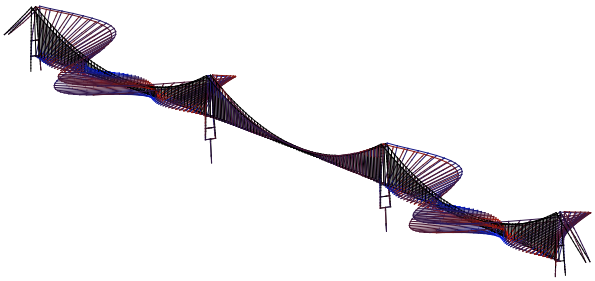

Mode Shape 52

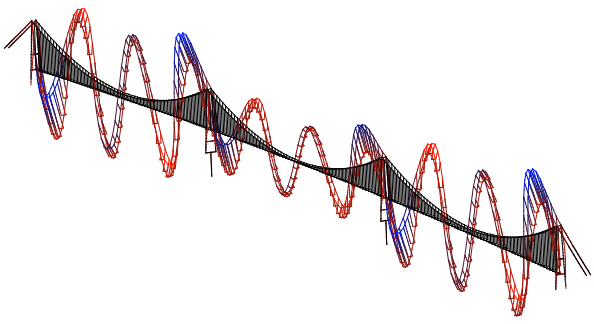

Mode Shape 53

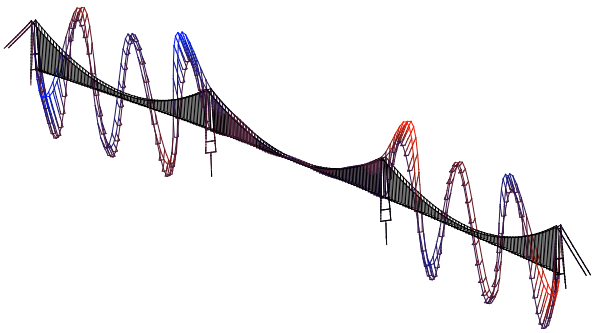

Mode Shape 54

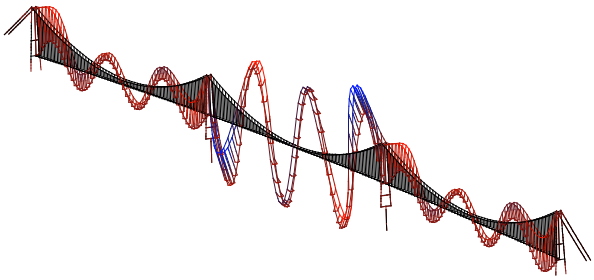

Mode Shape 55

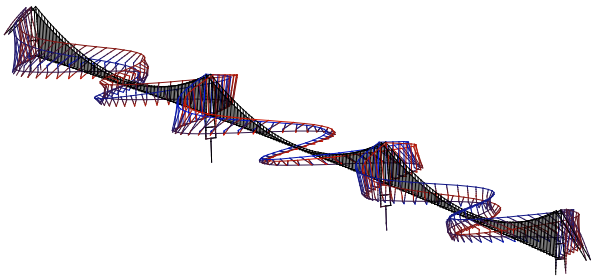

Mode Shape 56

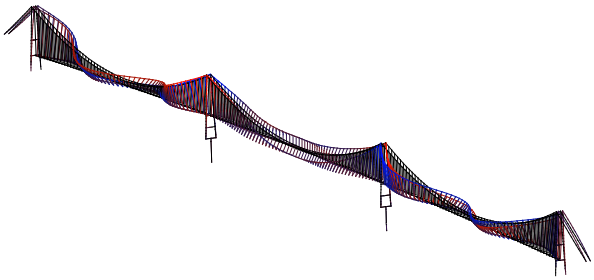

Mode Shape 57

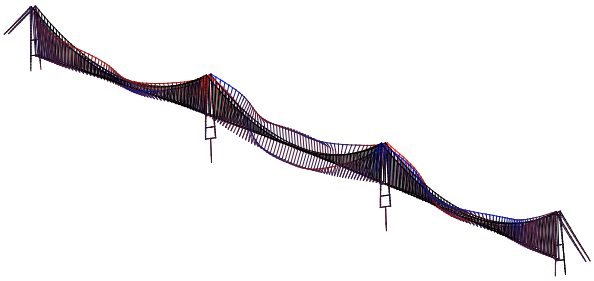

Mode Shape 58

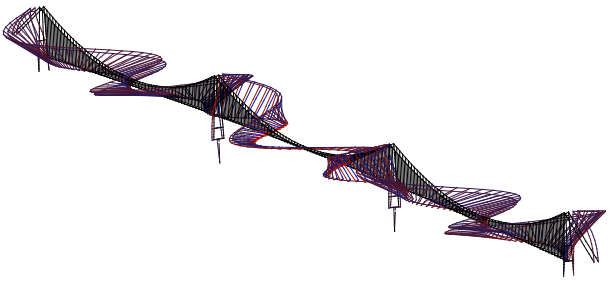

Mode Shape 59

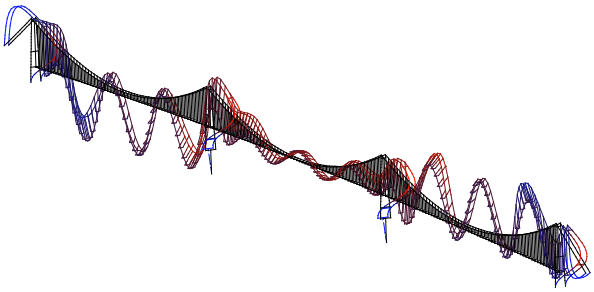

Mode Shape 60

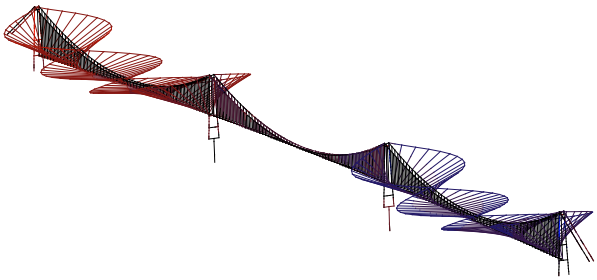

Mode Shape 61

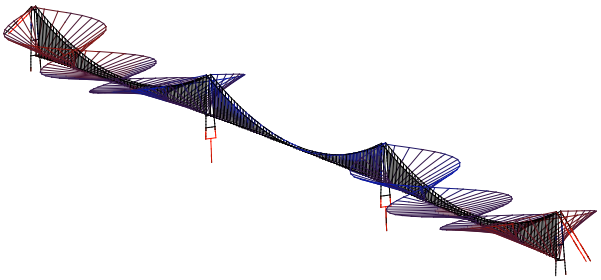

Mode Shape 62

References

[1] NPRA, "Haradngerbrua-beregninger. Kapitel 1: Grunnlag," 2008.

[2] P. N. Larsen. and S.-E. Jacobsen., "Mulighetsstudie for kryssing av Sognefjorden med flytrebruFerjefri E39 -Flyttebru," *Brunkonferransen 2012, Vegvesenet (Bridge Conference 2012, Norwegian Public Road Administatrtion),* 2012.

[3] M. Patel, "Dynamics of Offshore Structures," *Computational Mechanics Publications*, 1987.

[4] E. C. Tupper, *Introduction to Naval Architecture* 4th. ed. New York, USA: Elsevier, 2004.

[5] F. M. White, *Fluid mechanics*, 6th ed. Boston, Massachusetts, USA: McGraw-Hill, 2008.

[6] A. H. Techet, "2.016 Hydrodynamics Reading #6," 2005.

[7] J. N. Newman, *Marine Hydrodynamics*. Massachusetts, USA: MIT Press, 1977.

[8] O. Faltinsen, "Sea Loads on Ship and Offshore Structures," *Ocean Technology Series, Cambridge University Press, UK*, 1989.

[9] R. Mansouri and H. Hadidi, "Comprehensive Study on the Linear Hydrodynamic Analysis of a Truss Spar in Random Waves," *World Academy of Science, Engineering and Technology,* 2009.

[10] A. Incecik, "Design Aspects of Hydrodynamics and Structural Loading on Floating Offshore Platforms under Wave Excitation," *PhD thesis University of Glasgow, UK,* 1982.

[11] M. Patel and J. Witz, *Compilant Offshore Structures*. Oxford, UK: Heinmann Ltd., 1991.

[12] N. J. Gimsing, *Cable Supported Bridges: Concept and Design*, 2nd ed. Chichester: John Wiley & Sons, 1997.

[13] S. O. H. ApS, *The Hardanger Bridge: Static and dynamic wind tunnel tests with a section model*. Copenahgen, Denmark, 2006.

[14] NPRA, "Hardangerbrua: Arbeidstegninger," 2011.

[15] NPRA, "Technical Brochure Hardanger Bridge," 2012.

[16] R. C. Hibbeler and S. C. Fan, *Engineering mechanics: statics*. Singapore: Pearson Prentice Hall, 2010.

[17] S. K. Chakrabarti, *Handbook of offshore engineering*. Amsterdam, Netherlands: Elsevier, 2005.

[18] R. Pérez Fernández and M. Lamas Pardo, "Offshore concrete structures," *Ocean Engineering*, 2013.

[19] S. Norway, "NS-EN 1991-1-4:2005+NA:2009: Eurocode 1: Actions on structures - Part 1-4: General actions - Wind action," ed: Standard Norway, 2005.

[20] F. Irgens, *Dynamikk*. Trondheim, Norway: Tapir Forlag, 1999.

[21] A. K. Chopra, *Dynamics of Structures: Theory and Applications to Earthquake Engineering*. Boston, Massachusetts: Prentice Hall, 2007.

[22] S. Norway, "NS-EN 1991-2:2003+NA:2010: Eurocode 1: Actions on structures - Part 2: Traffic loads on brdiges," ed: Standard Norway, 2010.

[23] D. J. Inman, *Engineering Vibrations*: Pearson Prentice Hall, 2008.

[24] E. N. Strømmen, *Theory of bridge aerodynamics*. Germany, Berlin: Springer, 2010.